Structures and Materials Research
Department of Civil Engineering
Division of Structural Engineering
and Structural Mechanics

BEHAVIOR OF SKEW HIGHWAY BRIDGES

by

G. H. Powell
Assistant Professor of Civil Engineering

J. G. Bouwkamp
Professor of Civil Engineering

and

I. G. Buckle
Assistant Specialist

to

the Division of Highways
Department of Public Works
State of California
Under Research Technical Agreement
No. 13945-14120
and
U.S. Department of Transportation
Federal Highway Administration
Bureau of Public Roads

College of Engineering
Office of Research Services
University of California
Berkeley, California

February 1969

TABLE OF CONTENTS

Chapter Page

Chapter | Page

Chapter | Page

ACKNOWLEDGEMENT

This research investigation was conducted under the sponsorship of the Division of Highways, Department of Public Works, State of California, and the Bureau of Public Roads, Federal Highway Administration, United State Department of Transportation. The opinions, findings and conclusions in this report are those of the authors and not necessarily those of the Bureau of Public Roads.

Close liason and support from the Bridge Department of the Division of Highways, State of California was provided by Mr. G. D. Mancarti, Assistant Bridge Engineer and Mr. R. E. Davis, Senior Bridge Engineer of the Research and Development Section.

For the University of California, Professors J. G. Bouwkamp and G. H. Powell acted as faculty investigators. The reduction and plotting of data by Mr. R. Todeschini, Research Assistant, is also acknowledged.

CHAPTER 1

INTRODUCTION

This report is the second in a series of reports dealing with the behavior, analysis and design of rib- or girder-supported bridge decks of a variety of shapes. A program of study extending in several phases over approximately a six year period has been envisaged. The proposed activities include literature surveys, development of refined techniques for analysis and design, and laboratory and field studies of model and prototype structures.

The first report in the series [1]* described a computer oriented method of analysis for skew bridges, in which the bridge structure was idealized as a thin plate with eccentrically connected ribs, and was analyzed by the finite element method. Since the completion of that report, work has continued on the development of analytical techniques and computer programs. The techniques being investigated and compared include extensions of the ribbed plate method, and also methods in which the structure is idealized as an anisotropic plate, as a discrete gridwork, and as a simple beam.

In this report, these methods are reviewed briefly. However, the main purpose of the report is to investigate the anisotropic plate method of analysis, and to use this method to study the behavior of skew bridges. The report is therefore arranged as follows.

In Chapter 2, several analytical methods of both historical and contemporary importance are reviewed and contrasted. Particular attention

---

* See References

is given to the anisotropic plate method, as it is used extensively in the later chapters. In Chapter 3, the theory of the anisotropic plate method is presented, and a computer program to apply the method is described. In Chapter 4, a typical class of skew bridges is selected, and a study is carried out in which the angle of skew, diaphragm layout and loading are varied. The results are discussed extensively, with the aim of demonstrating how skew bridges behave, and how they differ from right bridges. In Chapter 5, the behavior of a skew, two-span slab bridge is investigated both analytically and experimentally, and the results are compared. In Chapter 6 a study of the local behavior of skew-supported deck slabs is carried out, in order to determine whether skew supports significantly influence deck slab behavior. Conclusions about specific aspects of behavior are presented at the end of each chapter.

In future reports, other methods will be described in detail and will be critically compared on the basis of accuracy and suitability for both research and design use.

CHAPTER 2

REVIEW OF METHODS OF BRIDGE DECK ANALYSIS

2.1 INTRODUCTION

A number of important methods of highway bridge deck analysis are reviewed in this chapter. To assist in this review, the methods have been classified according to the type of mathematically idealized model selected to represent the real structure, and according to the method used to analyze the idealized model.

Three major classes of idealized model, and one miscellaneous class, can be recognized. These are:

1. Equivalent plate model.
2. Equivalent grid model.
3. Ribbed plate model.
4. Miscellaneous models.

In each case, the model is obtained by making assumptions about the character and behavior of the real structure. The accuracy with which the results obtained from analyses of the model can be applied to the real structure depends, therefore, on the accuracy of the assumptions, and it is important for the analyst to bear this fact constantly in mind.

The analysis techniques which have been applied to the idealized models also fall into four classes. These are:

1. Series solution of a differential equation.
2. Finite difference solution of a differential equation.
3. Analysis of an assemblage of discrete structural members.
4. Analysis by empirical or semi-empirical methods.

In the following sections, methods of both historical and contemporary importance are reviewed according to the idealized model and analytical technique used. The equivalent anisotropic plate idealization is given particular attention because it is used in later chapters of this report. Other idealization procedures, such as the grid and ribbed plate techniques, will be considered in future reports of this series, and will be explained in greater detail in those reports.

2.2 EQUIVALENT PLATE IDEALIZATION

2.2.1 Idealization

The basis of the equivalent plate procedure is the idealization of the bridge deck as an equivalent elastic plate with anisotropic properties. The stiffnesses of the plate are obtained by "smearing" the stiffnesses of the girders and diaphragms, as explained in detail in Chapter 3. The major sources of inaccuracy in the idealization are as follows:

1. If either the girders or diaphragms of the actual deck are widely spaced, the "smearing" of their stiffnesses may not be justified. However, this problem can be overcome, as noted subsequently, by representing the girders or diaphragms as discrete beams.

2. It may be difficult to assign an appropriate torsional stiffness to the equivalent plate.

3. The real deck is actually a three dimensional structure, with ribs eccentrically connected to a deck slab. However, this three dimension aspect is ignored when the structure is idealized as a thin plate. In particular, shear lag effects in the deck slab are essentially ignored.

The methods reviewed in this section are believed to be representative of the many investigations which have been reported. The analytical techniques used and the methods of presenting the results are described in general terms for each case, for the purposes of comparison and contrast. However, for detailed explanations of the methods, the original reports should be studied. Where different workers have adopted different procedures for idealizing the deck structure this fact is noted, but details are not presented. A recommended procedure for idealization of the structure is presented in Chapter 3.

2.2.2 Distribution Coefficient Method

The distribution coefficient method is a variation of the series solution technique applied to orthotropic plates. The method is treated separately here because it forms the basis of an extensively used book by Rowe [2].

The term "distribution coefficient" refers to the particular method used to present the results of the analysis. The method is based on the Guyon-Massonet solution of the governing differential equation for rectangular orthotropic plates (Huber's equation), namely

$$D_x \frac{\partial^4 w}{\partial x^4} + 2H \frac{\partial^4 w}{\partial x^2 \partial y^2} + D_y \frac{\partial^4 w}{\partial y^4} = q\ (x,y) \qquad (2.1)$$

in which: D_x and D_y are the flexural stiffnesses per unit width of the idealized plate in the x and y directions respectively;

H is a constant depending on the equivalent flexural and

torsional stiffnesses selected for the plate;

w is the lateral displacement;

and q is the applied load per unit area.

The initial idealization was made by Guyon [3], who ignored torsional stiffness. Massonet [4] subsequently proposed a method of accounting for torsion. The solution technique was then refined by Morice, Little and Rowe [2,5].

The solution technique is the single series procedure of Levy [6], in which displacements in the x direction are expanded in Fourier series, with the effect that the partial differential equation in x and y is reduced to an ordinary differential equation in y only. This equation can then be solved comparatively easily. The technique is well known, and has been applied in recent years to a wide variety of plate and shell problems. Its overwhelming disadvantages are that the properties of the idealized plate must be uniform in the direction of the span (the x direction), the plate must be simply supported along two opposite edges, and only rectangular plates can be considered. However any pattern of loading on the bridge can be taken into account, by expanding the load function in Fourier series. Loads corresponding to each term of the series are applied separately, and the final results are then obtained by superposition.

Morice, Little and Rowe observed that the displacement variation across the width of the bridge caused by any loading pattern was generally similar to the displacement distribution caused by only the first term of the Fourier series for that loading pattern. Accordingly, they carried out

parameter studies for the comparatively simple case of loading by the first Fourier term only, and presented the results as a series of "distribution coefficients." For a plate with specified stiffness properties, the deflection at a point, x = a, y = b, on the bridge due to a line of wheel loads applied along a line, y = c, can be calculated as

$$w = k_1 W \tag{2.2}$$

in which: w = deflection at point (a,b);

k_1 = the distribution coefficient, which depends on the properties of the slab and the values of b and c;

and W = average deflection of the complete bridge cross section at x = a, caused by the actual line of wheels and computed by treating the complete bridge as a simple beam.

By this procedure, the deflections due to any combinations of wheel loads can be estimated.

An exactly similar procedure, using essentially the same distribution coefficients, is applied to determine the longitudinal plate bending moment per unit width at a point. However, the distributions of bending moment across the bridge width caused by the actual wheel loads and the first Fourier term respectively are not as closely similar as the distributions of deflection (mathematically, this is because the series for bending moment converges less rapidly than the series for deflection). As a result, the method is less satisfactory for moment computations. The procedure recommended by Rowe et al [2,5] is to apply the equation

$$m_x = 1.1\ k_1 M_x \tag{2.3}$$

in which: m_x is the plate bending moment per unit width at point (a,b);

k_1 is the distribution coefficient, as before, and the 1.1 is is an approximate correcting factor;

and M_x is the average bending moment on the bridge section at x = a, caused by the actual line of wheels and computed by dividing the simple beam moment by the bridge width.

A procedure for the computation of transverse bending moments is also presented but in a much less convenient form.

The distribution coefficient method was developed for use in England, where the critical design loadings for short span bridges are exceptionally heavy wheel loads representing special vehicles, and where the ability of the bridge deck to distribute such heavy loads is of primary importance. The method can be applied fairly easily, and has been widely used in England. In the United States, however, design loadings are specified differently, and different methods of analysis have evolved. It is doubtful whether the distribution coefficient method will have much application in the United States, except for special problems.

The weaknesses of the distribution coefficient method should also be emphasized. The method is strictly applicable to simple span right bridges only, and must be treated with caution if applied to skew or continuous bridges. Equally important is the fact that transverse diaphragms must be "smeared", in order to produce uniform equivalent plate properties. If the diaphragms are widely spaced, considerable error may result, as noted in Chapter 4 of this report.

2.2.3 Other Series Solutions of the Differential Equation

The Guyon-Massonnet solution of the equivalent plate assumed that the plate had free longitudinal edges, and hence did not permit edge beams to be taken into account. Cornelius [7] presented a solution of the plate equation for the case where the plate edge was supported by an edge beam possessing flexural stiffness but no torsional stiffness. A Levy type of solution was still used, but different boundary conditions were inserted in the solution of the ordinary differential equation in y. It may be observed that this did not represent a major theoretical advance, as a general theory of edge beam-structure interaction, including both torsional effects and eccentric connection, had been presented earlier for the more complex cylindrical shell problem by Jenkins [8].

The Cornelius solution was improved and applied to bridges by Chu and Krishnamoorthy [9]. They emphasized the importance of integrating the plate moments to estimate the moments in the girders of the actual deck, and discussed practical problems of assigning flexural and torsional stiffnesses to the plate. They also showed that the transverse distributions of moment and deflection in a plate differed substantially, thus contradicting a key assumption of Rowe's distribution coefficient method. They further pointed out that the transverse bending moments computed for the equivalent plate do not provide a good measure of the slab moments in the actual bridge. Giencke [10,11] improved the methods of idealizing the structure by proposing more realistic definitions for the properties of the equivalent plate than those which had been previously used. Heins and Looney [12,13] have extended the theory of interacting plates and beams to consider more complex geometrical configurations.

A variation of the series solution technique, which combines the series procedure with the finite element method has been described by

Cheung [14] and Powell and Ogden [15]. This technique actually eliminates the need to set up and solve the differential equation of the orthotropic plate, and is rather more general than other procedures. However, it is most appropriately classified as a series technique, and suffers from most of the restrictions of the other series methods.

An elegant application of orthotropic plate theory to the special problem of orthotropic steel plate deck bridges has been presented by Pelikan and Esslinger [16] and has been adopted in the A.I.S.C. Design Manual [17] for these structures. Mathematical idealizations specifically suited to steel decks with open and closed ribs are first developed. The analysis is then carried out by forming expressions for the influence surfaces of orthotropic plates which are continuous over rigid beams, and determining from these the maximum effects due to truck loadings. In the A.I.S.C. Design Manual, charts permitting easy computation of maximum effects are presented.

2.2.4 Finite Difference Solution of Differential Equation

Because of the limitations of series solutions, the finite difference method has been extensively applied to obtain approximate solutions of the differential equation of equivalent plates. The method was developed by Jensen [18] for solid isotropic plates with both skew and right supports, and was used for the analysis of flat slabs. The theory was then extended by Newmark and Siess [19] and by Chen, Siess and Newmark [20] to the analysis of right and skew bridge decks. The method used was to idealize the structure not as an anisotropic plate, but as an isotropic plate in which discrete beams were imbedded. This idealization is actually superior to the anisotropic plate idealization as it avoids the problem of "smearing"

the girder and diaphragm stiffnesses. However, similar assumptions are made in reducing the bridge deck to an equivalent thin plate system. In the first report by Newmark and Siess [19], analyses for a variety of right angled decks were carried out, and as a result of these analyses recommendations leading to the well known S/5.5 rule were made [19,21]. In the later application to skew decks [20] similar recommendations were made, which modified the rule to allow for the effects of skew. The finite difference technique has recently been extended and applied to a variety of structures by Heins and Looney [22,23].

Finite difference analyses of skew bridge decks idealized as equivalent orthotropic plates have been carried out by Naruoka and Ohmura [24]. An attempt was made to present the results as distribution coefficients of the type used by Rowe. However, because of the larger number of parameters which can be varied in skew decks, the coefficients did not cover a sufficiently wide range of cases to be of practical value. Finite difference analyses of orthotropic plates have also been carried out by Heins and Looney [12,13].

Although a much wider range of structures can be analyzed by the finite difference method than by the series solution method, the finite difference technique is still rather inflexible. In particular, difficulties arise at the edges of the structure, especially if the edge is not straight or is supported in a complex fashion. The finite difference equations may also be poorly conditioned for solution, and significant inaccuracy may result.

2.2.5 Finite Element Analysis

The finite element method is a modern, computer oriented method which can be applied to the analysis of an extremely wide variety of

complex structural systems. The method can be applied to both anisotropic plates and plates with imbedded beams. Plates of virtually any shape and with arbitrary support conditions can be analyzed. The method is not exact, but will generally yield more accurate results than the finite difference method. It should be remembered, however, that the results of the analyses are still no better than the assumptions made in setting up the equivalent plate idealization.

The finite element method has been used in later chapters of this report to conduct a parameter study of skew bridge decks. The theory used is described in Chapter 3.

2.3 EQUIVALENT GRID IDEALIZATION

The equivalent plate method of idealization replaces the bridge deck by an equivalent continuum. By contrast, the grid method replaces the bridge by a framework of discrete beam elements. Each beam is assigned flexural and torsional stiffnesses selected to represent the strip of deck structure which it replaces. The idealized structure is then analyzed as a discrete element system, and the member forces are used to estimate the forces in the actual deck.

Early attempts to apply grid methods of analysis to bridge decks were handicapped by the amount of numerical calculation involved. Frequently, series types of solution were sought, and in some cases discrete grids were actually converted to either equivalent plates or plates with imbedded beams to permit series solution techniques to be applied. With the introduction of digital computers, however, the analysis of

grids by the displacement method became a routine task. The technique was pioneered by Hendry and Jaeger [25] and Lightfoot and Sawko [26]. More recently Bouwkamp and Powell [27] have idealized orthotropic steel plate deck bridges as large grids with excellent results. The technique generally avoids the complex mathematics of other idealizations and can be expected to have wide application in bridge deck analysis. The method will be investigated in detail in future reports of this series.

2.4 RIBBED PLATE IDEALIZATION

Both the equivalent plate and equivalent grid procedures reduce the three-dimensional bridge deck to essentially a plane system. Ribbed plate idealizations, however, attempt to treat the structure as a plate with eccentrically connected ribs.

Trenks [28], Pfluger [29] and Vitols, Clifton and Au [30], have also "smeared" the rib stiffnesses, but by accounting for the rib eccentricity they have developed 8th order differential equations to represent the system. These equations can be solved for simple cases by series techniques, but the method is mathematically complex and not of practical importance. Massonnet [31] has sought a compromise solution which incorporates the effects of eccentric ribs into equivalent orthotropic plate equations of 4th order. Basically, the technique is to allow the positions of the neutral axes in the ribs of the combined rib and plate system to vary, and to determine those positions of the neutral axes which lead to minimum total potential energy of the complete plate. By contrast, in the usual equivalent plate method the positions of the neutral axes are estimated in advance and are fixed. Some increase in accuracy is achieved, but the mathematics of the problem is made considerably

more complex, and the basic assumptions, restrictions and errors of the equivalent plate idealization are retained. In can be concluded, therefore, that this type of method is also not of practical importance.

Ribbed plates can also be analyzed by the finite element method without "smearing" the rib stresses. The idealized structure in this case consists of a thin isotropic plate possessing both flexural and extensional stiffness, representing the deck slab, to which discrete ribs, also with both flexural and extensional stiffness, are connected. For composite action, compatibility of both the in-plane and out-of-plane displacements at the interface of the plate and ribs is then established during the analysis, whereas for noncomposite action compatibility of only the out-of-plane displacements is established.

The application of this method to skew bridges has been investigated by Mehrain [1] in a previous report in this series, and a somewhat similar procedure has been reported independently by Gustafson and Wright [32]. Although the method is not strictly "exact" (for example, the cracking of concrete sections is not taken into account), the procedure is the most precise one currently available. However, because it is time consuming, and therefore costly, to use, it does not appear to be feasible to apply the method in design at present, except in unusual cases. Nevertheless, the method is extremely valuable because it can be used to check simpler and more approximate methods. A considerably extended version of Mehrain's computer program has been developed, which permits stringer-supported decks of completely arbitrary plan shape and with arbitrary properties and loading to be analyzed. This program is being used to analyze curved

bridges and bridges with varying skew to study their behavior and to check results obtained by other methods of analysis. This work will be reported in detail in a future report in this series.

2.5 OTHER IDEALIZATIONS

2.5.1 General

In this section three other methods of idealization are considered, namely the equivalent beam method (AASHO "S/6" rule), the multibeam method and model testing.

2.5.2 AASHO "S/6" Rule

One of the major difficulties faced by the bridge designer is that the loads (whether design loads or actual loads) can be placed anywhere on the structure, often in combination, and the absolute maximum effects of these loads must be determined. All of the methods of analysis described in this chapter require substantial numerical effort to determine the effects of loads acting in any one position on the structure, and may require tremendous effort if all possible load positions are to be investigated. Even if the method is one in which influence surfaces are generated, substantial simplification will result only if there are a few critical sections in the bridge which can be easily identified, so that only limited numbers of influence lines have to be constructed. It may happen that as computer programs for use by the bridge designer are developed, it will be possible for maximum effects to be determined from rational

theories automatically with moderate cost and effort. Indeed, programs of this type are being studied as part of the investigations being carried out by the authors. At present, however, such programs do not exist. As a result, the use of a simplified idealization such as the "S/6" rule is essential.

The "S/6" type of rule can be criticized because it takes into account only one parameter, the girder spacing, out of several parameters which may influence the load distribution in the bridge. Thus, Scordelis and Meyer [33] have proposed that additional parameters be considered in establishing this type of rule for box girder bridges. It is noted, however, that the original recommendations of Newmark et al [19,20,21] on which the "S/6" rules appear to be based, also took account of parameters other than the girder spacing. It has not been firmly established whether the rules now in use are accurate for skew bridges or bridges of other shapes, and part of the work being carried out by the authors is to review these rules. It can be anticipated that rules of this type offer the best compromise between simplicity and accuracy for typical bridges, especially considering the lack of knowledge about the true loading patterns on bridges. However, for bridges of unusual shape it is probable that more rational investigations are warranted.

2.5.3 Multibeam Idealization

Multibeam bridges, consisting of discrete precast beams connected by longitudinal "hinges", can be analyzed as beam-hinge systems. Series solutions have been proposed by Pool, Arya, Robinson and Khachaturian [34] and by Powell, Ghose and Buckle [35], and a transfer matrix method by Buckle [36]. Because the hinges are usually assumed to transfer no moment, load is transferred

from beam to beam essentially by shear only, and the degree of load transfer depends on the torsional stiffness of the beams. Nevertheless, approximate analyses of stringer supported bridges with monolithic deck slabs can be carried out by multibeam theory if the transverse flexural stiffness of the bridge is small. A feature of the method described by Powell, Buckle and Ghose is that nonzero flexural stiffnesses can be assigned to the hinges, so that decks with significant transverse flexural stiffness could also be analyzed.

2.5.4 Model Tests

If there is no analytical technique available which can be applied with sufficient confidence by the designer, resort to model testing is usually necessary. Frequently, the information sought from the physical model is the same as that which might have been found from a mathematical model, namely elastic deflections and stresses. As the range of structures which can confidently be analyzed increases, however, the need for this type of model test decreases. Such tests are therefore used mainly to check the theoretical results obtained in research programs rather than as aids to design.

At the same time that small scale elastic models have less use, however, prototype or large model testing, aimed at studying the true behavior of actual structures, is required more and more. Such tests are required to determine the deflections and stresses in real structures under actual loading and environmental conditions, and to determine whether the analytical methods being used or proposed for use in design are adequate. As safety factors are reduced, and as structures become more complex and analytical techniques become apparently more refined, more large scale tests are essential.

2.6 SUMMARY

2.6.1 Review of Idealized Models

The major types of idealized model for use in bridge analysis are:

a. The equivalent plate model;

b. The equivalent grid model;

c. The ribbed plate model;

and d. The equivalent beam model.

The equivalent plate method should be satisfactory for the analysis of bridge decks with closely spaced stringers or ribs, but can be expected to be inaccurate if the ribs are widely spaced. In such cases, the method can be extended by idealizing the structure as a plate in which discrete beams are imbedded.

Whereas the equivalent plate method idealizes the actual structure as a continuum, the equivalent grid method idealizes it as an assemblage of discrete beams, but otherwise the level of approximation is very similar. The grid method has the advantage of simplicity, yet permits very complex systems to be analyzed, provided judgement is exercised in the selection of the equivalent beam properties. Whereas a grid analysis can be shown to give poor results for solid isotropic plates, good results can be expected for ribbed plates, especially if they are strongly anisotropic. For bridge structures, the accuracy achieved should generally be comparable with the accuracy with which the loading and bridge properties are known, and the grid method can be expected to have wide application in bridge analysis.

The ribbed plate method attempts to idealize the structure in as accurate a manner as possible, and to account for effects which are ignored in the simpler plate and grid methods. The increased refinement is achieved, however, at the expense of greater complexity. Hence, although the method is valuable as a tool for research and investigation, it is doubtful whether it will become a standard method for use in design.

The equivalent beam method has the advantage of extreme simplicity, and has served designers well for many years. There is no doubt that it will continue in use. Nevertheless, the method in its current form can be criticized because it does not take account of many important parameters which influence bridge deck behavior. Accordingly, the method deserves to be re-examined, in order to determine whether a more rational form should be developed.

2.6.2 Techniques of Analysis

In certain restricted cases, equivalent plate models can be analyzed by series solution of the differential equation, either directly (in which case a computer is desirable) or with the aid of design charts. For a wider variety of cases, the finite difference method can be used, but the use of a computer is virtually essential. The finite element method, for which a computer is absolutely essential, can be applied to a still wider variety of cases, and is generally superior to the finite difference method. It is therefore recommended for cases in which series solution or charts can not be used. It may be observed that there is no reason why a computer should not be as common a design office tool as a slide rule. Many analysis and design techniques which are currently in use

have been developed more with regard to simplicity for hand computation than with regard to rationality. There can be no doubt that in the near future virtually all routine calculation will be performed by machine, and that more elaborate and rational techniques will be commonly used.

The grid method also requires the use of a computer, as do the finite element techniques for the analysis of ribbed plate models. Even the analysis of equivalent beam models may require a great deal of numerical computation, and can profitably be carried out by computer. In all cases, however, appropriate computer programs, which are easy to use in the design office, must be developed.

CHAPTER 3

ANISOTROPIC PLATE THEORY

3.1 INTRODUCTION

The equivalent plate model can be used for the analysis of bridge decks having closely spaced ribs in a variety of configurations. In this chapter, a procedure for idealizing a bridge deck as an equivalent anisotropic plate is presented, and the theory of the anisotropic plate is developed. A computer program developed to analyze skew plates is then described. This program is subsequently used for the parameter studies in Chapter 4.

The equivalent plate method can be extended to bridge decks which have widely spaced beams (or a combination of widely spaced girders with closely spaced ribs), by idealizing the structure as an isotropic or anisotropic plate with imbedded discrete beams. This type of model can also be analyzed by the computer program described in this chapter.

3.2 BRIDGE PROPERTIES

3.2.1 Bridge Axes

Fig. 3.1 shows a plan of a skew bridge. Axes Ox and Ox' act parallel to one pair of edges of the bridge (in this report, the span direction), as shown. Axis Oy' is then defined normal to Ox', so that coordinates x',y' are in a rectangular system. However, axis Oy is defined parallel to the other pair of edges of the bridge (in this report, parallel to the supports), so that coordinates x, y are in a skew system. The angle

β is the "external" angle of skew, as shown.

3.2.2 Beam Systems

The beam systems in a skew bridge may follow several patterns, three of which are shown in Fig. 3.2. These are as follows:

a. Girders and diaphragms parallel to the skew axes, Ox and Oy (Fig. 3.2.a) This system is most common in concrete bridges, and is not orthotropic.

b. Girders and diaphragms parallel to the rectangular axes, Ox' and Oy' (Fig. 3.2.b) This system is equivalent to that commonly used in steel bridges and is orthotropic.

c. Girders and diaphragms at right angles to the skew axes, Ox and Oy (Fig. 3.2.c). This system, or other systems, might be used in special cases. It is included here to show that the method is not restricted to the two cases above.

Note that in right bridges these three systems are all identical.

3.2.3 Beam Axes

In each of the above three cases, the beam directions define a pair of beam axes in the bridge, which are identified as directions 1 and 2 respectively, as shown in Fig. 3.2. Each set of beams will have both bending and torsional moments acting on it. The bending moments are identified respectively as M_1 and M_2, as shown in Fig. 3.3, and the torsional moments as M_{31} and M_{32}.

3.2.4 Bridge Properties in Beam Axes

The stiffness properties of the bridge depend on the elastic constants of the structural material and the dimensions of the beams and slab. Let Young's modulus and Poisson's ratio be E and ν, so that the shear modulus is $G = E/2(1+\nu)$. Let I_1 and I_2 be the moments of inertia of single beams in the 1 and 2 directions respectively. If the beams are closely spaced, that part of the deck slab which is tributary to each beam should be assumed to be a part of the beam cross section. If the beams are widely spaced, and effective width of slab should be assumed, commonly one third of the total beam length, but not exceeding the beam spacing. This procedure allows approximately for shear lag effects in the slab. If the beams and slab are not composite, their I values should be computed separately and added. Let J_1 and J_2 be the effective torsional inertias in the 1 and 2 directions respectively. These are usually determined by dividing the effective beam sections into rectangles and summing the St. Venant torsional inertias of the individual rectangles. However, for rectangles representing the deck slab, the equivalent torsional inertia should be put equal to $bh^3/6$, in which h = slab thickness and b = rectangle width. This procedure is rather crude, but in view of other approximations in the methods of analysis, and because the torsional behavior of an actual bridge deck is extremely complex, the method is believed to be justified.

3.2.5 Bridge Moment-Deformation Relationships in Beam Axes

Moment-curvature and moment-twist relationships are assumed to be expressible in the following form:

$$\begin{Bmatrix} M_1 \\ M_2 \\ M_{31} \\ M_{32} \end{Bmatrix} = \begin{bmatrix} D_{11} & D_{12} & 0 & 0 \\ D_{12} & D_{22} & 0 & 0 \\ 0 & 0 & D_{31} & 0 \\ 0 & 0 & 0 & D_{32} \end{bmatrix} \begin{Bmatrix} \chi_1 \\ \chi_2 \\ \chi_{31} \\ \chi_{32} \end{Bmatrix} \qquad (3.1)$$

in which: χ_1 and χ_2 are beam curvatures;

χ_{31} and χ_{32} are beam rates of twist;

D_{11} and $D_{22} = EI_1$ and EI_2 respectively;

D_{31} and $D_{32} = GJ_1$ and GJ_2 respectively;

and D_{12} represents the coupling, through Poisson's effect, between the flexural behavior in the 1 and 2 directions.

The assumption that actions M_1 and M_2 are coupled only by Poisson's effect and M_{31} and M_{32} are uncoupled is reasonable for the orthotropic system in Figs. 3.2.b. However, the situation is more complex in the skew systems shown in Figs. 3.2.a and 3.2.c, and coupling among the flexural and torsional actions must be expected through shear effects in the slab. Such coupling effects are, however, very difficult to determine, and for simplicity it is assumed that Eq. 3.1 applies for this case also. If a more accurate analysis is required, then a more refined idealization of the structure, such as a ribbed plate model, should be selected.

3.3 EQUIVALENT PLATE PROPERTIES

3.3.1 Plate Axes

Axes Ox', Oy' and Ox, Oy, as in Fig. 3.1, are selected for the equivalent plate as well as the actual bridge.

3.3.2 Plate Moment Coordinate Systems

The equivalent plate which will be analyzed is (with the exception of certain torsional features, as noted later) conceived as a solid plate of orthotropic material. If a segment of the plate, as shown in Fig. 3.4.a is removed, then the normal stresses and shear stresses acting on a unit length of the plane face, AB, combine to give a resultant moment per unit length, shown as the vector R in Fig. 3.4.b. This resultant moment can now be resolved into component moments in several different ways, some of which are significant in the development of skew plate theory and in the interpretation of the results of skew plate analyses.

The simplest component moment vectors are those taken normal and parallel to the face AB, as shown in Fig. 3.4.c, and are respectively the torsional moment and bending moment per unit length on AB. The component vectors might also, however, be taken normal to the rectangular axes, Ox' and Oy', as shown in Fig. 3.4.d, or normal to the skew axes, Ox and Oy, as shown in Fig. 3.4.e. It happens that the system shown in Fig. 3.4.c is most convenient for interpreting the results of skew plate analyses, because the bending and torsional moments on the rib cross sections can be determined from this system. However, for the development of skew plate theory the system shown in Fig. 3.4.e is commonly selected for the reason given in the next paragraph. It should be noted that the component moment vectors are not orthogonal in this case, and therefore must be treated with care.

Fig. 3.5 shows a rectangular element and a skew element in a skew plate. Anisotropic plate theory can be developed using the system shown in Fig. 3.5.a, and for the particular case of orthotropic slabs

it will lead to a simple formulation. However, it is difficult to insert the skew boundary conditions in an analysis being conducted with this system. Further, the displacement compatibility characteristics of finite elements for skew plate analysis can be improved substantially if the displacement degrees of freedom are expressed in the skew coordinate system. Hence, the skew system shown in Fig. 3.5.b is more convenient, and has been adopted for the finite element solutions used in this report.

3.3.3 Plate Moment-Deformation Relationships in Beam Axes

In order to convert from bridge beam stiffnesses in the 1 and 2 directions to equivalent plate stiffnesses in these same directions, put

$$i_1 = \frac{I_1}{S_1} \tag{3.2}$$

in which S_1 is the spacing of the girders and i_1 is therefore the plate stiffness in the 1 direction per unit width of plate. Similarly, put

$$i_2 = \frac{I_2}{S_2} \tag{3.3}$$

$$j_1 = \frac{J_1}{S_1} \tag{3.4}$$

$$j_2 = \frac{J_2}{S_2} \tag{3.5}$$

Assume, now, that plate moment-deformation relationship in beam axes can be written as:

$$\begin{Bmatrix} m_1 \\ m_2 \\ m_{31} \\ m_{32} \end{Bmatrix}_B = \begin{bmatrix} d_{11} & d_{12} & 0 & 0 \\ d_{12} & d_{22} & 0 & 0 \\ 0 & 0 & d_{31} & 0 \\ 0 & 0 & 0 & d_{32} \end{bmatrix}_B \begin{Bmatrix} \chi_1 \\ \chi_2 \\ \chi_{31} \\ \chi_{32} \end{Bmatrix}_B \qquad (3.6)$$

or $$\{m_B\} = [d_B]\{\chi_B\} \qquad (3.7)$$

in which d_{11} and d_{22} = Ei_1 and Ei_2 respectively;

d_{31} and d_{32} = Gj_1 and Gj_2 respectively;

d_{12} represents the coupling, through Poisson's effect, between the flexural behavior in the 1 and 2 directions;

and m_1, m_2 are the bending and m_{31}, m_{32} are the torsional moments in the beam axes per unit length of plate in each direction.

3.3.4 Plate Moment-Deformation Relationships in Rectangular Axes

For convenience, the rectangular axes Ox' and Oy' are selected as reference axes, and the plate moment deformation relationships for each of the three cases shown in Fig. 3.2 are transformed from the beam axes to these reference axes. If the analysis is to be carried out in the skew axes, Ox and Oy, a further transformation can then be made.

The plate moments in the rectangular axes are shown in Fig. 3.5.a. The relationship between the moments in the rectangular and beam axes can be written as:

$$\begin{Bmatrix} m_{x'} \\ m_{y'} \\ m_{x'y'} \\ m_{y'x'} \end{Bmatrix} = [t_1] \begin{Bmatrix} m_1 \\ m_2 \\ m_{31} \\ m_{32} \end{Bmatrix}_B \tag{3.8}$$

or

$$\{m_R\} = [t_1]\ \{m_B\} \tag{3.9}$$

in which: $\{m_R\}$ are the moments in the rectangular axes Ox', Oy' ;

$\{m_B\}$ are the moments in the beam axes;

and $[t_1]$ is a transformation matrix, which is as follows for each of the cases shown in Fig. 3.2.

(a) For the case in Fig. 3.2.a

$$[t_1] = \begin{bmatrix} 1 & 0 & 0 & 0 \\ 0 & 1 & \frac{s}{c} & -\frac{s}{c} \\ 0 & 0 & 1 & 0 \\ -\frac{s}{c} & \frac{s}{c} & 0 & 1 \end{bmatrix} \tag{3.10}$$

in which $s = \sin \beta$;

$c = \cos \beta$;

and β = external angle of skew.

(b) For the case in Fig. 3.2.b.

$$[t_1] = \begin{bmatrix} 1 & 0 & 0 & 0 \\ 0 & 1 & 0 & 0 \\ 0 & 0 & 1 & 0 \\ 0 & 0 & 0 & 1 \end{bmatrix} \tag{3.11}$$

(c) For the case in Fig. 3.2.c

$$[t_1] = \begin{bmatrix} 1 & 0 & \frac{s}{c} & -\frac{s}{c} \\ 0 & 1 & 0 & 0 \\ -\frac{s}{c} & \frac{s}{c} & 1 & 0 \\ 0 & 0 & 0 & 1 \end{bmatrix} \tag{3.12}$$

The moment-deformation relationships in the rectangular axes can now be written as:

$$\begin{Bmatrix} m_{x'} \\ m_{y'} \\ m_{x'y'} \\ m_{y'x'} \end{Bmatrix} = [d_R] \begin{Bmatrix} \chi_{x'} \\ \chi_{y'} \\ \chi_{x'y'} \\ \chi_{y'x'} \end{Bmatrix} \tag{3.13}$$

or

$$\{m_R\} = [d_R] \{\chi_R\} \tag{3.14}$$

In which, for each case:

$$[d_R] = [t_1] [d_B] [t_1]^T \tag{3.15}$$

where $[d_B]$ is given by Eq. 3.6.

Because the equivalent plate theory implicity assumes that the plate is a solid slab with anisotropic material properties, it now follows that the torsional moments, $m_{x'y'}$ and $m_{y'x'}$ are equal in magnitude but opposite in sign. The rates of twist, $\chi_{x'y'}$ and $\chi_{y'x'}$, are also equal in magnitude, each being numerically equal to $\partial^2 w/\partial x' \partial y'$. Hence, the 4 x 4 matrix, $[d_R]$, in Eq. 3.14 can be reduced to a 3 x 3 matrix, $[\bar{d}_R]$, in order to get an expression of the type generally used in plate theory, namely:

$$\begin{Bmatrix} m_{x'} \\ m_{y'} \\ m_{x'y'} \end{Bmatrix} = [\bar{d}_R] \begin{Bmatrix} \chi_{x'} \\ \chi_{y'} \\ 2\chi_{x'y'} \end{Bmatrix} \tag{3.16}$$

in which $[\bar{d}_R]$ is obtained from $[d_R]$ by the transformation

$$[\bar{d}_R] = [t_2]\,[d_R]\,[t_2]^T \tag{3.17}$$

and

$$[t_2] = \begin{bmatrix} 1 & 0 & 0 & 0 \\ 0 & 1 & 0 & 0 \\ 0 & 0 & \frac{1}{2} & -\frac{1}{2} \end{bmatrix} \tag{3.18}$$

3.3.5 Plate Moment-Deformation Relationships in Skew Axes

As noted in section 3.3.2, it is convenient, for the analysis of plates on skew supports, to work in the skew coordinate system. An element of plate in this system, and the plate moments acting on it, are shown in Fig. 3.5.b. Note that these plate moments are not the same as the moment in the beam axes, and that the moment components on any face are not orthogonal. In this system the "torsional" moments, m_{xy} and m_{yx} are also numerically identical, which allows the following expression to be written:

$$\begin{Bmatrix} m_x \\ m_y \\ m_{xy} \end{Bmatrix}_S = [\bar{d}_S] \begin{Bmatrix} \chi_x \\ \chi_y \\ 2\chi_{xy} \end{Bmatrix}_S \tag{3.19}$$

or

$$\{\bar{m}_S\} = [\bar{d}_S]\,\{\bar{\chi}_S\} \tag{3.20}$$

in which

$$[\bar{d}_S] = \cos\beta\,[t_3]\,[\bar{d}_R]\,[t_3]^T \tag{3.21}$$

and

$$[t_3] = \begin{bmatrix} 1 & \frac{s^2}{c^2} & \frac{2s}{c} \\ 0 & \frac{1}{c^2} & 0 \\ 0 & \frac{s}{c^2} & \frac{1}{c} \end{bmatrix} \tag{3.22}$$

3.3.6 Output Coordinate System

Regardless of whether the rectangular or skew coordinate system is used in the analysis, the final moments should be computed as bending and torsional moments in the beam coordinate system. Transformations from

the moments $\{\bar{m}_R\}$ or $\{\bar{m}_S\}$, in rectangular or skew axes respectively, to the moments $\{m_B\}$, in beam axes, are therefore needed. The transformations are as follows:

(a) From the skew system, $\{\bar{m}_S\}$, to the reduced rectangular system, $\{\bar{m}_R\}$:

$$\{\bar{m}_R\} = [t_4] \{\bar{m}_S\} \tag{3.23}$$

in which

$$[t_4] = \begin{bmatrix} \frac{1}{c} & \frac{s^2}{c} & -\frac{2s}{c} \\ 0 & c & 0 \\ 0 & -s & 1 \end{bmatrix} \tag{3.24}$$

(b) From the rectangular system, $\{\bar{m}_R\}$, to the beam system of Fig. 3.2.a:

$$\{m_B\} = [t_5] \{\bar{m}_R\} \tag{3.25}$$

in which

$$[t_5] = \begin{bmatrix} 1 & 0 & 0 \\ s^2 & c^2 & -2sc \\ 0 & 0 & 1 \\ sc & -sc & (c^2-s^2) \end{bmatrix} \tag{3.26}$$

(c) From the skew system, $\{\bar{m}_s\}$, to the beam system of Fig. 3.2.a:

$$\{m_B\} = [t_5] [t_4] \{\bar{m}_S\} \tag{3.27}$$

(d) From the rectangular system, $\{\bar{m}_R\}$, to the beam system of Fig. 3.2.b:

$$\{m_B\} = [t_6] \{\bar{m}_R\} \tag{3.28}$$

in which

$$[t_6] = \begin{bmatrix} 1 & 0 & 0 \\ 0 & 1 & 0 \\ 0 & 0 & 1 \\ 0 & 0 & -1 \end{bmatrix} \tag{3.29}$$

(e) From the skew system, $\{\bar{m}_S\}$, to the beam system of Fig. 3.2.b:

$$\{m_B\} = [t_6] [t_4] \{\bar{m}_S\} \tag{3.30}$$

(f) From the rectangular system, $\{\bar{m}_R\}$, to the beam system of Fig. 3.2.c:

$$\{m_B\} = [t_7] \{\bar{m}_R\} \tag{3.31}$$

in which

$$[t_7] = \begin{bmatrix} c^2 & s^2 & -2sc \\ 0 & 1 & 0 \\ sc & -sc & (c^2-s^2) \\ 0 & 0 & 1 \end{bmatrix} \tag{3.32}$$

(g) From the skew system, $\{\bar{m}_S\}$, to the beam system of Fig. 3.2.c:

$$\{m_B\} = [t_7]\,[t_4]\,\{\bar{m}_S\} \tag{3.33}$$

The final beam moments in any case are obtained by integrating the plate moments over the widths which are tributary to the beams.

3.4 DIFFERENTIAL EQUATION

Although the differential equation is not required for the finite element method of analysis, it is of interest to note its form, as follows:

$$d_{11}\frac{\partial^4 w}{\partial x^4} - 4d_{13}\frac{\partial^4 w}{\partial x^3\,\partial y} + 2(d_{12} + 2d_{33})\frac{\partial^4 w}{\partial x^2 \partial y^2} - 4d_{23}\frac{\partial^4 w}{\partial x \partial y^3} + d_{22}\frac{\partial^4 w}{\partial y^4} = q(x,y) \tag{3.34}$$

For the rectangular coordinate system shown in Fig. 3.5.a, the constants d_{11}, d_{12} etc. are the terms of $[\bar{d}_R]$, as defined by Eq. 3.16: For the special case in which the beams are also at right angles, as in Fig. 3.2.b, $d_{13} = d_{23} = 0$, and hence the differential equation reduces to the well known orthotropic plate equation:

$$D_x\frac{\partial^4 w}{\partial x^4} + 2H\frac{\partial^4 w}{\partial x^2 \partial y^2} + D_y\frac{\partial^4 w}{\partial y^4} = q(x,y) \tag{3.35}$$

in which:

$$D_x = d_{11}\ ;$$

$$D_y = d_{22}\ ;$$

and

$$H = d_{12} + 2d_{33}\ ;$$

For the skew coordinate system shown in Fig. 3.5.b, the constants d_{11}, d_{12} etc. are coefficients of $[\bar{d}_S]$, as defined by Eq. 3.20.

Although the equivalent anisotropic plate is, by implication, a solid plate, the true structure is ribbed, and hence has a much lower torsional stiffness than a solid plate. Because they have begun with the differential equation, Eq. 3.35, a number of workers have introduced a modifying factory, α_T , to account for the reduced torsional stiffness. This factor is defined for an orthotropic plate as

$$\alpha_T = \frac{H}{\sqrt{D_x D_y}} \tag{3.36}$$

Early attempts at using Eqn. 3.35 required arbitrary estimates of α_T , ranging from 0.0 for torsionless slabs to 1.0 for solid isotropic slabs. Subsequently, Rowe et al [2,5], gave an explicit expression for α_T in terms of the bridge deck properties. If Eqs. 3.6 and 3.35 are substituted into Eq. 3.36, it can be shown that:

$$\alpha_T = \nu \sqrt{\frac{i_2}{i_1}} + \frac{j_1 + j_2}{4(1+\nu)\sqrt{i_1 i_2}} - \tag{3.37}$$

The equation given by Rowe is similar to this but assumes $\nu = 0$. It should be noted however, that the essential equations of the anisotropic plate are Eqns. 3.1 through 3.33, and that α_T needs to be introduced only if the differential equation method of solution is employed.

3.5 FINITE ELEMENT ANALYSIS

Details of a finite element technique for the analysis of skew isotropic plates have been presented in a previous report by Mehrain. The extension of the theory to include anisotropic plates is straightforward, requiring simply that the moment-deformation relationship for the anistropic plate, Eq. 3.19, be used in place of Mehrain's relationship for the isotropic plate. A major advantage of the finite element method is that an extension such as this can be made comparatively easily.

A computer program has been developed to analyze skew anisotropic plates, and has been used for the studies presented in this report. The program is named FEASAP (Finite Element Analysis of Skew Anisotropic Plates), and possesses the following features:

1. Optional input of either
   (a) the plate inertias per unit length (i_1,i_2,j_1 and j_2 as defined in Eqns. 3.2, 3.3, and 3.4), together with the elastic constants (E and ν), or
   (b) the elastic moduli, Poisson's ratios, and thickness of the plate (E_1,E_2,ν_1,ν_2 and h).
2. Specification of either of the two beam systems shown in Fig. 3.2.a and 3.2.b.
3. Provision for discrete beams, imbedded in the plate.
4. Provision for single concentrated loads, patch loads and truck loads.
5. Ability to consider curved bridges over parallel supports by varying the angle of skew along the bridge.

6. Output of:
   a. displacements at all nodal points;
   b. reactions at the supported nodal points;
   c. moments per unit length at all nodal points and all element centers, which may be output in the skew, rectangular or beam coordinates;
   d. effective shear force distributions along the supported boundaries;
   and
   e. beam moments and shears if beams are present in the plate.

A listing of the program and detailed instructions for its use will be included in a future report. In the meantime, a copy of the program and a tentative set of instructions are available on request.

3.6 EQUILIBRIUM CHECK IN SKEW PLATES

In skewed plates , which are simply supported on two opposite edges, it is a requirement of equilibrium that the integral of the plate bending moments across any transverse section, must equal the attacking couple of the applied load acting at that section.

Fig. 3.6.a shows, in plan, a single span skew plate of span L, measured normal to the support lines. Under the action of a point load P acting at a distance a from one support, the attacking couple on any section, Z-Z, cut parallel to a support and at distance z from it, will be $P(L-a)z/L$. For a uniformly distributed load of total weight W, this same couple will be $Wz(1-z/L)/2$.

If the plate represents a bridge, this couple can be termed the "total bridge moment" at the particular section. If analyses are being carried out by the finite element method, this equilibrium requirement provides a useful means of checking the solution.

Fig. 3.6.b shows one half of the skew plate of Fig. 3.6.a. For the midspan cross section, C-C, the attacking couples are PL/4 and WL/8 for the point and distributed loads respectively. The integral of the computed bending stress resultants on section C-C must therefore equal these values. This check has been carried out for the structures considered in Chapter 4, and in all cases the agreement was excellent.

In a right-angled bridge, the moment M_{C-C} is also equal to the sum of the girder moments, and may be termed the "total bridge moment". In order to study the load distribution in skew bridges, it is convenient to define a corresponding "total bridge moment", but in this case the problem is rather more complex, as follows.

Fig. 3.6.c shows an element cut from a skew plate at some point along the section C-C. The bending and torsional stress resultants per unit length on C-C, and also on lines parallel to the axes Ox' and Oy', are shown. It follows from the relationships presented in this Chapter, that the girder bending moments are obtained by integrating the plate moment $m_{x'}$, over the tributary widths of the girders. Hence, the sum of the midspan girder moments in a skew bridge does not equal the moment M_{C-C}. Rather, the following equilibrium relationship can be written:

$$M_{C-C} = \int_{y'=0}^{b} m_{x'} \cos\beta \, dy'$$

$$+ \int_{y'=0}^{b} m_{y'} \sin\beta \tan\beta \, dy'$$

$$+ 2 \int_{y'=0}^{b} m_{x'y'} \sin\beta \, dy' \qquad (3.38)$$

If this equation is divided by $\cos\beta$, the result is

$$M_{C-C} \sec\beta = \int_{0}^{b} m_{x'} \, dy'$$

$$+ \int_{0}^{b} m_{y'} \tan^2\beta \, dy'$$

$$+ 2\int_{0}^{b} m_{x'y'} \tan\beta \, dy' \qquad (3.39)$$

The first term on the right hand side of Eq. 3.39 is the sum of the girder midspan moments, and the left hand side is the total bridge moment which would be present in a right bridge of span $L\sec\beta$ (the skew span) subjected to the same loading. The quantity $M_{C-C}\sec\beta$ is therefore conveniently regarded as the "total bridge moment" for a skew bridge. This definition has been used in Chapter 4 in studies of the load distribution in skew bridges. In a bridge which has negligible torsional stiffness and transverse bending stiffness, the last two terms on the right hand side of Eq. 3.39 will be negligible, and the sum of the girder moments will equal the total bridge moment. In other cases, however, this will not apply, as discussed in Chapter 4.

3.7 VERIFICATION OF FEASAP PROGRAM

To check the accuracy of the results available with the FEASAP program, an analysis has been carried out of a right-angled orthotropic plate previously studied by Clifton, Chang and Au [37]. These workers have analyzed this structure using an equivalent plate theory proposed by Giencke [10,11] and by a ribbed plate theory based on an eigth order differential equation. The structure has been described in detail in their paper. It consisted of a steel deck plate reinforced by two sets of orthogonal ribs. The panel was simply supported on four sides and loaded with a patch load at the center of the panel. The principal, results are shown in Table 3.1.

TABLE 3.1

Check on FEASAP Program

Method	Deflection Under Load	x-Stresses		y-Stresses	
		Top Plate Fiber	Bottom Rib Fiber	Top Plate Fiber	Bottom Rib Fiber
Giencke	.00426	-220	937	-280	999
Clifton et al	.00451	-163	1059	-230	1092
FEASAP	.00455	-177	1148	-242	1056

The FEASAP program is seen to be within 10% of the more refined method of Clifton et al, and significantly better than the method of Giencke for this structure.

CHAPTER 4

BEHAVIOR OF SINGLE SPAN SKEW BRIDGE DECKS

4.1 PARAMETER SELECTION

Although the behavior of right bridge systems has been thoroughly studied, there are certain unusual features of skew systems which are not well understood. In this chapter the results of a parameter study of skew bridge decks are presented. The aim is to emphasize the important characteristics of skew systems and to show how they differ from right systems.

The parameters which characterize a bridge are large in number, including such primary variables as span, width, angle of skew and loading, and also such variables as girder and diaphragm type and spacing, degree of composite action, etc. For the purposes of the parameter study described herein, the parameters of major importance were assumed to be the angle of skew, the ratio of girder to diaphragm stiffnesses (degree of anisotropy) and the type of loading. Accordingly, only these parameters were varied.

The analyses were carried out using the program FEASAP, described in Chapter 3. The parameters used in the analyses were selected following an examination of several bridges constructed in California in recent years. It was found that the essential parameters did not vary widely, even between bridges with quite different types of construction. Hence, a "typical" bridge, which gave "typical" values of the essential parameters, was selected. This bridge was a four lane single span bridge of 52'-6" span, with seven precast prestressed girders at 7'-6" centers acting compositely with an in-situ deck slab, as shown in Figs. 4.1 and 4.2.

The external angle of skew of this bridge, β, was assigned values of 0°, 20°, and 40°. As this angle was varied, the right (short) span and width were both held constant. That is, the roadway widths at both the elevated and grade levels were fixed.

The degree of anisotropy, $\delta_i = i_1/i_2$, was assigned values of 1, 12 and 163, by holding i_1 (a measure of the girder stiffness) constant and varying i_2 (a measure of the diaphragm and slab stiffness). The value $\delta_i = 1$ represents an unusual case with very closely spaced diaphragms, the value $\delta_i = 12$ represents a typical case with one or two diaphragms in the span, and the value $\delta_i = 163$ represents a case with no diaphragms at all. Two additional cases were also studied. The first was a solid isotropic slab, which also has $\delta_i = 1$ but a much larger torsional stiffness than the ribbed slab with $\delta_i = 1$. This case was included to demonstrate the differences between solid and ribbed slabs and is designated δ_i = SLAB. The second case was a plate with $\delta_i = 163$, but with a single concentrated beam (diaphragm) imbedded in the plate at midspan, and assigned a stiffness giving an overall δ_i of 12. This case was included to study errors which are introduced when widely spaced diaphragms are "smeared", and is designated as $\delta_i = 163 + D$. In all cases the diaphragms were assumed to be composite with the deck slab, to have full continuity over the girders, and to be parallel to the supports. A summary of the anisotropic parameters for bridges of the same general type as that investigated is shown in Table 4.1. This table indicates how the δ_i values were selected.

In the equivalent plate analyses an elastic modulus of 5000.0 k/in^2 and a Poisson's ratio of 0.15 were assumed for the bridge material,

TABLE 4.1 SUMMARY OF ANISTROPIC PARAMETERS

Number of Transverse Diaphragms (excluding end diaphragms)	i_1	i_2	δ_i	j_1	j_2	δ_j	α_T	DESIGNATION
0	2993.5	18.4	162.6	118.7	36.0	3.3	.15503	δ_i = 163
1	2993.5	248.2	12.1	118.7	48.4	2.5	.08526	δ_i = 12
2	2993.5	349.4	8.6	118.7	54.6	2.2	.08797	
Large	2993.5	2993.5	1.0	118.7	231.1	0.51	.01724	δ_i = 1
Solid Slab	2993.5	2993.5	1.0	5852.3	5852.3	1.0	1.0	δ_i = SLAB

except that for selected cases the effect of reducing Poisson's ratio to zero was studied. This effect was found to be negligible except for certain analyses with $\delta_i = 1$, in which case unusual behavior near the edge of the plate was observed for $\nu = 0.15$. Accordingly, the case $\delta_i = 1$ was analyzed with Poisson's ratio equal to zero, and it is recommended that this value be generally used for the analysis of concrete bridge decks by the equivalent plate method.

Three loading cases were examined, namely a point load of 18 k at midspan on the bridge centerline, a point load of 18 k at midspan over the edge girder, and a uniform load of 64 lb. per sq. ft. over the whole bridge.

4.2 FINITE ELEMENT SUBDIVISION

The finite element subdivision used in the analysis is shown in Fig. 4.3. The mesh is basically 8 elements by 9 elements (width by length), with longitudinal divisions corresponding to the seven longitudinal girders. However, the mesh was refined both longitudinally and transversely under the loads, in order to determine the peak moments more accurately. The mesh was also refined at the edges, in order to provide small elements near the obtuse corners of the skew plate, at which points thin plate theory may predict high bending moment intensities. The final mesh was therefore 14 elements by 14 elements, giving a total of 196 elements and 225 nodal points.

The concentrated loads were applied at nodes 113 and 108, as shown in Fig. 4.3. The uniform load was applied at the nodal points according to the tributary area of each point.

4.3 PRESENTATION OF RESULTS

As noted in Chapter 3, care must be taken when interpreting the bending moment results of an equivalent skew plate analysis. In the discussion of the analyses considered in this chapter, the moment $m_{x'}$ (see Fig. 3.5a) has been chosen as the most important quantity, because the girder bending moments for design are obtained by integrating $m_{x'}$ over the girder widths.

The variations of $m_{x'}$ at a midspan cross section of the plate for varying angles of skew, degrees of anisotropy and load positions are first studied. The influence of the different parameters on these variations are discussed. The values of girder moment, obtained by integration of the $m_{x'}$ variation, are also examined and compared with the "total bridge moment." The sums of all girder moments are similarly determined and compared with the total bridge moment. The deflections at the midspan cross section are also studied.

Following the discussion of effects at midspan, the behavior of the complete plate, and in particular the behavior at the obtuse corner, is examined for the cases with 40° skew. The characteristics of plates with different anisotropic ratios are compared, and the significance of the moments in the obtuse corner is discussed.

4.4 BEHAVIOR AT MIDSPAN

4.4.1 General

In the discussion of effects at midspan, the three cases δ_i = 1, 12, and 163 permit the influence of a progressive change in degree of anisotropy to be investigated. Comparisons between the cases δ_i = 12

and 163 + D then demonstrate the effects of smearing the diaphragms. In each case, the effects of varying β from 0° to 20° and to 40° show how the behavior is influenced by the angle of skew, and each of the different loading conditions emphasizes a different aspect of the structural behavior.

4.4.2 Influence of Degree of Anisotropy on Load Distribution by the Deck

For point loads at both the centerline of the bridge (Figs. 4.4 through 4.6) and near the edge (Figs. 4.7 through 4.9) it can be seen that as δ_i varies from 1 to 12 to 163, the moment and deflection variations all become more sharply peaked. This is an obvious result, and simply reflects the decreasing ability of the plate to distribute loads transversely as δ_i increases. The same effect is seen if the m_x, values are integrated over the width of the loaded girders to obtain the girders bending moments, as shown in the following table for the case of zero skew.

TABLE 4.2
BENDING MOMENT IN LOADED GIRDER (k.in.)
POINT LOAD. $\beta = 0°$.

	Load at centerline	Load at edge
$\delta_i = 1$	751	1541
$\delta_i = 12$	1125	1909
$\delta_i = 163$	1584	2185

It can be seen that the girder moments are larger when the load is applied near the edge of the bridge, obviously because the ability of the deck to distribute the load is reduced by the presence of the free

edge. It can also be seen that the bending moment in the loaded girder as the load moves from the centerline to the edge increases more for δ_i = 1 than for δ_i = 163. This is because in the case with δ_i = 163 the ability of the deck to distribute load transversely is already small, and is proportionately less strongly affected by the free edge.

4.4.3 Effect of Torsional Stiffness on Peak Moment and Deflection Values Under Center Load

With a point load at the bridge centerline and $\beta = 0°$ (Fig. 4.4), the difference between the peak values of m_x, for the cases δ_i = 1 and δ_i = SLAB is rather small. The difference reflects the greater ability of the solid slab to distribute load transversely. The deflections, w, under the load are also fairly close. However, as the angle of skew increases to 20° (Fig. 4.5) and 40° (Fig. 4.6), the differences in both m_x, and w increase significantly. The moment changes are summarized in the following table.

TABLE 4.3 PLATE MOMENT UNDER CENTER POINT LOAD FOR VARYING ANGLE OF SKEW

Moment in k. in./in.

	$\beta = 0°$	$\beta = 20°$	$\beta = 40°$
δ_i = 1	10.4	10.0	8.4
δ_i = SLAB	8.9	8.3	6.5
% difference	14.4	17.0	22.6

The reason for the difference is that the solid slab, having equal flexural stiffnesses in all directions, carries the load to the supports by the shortest possible route, namely a path normal to the supports.

On the other hand, the ribbed plate does not have equal flexural stiffnesses in all directions, but is very flexible under the action of diagonally applied bending. This is because diagonally applied bending is largely carried by torsion in the ribs, and their torsional stiffnesses are small. As a result, the ribbed plate can not readily span normal to the supports, and must essentially span in the skew direction, along the ribs.

This fact can be emphasized if the principal moments in the plate are examined, rather than the moments $m_{x'}$. The following table shows both the principal bending moments, m_p, and the moments $m_{x'}$ under the load for a plate with 40° skew. The angle from the x axis to the p axis is also shown.

TABLE 4.4 MOMENTS UNDER CENTER POINT LOAD IN SKEW PLATE

Moment in k. in./in.; $\beta = 40°$

	$\delta_i = 1$	δ_i = SLAB
Moment $m_{x'}$	8.5	6.5
Moment m_p	8.5	8.3
Angle	9.3°	49.6°

It can be seen that for the ribbed plate the principal moment is only 10° away from the rib direction, indicating that the load is being carried essentially in this direction. It may be noted that for the higher values of δ_i, this angle was less than 1°. For the solid slab, however, the principal moment direction is nearly normal to the supports, indicating that the slab is spanning in this direction. The angle of

49.6° actually indicates a direction of span which lies between the x axis and the diagonal between the obtuse corners. It appears, therefore, that there is also a tendency to span between the corners.

The deflections under the load reflect similar behavior, as summarized in the following table.

TABLE 4.5 DEFLECTION UNDER CENTER LOAD FOR VARYING ANGLE OF SKEW

Deflections in inches

	δ_i = SLAB	δ_i = 1
$\beta = 0°$	.0111	.0129
$\beta = 20°$	.0109	.0139
$\beta = 40°$	.0104	.0179

The deflections in the solid slab actually decrease slightly, presumably because of the stiffening effects originating in the obtuse corners. The deflections in the ribbed plate, however, increase as the skew span increases.

The manner in which the load travels to the supports is of interest to the designer, especially if solid slab bridges are being designed. It would obviously be incorrect to reinforce a solid concrete slab for the bending moments $m_{x'}$, because the larger principal moments would cause the concrete to crack, and hence would invalidate the solid slab analysis. Thus, unless the influence of cracking on the distribution of slab moments is taken into account, the slab should be reinforced to

resist the principal moments. In a rectangular slab bridge the principal moment directions are known, and essentially do not change if the slab cracks. In a skew slab, however, the principal moment directions are more difficult to determine, and the influence of cracking on both the directions and magnitudes of the moments may be considerable.

4.4.4 Effect of Torsional Stiffness On Peak Moment and Deflection Values Under Edge Load

When a point load is applied near the edge of the plate, the differences in both moments and deflections for $\delta_i = 1$ and $\delta_i = SLAB$ are large for all angles of skew (see Figs. 4.7 through 4.9). The following table can be compared with Table 4.3.

TABLE 4.6 PLATE MOMENT UNDER EDGE POINT LOAD FOR VARYING ANGLE OF SKEW

Moment in k. in./in.

	$\beta = 0°$	$\beta = 20°$	$\beta = 40°$
$\delta_i = 1$	19.3	18.1	16.4
$\delta_i = SLAB$	12.6	12.1	11.0
% difference	34.7	33.1	32.9

It can be seen that the difference is larger than for the center load case, but that it remains essentially constant for all angles of skew. The moments in the solid slab cases are substantially smaller because the load, being applied eccentrically on the bridge, applies a torsional moment to the bridge as a whole. Because the solid slab is much stiffer in torsion it deflects less, and also carries less load by bending and more by pure torsion. Note that in practice, this behavior assumes that the torsional

strength of the solid slab is adequate. If it is not, then the analysis is not correct.

The differences between the behavior in the ribbed and solid slab cases remain essentially constant because the solid slab can not now span normal to the supports, but must span essentially parallel to the free edge. This action can be seen from the following table, which can be compared with Table 4.4, and which shows that the principal moment direction in the solid slab case is fairly closely parallel to the plate edge.

TABLE 4.7 MOMENTS UNDER EDGE POINT LOAD IN SKEW PLATE

Moments in k. in./in.; $\beta = 40°$

	$\delta_i = 1$	δ_i = SLAB
Moment $m_{x'}$	16.7	11.0
Moment m_p	16.7	11.7
Angle ~	0.3°	17.6°

4.4.5 Effect of Angle of Skew and Degree of Anisotropy on Peak Plate and Girder Moments Under Point Loads

For a central point load on plates with varying angles of skew and degrees of anisotropy, the peak $m_{x'}$ values can be obtained from Figs. 4.4 through 4.6. These values are summarized in the following table.

TABLE 4.8 PLATE MOMENT UNDER CENTER POINT LOAD FOR VARYING SKEW AND DEGREE OF ANISOTROPY

Moments, $m_{x'}$ in k. in./in.

	$\beta = 0°$	$\beta = 20°$	$\beta = 40°$
$\delta_i = 1$	10.4	10.0	8.4
$\delta_i = 12$	19.1	18.5	16.7
$\delta_i = 163$	29.9	30.0	30.1

The unusual result here is that the peak moments for $\delta_i = 1$ and 12 decrease as the angle of skew increases, and that even the moments for $\delta_i = 163$ barely increase. Because the ribbed plates span essentially along the x direction, an increase in moment would be expected as the skew span increases, especially for the $\delta_i = 12$ and 163 cases. It must be remembered, however, that the plate moments are obtained by finite element theory, and that the peak values are merely approximations to the values predicted by "exact" thin plate theory under a point load. The values are not completely unreliable, because similar meshes have been used for all the analyses, and hence comparative studies should still have some meaning. For the bridge engineer, however, the quantity which is of much greater importance is the bending moment in the loaded girder, which is obtained by integrating the $m_{x'}$ distribution. These girder moments are shown in the following table. In each case both the girder moment and its percentage of the "total bridge moment" are given.

TABLE 4.9 MOMENT IN LOADED GIRDER UNDER CENTER POINT LOAD FOR VARYING SKEW AND DEGREE OF ANISOTROPY

Moments in k. in.

	$\beta = 0°$	$\beta = 20°$	$\beta = 40°$
$\delta_i = 1$	751 (26.5%)	748 (24.8%)	665 (18.0%)
$\delta_i = 12$	1125 (39.7%)	1112 (36.9%)	1084 (29.3%)
$\delta_i = 163$	1584 (55.9%)	1607 (53.3%)	1673 (45.2%)

It can be seen that for both $\delta_i = 1$ and $\delta_i = 12$ bending moments decrease as the angle of skew increases, although at a slower rate than the peak m_x, values, and that the girder moment for $\delta_i = 163$ increases modestly as the angle of skew increases. More importantly, the percentage of the total bridge moment carried by the loaded girder decreases consistently as the angle of skew increases, with percentage decreasing less rapidly as δ_i = increases. It has already been shown in Section 4.4.4 that these plates appear to span in the skew direction, and yet there is undoubtedly some effect present in the skew plates which make them different from the plates with zero skew. This effect is in two parts, as follows.

First, a skew plate appears to posses an inherently greater ability to distribute loads transversely than an equivalent plate without skew. In Figs. 4.4 through 4.6 this can be seen as a tendency for flattening of the m_x, distributions as the angle of skew increases. Second, it must be remembered that the m_x, moments are not the only moments which resist the "total bridge moment", but the moments m_y, and $m_{x'y'}$ are also effective

as noted in Chapter 3. The effects of $m_{y'}$ and $m_{x'y'}$ can be seen if the $m_{x'}$ distribution is integrated over the full width of the bridge (that is, if the moments in all of the girders are added), and the resulting moment is compared with the total bridge moment. The difference between the two will represent the effects of $m_{y'}$ and $m_{x'y'}$. These values are shown in the following table, in which the total integrals of $m_{x'}$ are given and are expressed as percentages of the total bridge moment.

TABLE 4.10 SUM OF MOMENTS IN
ALL GIRDERS FOR CENTER POINT LOAD.
VARYING SKEW AND DEGREE OF ANISOTROPY.
Moments in k. in.

	$\beta = 0°$	$\beta = 20°$	$\beta = 40°$
$\delta_i = 1$	2835 (100.0%)	2897 (96.0%)	2871 (77.6%)
$\delta_i = 12$	2835 (100.0%)	2962 (98.2%)	3342 (90.3%)
$\delta_i = 163$	2835 (100.0%)	2999 (99.4%)	3575 (96.6%)
Total Bridge Moment	2835	3017	3701

It can be seen that as the angle of skew increases, the percentage of the total bridge moment carried by the girder moments decreases. It follows that the girder moments in a skew bridge deck under a central point load will be overestimated if the skew deck is replaced by a right deck with a span equal to the skew span. Similar conclusions are drawn subsequently for edge loads and uniform loads. It is possible that some reduced equivalent span can be determined, which is sufficiently accurate for design purposes when abusolute maximum effects are considered. However,

procedures for selecting the equivalent span remain to be determined.

From Table 4.10 it can be seen that the difference between the girder moments and the total bridge moment is decreasing for increasing values of δ_i. It is interesting to note that for $\delta_i = 1$ the girder moments reach a maximum absolute value between $\beta = 20°$ and $40°$, and thereafter appear to decrease.

Similar conclusions follow for the effects due to a point load near the edge of the bridge. The following tables correspond to Tables 4.8, 4.9 and 4.10, but are for this different loading case.

TABLE 4.11 PLATE MOMENT UNDER EDGE LOAD FOR VARYING SKEW AND DEGREE OF ANISOTROPY

Moments, $m_{x'}$, in k. in./in.

	$\beta = 0°$	$\beta = 20°$	$\beta = 40°$
$\delta_i = 1$	19.3	18.1	16.4
$\delta_i = 12$	27.6	27.6	27.2
$\delta_i = 163$	36.5	37.3	39.6

TABLE 4.12 MOMENT IN LOADED GIRDER UNDER EDGE POINT LOAD FOR VARYING SKEW AND DEGREE OF ANISOTROPY

Moments in k. in.

	$\beta = 0°$	$\beta = 20°$	$\beta = 40°$
$\delta_i = 1$	1541 (54.4%)	1461 (48.4%)	1372 (37.1%)
$\delta_i = 12$	1909 (67.3%)	1936 (64.2%)	2003 (54.1%)
$\delta_i = 163$	2185 (77.1%)	2264 (75.1%)	2519 (68.1%)

TABLE 4.13 SUM OF MOMENTS IN ALL GIRDERS
FOR EDGE POINT LOAD.
VARYING SKEW AND DEGREE OF ANISOTROPY.
Moments in k. in.

	$\beta = 0°$	$\beta = 20°$	$\beta = 40°$
$\delta_i = 1$	2835 (100.0%)	3102 (102.8%)	3617 (97.7%)
$\delta_i = 12$	2835 (100.0%)	3033 (100.5%)	3703 (100.0%)
$\delta_i = 163$	2835 (100.0%)	3387 (112.3%)	3629 (98.1%)
Total Bridge Moment	2835	3017	3701

Again, the values in Table 4.11 are not particularly meaningful to the bridge designer. In Table 4.12 it can be seen that the percentages of the total bridge moment carried by the loaded girder decrease as the angle of skew increases, but that the rate of decrease is somewhat slower than for the central point load. Surprisingly, Table 4.13 shows that the sum of the girder moments may actually exceed the total bridge moment. From this it follows that the reduction in the percentages in Table 4.11 must result from an improved ability of the skew bridge to distribute load transversely. This can be seen in a general flattening of the curves from Fig. 4.7 through Fig. 4.9.

4.4.6 Effects of Uniformly Distributed Load

Fig. 4.10 shows that for a plate without skew both the plate moments and the deflections are unaffected by the degree of anisotropy, and are constant over the bridge width with the exception of small pertubations

near the free edges. However, as the angle of skew increases, substantial differences in behavior develop, as shown in Figs. 4.11 and 4.12.

The most noticeable difference is that the solid slab becomes much stiffer than the ribbed slabs, and that $m_{x'}$ in the solid slab is much less than $m_{x'}$ in the ribbed slabs. It should be remembered, however, that $m_{x'}$ in the solid slab is substantially less than the maximum principal moment. A tendency for the solid slab to deflect more at the edges than near its center is also seen. This is because the center portion of the slab can span directly between supports, whereas the edge portions must span essentially along the edges, and are therefore less stiff.

This tendency for both moments and deflections to be smaller in the center than near the edge is most marked for the $\delta_i = 1$ case, indicating that it is more sensitive to the presence of the free edge than the solid slab. The tendency is much less for $\delta_i = 12$ and 163 because these cases span essentially in the x direction in any case, whether the load is near the center or the edge of the bridge.

A comparsion of the sums of the girders moments is presented below, for comparison with Tables 4.10 and 4.13.

TABLE 4.14
SUM OF MOMENTS IN ALL GIRDERS FOR UNIFORM LOAD
VARYING SKEW AND DEGREE OF ANISOTROPY
Moments in k. in.

	$\beta = 0°$	$\beta = 20°$	$\beta = 40°$
$\delta_i = 1$	13890 (100.0%)	15620 (99.2%)	21030 (88.9%)
$\delta_i = 12$	13890 (100.0%)	15610 (99.2%)	22450 (94.9%)
$\delta_i = 163$	13890 (100.0%)	15650 (99.5%)	22980 (97.1%)
Total Bridge Moment	13890	15730	23670

It can be seen that the sum of the girder moments is still significantly below the total bridge moment, but that the differences are smaller than for the point load cases.

4.4.7 Effect of Smearing Widely Spaced Diaphragms

The case δ_i = 12 was selected to represent a bridge with one intermediate diaphragm, at midspan of the bridge. It might, however, also represent a bridge built, for some reason, with a larger number of small transverse ribs. In the case where the diaphragms are closely spaced, the results obtained from an equivalent anisotropic plate analysis should be of ample accuracy for use in design. However, if the diaphragms are widely spaced, "smearing" their properties may introduce considerable error. Because a bridge with a single midspan diaphragm is a case where error may occur, the case δ_i = 163 + D has been investigated. The moment and deflection curves for this case are shown in Figs. 4.4 through 4.12. The obvious observation is that there is a marked difference between the cases δ_i = 12 and δ_i = 163 + D.

For the central point load, (Figs. 4.4 through 4.6) the deflections in the two cases are closely similar for $\beta = 0°$, with the δ_i = 12 case being slightly stiffer. However, as the angle of skew increases the difference in deflection becomes very marked. The same difference also develops under the action of the edge point load (Figs. 4.7 through 4.9).

For the central point load, the peak plate moments are consistently larger for the δ_i = 12 case, but because of the considerable differences in the distributions of the plate moments in the two cases, a comparison must be made on the basis of girder moments . The girder moments and the sums of the girder moments are given in the following two tables.

TABLE 4.15 MOMENT IN LOADED GIRDER UNDER CENTER POINT LOAD FOR VARYING ANGLE OF SKEW

Moments in k. ins.

	$\beta = 0°$	$\beta = 20°$	$\beta = 40°$
$\delta_i = 12$	1125 (39.7%)	1112 (36.9%)	1084 (29.3%)
$\delta_i = 163 + D$	892 (31.5%)	941 (31.2%)	1107 (29.9%)

TABLE 4.16 SUM OF MOMENTS IN ALL GIRDERS FOR CENTER POINT LOAD. VARYING ANGLE OF SKEW

Moments in k. ins.

	$\beta = 0°$	$\beta = 20°$	$\beta = 40°$
$\delta_i = 12$	2835 (100.0%)	2962 (98.2%)	3342 (90.3%)
$\delta_i = 163 + D$	2835 (100.0%)	3004 (99.6%)	3606 (97.4%)
Total Bridge Moment	2835	3017	3701

These tables immediately demonstrate the danger of smearing the diaphragms. In Table 4.15, whereas the girder moment decreases in value with increasing skew for $\delta_i = 12$, it increases for $\delta_i = 163 + D$. The percentage of the total bridge moment in the case $\delta_i = 163 + D$ remains essentially constant as the skew increases, whereas the corresponding percentage for $\delta_i = 12$ drops considerably. For zero skew the loaded girder in the case $\delta_i = 163 + D$ carries less moment than that in the case $\delta_i = 12$, but for $\beta = 40°$ the situation is reversed. In Table 4.16, the percentage of the total bridge moment balanced by the girder moments is consistently higher for $\delta_i = 163 + D$ than for $\delta_i = 12$. It is obvious, therefore,

that for a midspan load, applied directly above the diaphragm, the theoretical results assuming smeared and discrete diaphragms are inconsistent with each other. Differences for other load positions (for example, at quarter span) can be expected. There is not doubt that the δ_i = 163 + D analysis is more accurate for an actual bridge, and hence it can be concluded that widely spaced diaphragms should not be smeared in an analysis.

Tables of moment in the loaded girder and of the sum of all girder moments for a point load near the edge are given below. Similar conclusions follow.

TABLE 4.17 MOMENT IN LOADED GIRDER UNDER EDGE POINT LOAD FOR VARYING ANGLE OR SKEW
Moments in k. ins.

	β = 0°	β = 20°	β = 40°
δ_i = 12	1909 (67.3%)	1936 (64.2%)	2003 (54.1%)
δ_i = 163 + D	1831 (64.6%)	1930 (64.0%)	2265 (61.2%)

TABLE 4.18 SUM OF MOMENTS IN ALL GIRDERS UNDER EDGE POINT LOAD VARYING ANGLE OF SKEW
Moments in k. ins.

	β = 0°	β = 20°	β = 40°
δ_i = 12	2835 (100.0%)	3033 (100.5%)	3703 (100.0%)
δ_i = 163 + D	2835 (100.0%)	3012 (99.8%)	3669 (99.1%)
Total Bridge Moment	2835	3017	3701

The sums of all girder moments are given for the uniform load case in the following table.

TABLE 4.19 SUM OF MOMENTS IN ALL GIRDERS FOR UNIFORM LOAD. VARYING ANGLE OF SKEW. Moments in k. ins.

	$\beta = 0°$	$\beta = 20°$	$\beta = 40°$
$\delta_i = 12$	13890 (100.0%)	15610 (99.2%)	22450 (94.9%)
$\delta_i = 163 + D$	13890 (100.0%)	15680 (99.7%)	23240 (98.2%)
Total Bridge Moment	13890	15730	23670

A conclusion which now be drawn from Tables 4.16, 4.18 and 4.19 is that virtually all of the total bridge moment is resisted by the girder moment in each case, and hence it should be possible to reduce the skew bridge to a right bridge with a span equal to the skew span. While this may be true, it should be noted that the three loads considered were all applied symmetrically with respect to the diaphragm, and are therefore special cases. Analyses for a wider range of load positions are needed before definite conclusions can be drawn.

4.5 BEHAVIOR OF COMPLETE DECK

4.5.1 General

Figs. 4.13 through 4.26 show pictorial views of the surfaces for moment m_x, over the whole plate for plates with an angle of skew of 40°, for δ_i = SLAB, 1, 12, 163 + D and 163 respectively, and for each of the three load

cases previously considered. The aim of these diagrams is to show the behavior of the complete structure, rather than just the behavior at the midspan cross section, and in particular to show the moments developed in the obtuse corners of the plate.

The diagrams for the central point load are shown in Figs. 4.13 through 4.17. It can be seen that for all degrees of anisotropy the moments developed in the obtuse corners are not significant for this loading. In each of the cases δ_i = 12, 163 + D, and 163, a tendency for the plates to span normal to the supports can be seen at the quarter span sections, where the maximum moments are not at the bridge centerline, but are displaced towards the obtuse corners. In the cases δ_i = SLAB and 1, the tendency is for the maximum quarter span moments to be right at the edge of the plate. This behavior is difficult to explain, but is presumably associated with the torsional properties of the structure and effects originating at the free edge. The effect is probably not important in the design of actual bridges.

The diagrams for the point load near the edge of the plate are shown in Figs. 4.18 through 4.22. In all cases, it can be seen that the plate must span parallel to the edge towards the obtuse corner, but may tend to span normal to the support towards the acute corner. Significant negative moments at the obtuse corners are also developed for the cases δ_i = SLAB, 1 and 12, but the ratio of corner moment to midspan moment decreases as δ_i increases, and the corner moments are insignificant for the cases δ_i = 163 + D and 163.

Figs. 4.23 through 4.26 show the moment surfaces for the case of uniform load. The behavior of the plate under this load has already been

discussed and nothing more need be added except to note that the corner moments are again significant. Also, the moment surface for the case of δ_i = 163 + D has been omitted since it closely resembles the δ_i = 163 surface - the addition of the midspan diaphragm has little effect on the moment distribution in the plate for this type of loading.

4.5.2 Corner Moments

The corner moments originate with the boundary conditions specified along the supported edges. Where the edge is constrained to remain perfectly straight, as in the analyses carried out, the corner constraint leads to the development of negative moments in plates which have either significant torsional stiffness or significant transverse bending stiffness. The large moments occur only in the obtuse corner because such plates are able to span normal to the support at the acute corner and in all other parts of the plate. In plates which possess both low torsional stiffness and low transverse flexural stiffness, the distortions introduced at the supports do not lead to large moments, although such plates can not span normal to the supports to any great extent.

Because the analyses reported in this chapter have been carried out for idealized thin plate structures, results for localized effects such as the corner moments should be interpreted cautiously for application in bridge design. In an actual bridge the support is not constrained to remain perfectly straight, but rather consists of a diaphragm and a finite number of bearings. In the practical case, therefore, the constraint may be greatly reduced. Further, in the thin plate theory shearing deformations are ignored,

whereas if high moment gradients try to develop in a real situation, the resulting shearing deformations may not be negligible and the effective degree of constraint may be reduced. The local geometry of an actual bridge, consisting of a deck slab with discrete girders and diaphragms, is also quite different from an ideal solid slab, and the local behavior is likely to be greatly affected by these geometric details.

Accordingly, conclusions regarding the behavior in the obtuse corner can not be made from the results shown, and the problem must be investigated using better idealizations of the structure. Such investigations are being made using the ribbed plate finite element analysis procedure noted in Chapter 2, and will be described in detail in a future report. It is hoped to draw conclusions about the influence of the end diaphragm stiffness, the spacing of supports, and the thickness of the deck slab on the distribution of support reactions for skew bridges and on the development of negative girder moments at the support.

One important point can, however, be noted at this time, namely that the high corner moments represent a very localized effect. Plate analyses have been carried out in which the support, instead of holding the plate edge perfectly straight, merely prevented vertical deflection at a discrete number of points and allowed the edge to bend between these points. The effect of changing the support condition was to decrease the edge constraint and to greatly reduce the negative corner moment. At the same time, however, the deflection and positive moment under the load showed almost negligible increases. Also, the rotations at the support points which were required to release the edge constraint were found to be very small. This indicates that the corner effect is localized and is associated

with only a small amount of strain energy in the structure. It follows that in an inelastic structure only a small amount of yielding or cracking would be needed to eliminate the corner effects, and hence that they may not be critical in design. However, this conclusion remains to be confirmed following more detailed studies.

CHAPTER 5

BEHAVIOR OF TWO-SPAN CONTINUOUS SKEW BRIDGE SLABS

5.1 GENERAL

The mathematical complexity of deriving an analytical close-form solution of single span skew plates has prevented an accurate evaluation of the slab behavior under even the most simple load conditions. Hence, initially, incidental and experimental systematic studies have been carried out [38]. Only, through the use of finite difference methods and the more recent development of computer programs, with a finite element subdivision of the skew slab, has it become possible to solve this problem analytically [18][39][1].

The solution of the even more complex problem of continuous skew plates has also been pursued, first through experimental means. However, recent developments in computer programming (e.g. FEASAP) now also permits the solution of continuous slabs.

In the following sections the results of a systematic analytical study of two-span continuous isotropic bridge slabs is presented. The objective of this study is to evaluate the significant behavior of these slabs as influenced by the bridge skew and the width-span ratio. In addition to a study of these slabs under uniformly distributed loads over the entire plate an evaluation of the maximum moments under lane load conditions is also presented. Finally, a successful comparative study between experimental results, obtained through the Moiré-method [40], and analytical values is discussed.

5.2 ANALYTICAL STUDIES

5.2.1 Structural Configuration

In this study, nine, two-span continuous bridge slabs were selected and analyzed for a variety of loading conditions. These skewed slabs were assumed to be isotropic and of constant thickness, but the angle of skew and the width were varied.

Whenever possible unit values were assigned to these parameters, in order that the results of the ananlyses may be simply applied to other structures of different proportions. Consequently both span lengths, measured along the free edge, the thickness and the elastic modulus of the slab material were each set equal to 1.0. A Poisson's ratio of 0.3333 was assumed. The parameters studied were the angle of skew β, and the skew width of the slab measured along the support. Both parameters were studied in three steps, namely $\beta = 0°$, 30° and 45° and the skew width = 2.0, 1.0 and 0.5, thus resulting in a total of nine slabs. It can be noted that as the skew is varied the width is maintained constant.

Figure 5.1 shows a typical plan view of the continuous bridge slab with the x, y and x', y' axes, and illustrates the important geometric parameters.

5.2.2 Load Conditions

To effectively study the behavior of each two-span slab, six load cases were selected. Each load case consisted of a uniformly distributed load of unit intensity (load per unit area). The area of slab subjected to this load varied, as shown in Figure 5.2, and resulted in the following basic load cases:

1. Uniform load over entire slab (both spans).
2. Uniform load over entire left span, only.
3. Uniform load over first-quarter strip of the left span.
4. Uniform load over second-quarter strip of the left span.
5. Uniform load over third-quarter strip of the left span.
6. Uniform load over fourth-quarter strip of the left span.

The above load cases represent not only the overall load conditions (Cases 1 and 2) but also the conditions encountered under traffic lane loads.

5.2.3 Method of Analysis

Again the FEASAP computer program, described in Chapter 3, was used for the analyses. Since the slab was isotropic, the solid plate option of the program was selected. The finite element subdivision of the bridge slab used for the analysis is shown on Fig. 5.3. Also indicated are the longitudinal sections A, B, C, D, E and F and the transverse sections L, C, R for which plate response will be plotted. A finer subdivision in areas of high moment variation (near the obtuse corners and over the intermediate support) can be noted. The mesh comprised 578 elements and 630 modal points.

5.2.4 Analytical Results

The analytical results are presented in the form of curvature plots for $\chi_{x'}$, $\chi_{y'}$ and $\chi_{x'y'}$ along both longitudinal (A, B, C, D, E) and transverse (L, C, R) sections. Figures 5.4 to 5.6 present $\chi_{x'}$ plots along these longitudinal sections for a two-span slab with a width-to-span aspect ratio of 2.0 and angles of skew (β) of 0° (rectangular plate), 30° and 45°. Similar results are presented in Figures 5.9 to 5.11 and 5.14 to 5.16

for slabs with width-to-span aspect ratios of 1.0 and 0.5 respectively. The transverse curvature plots for $\chi_{y'}$ along the slab mid span L and R and center support C for each of the six load conditions are presented in Figures 5.7, 5.12, and 5.17. These figures represent the results for two-span slabs with aspect ratios of 2.0, 1.0 and 0.5 respectively. For the same slab configurations the angle of twist values $\chi_{x'y'}$ along the transverse sections (L, C, R) for the several load cases studied are presented in Figures 5.8, 5.13 and 5.18 respectively. Identification in general is by section (A, B, C, D, E, F, L, C, R) and load-case numbers.

To evaluate the plate moments $m_{x'}$, $m_{y'}$ and $m_{x'y'}$ the following applies:

$$m_{x'} = - D \ (\chi_{x'} + \nu \chi_{y'})$$

$$m_{y'} = - D \ (\chi_{y'} + \nu \chi_{x'}) \quad \text{and}$$

$$m_{x'y'} = - D \ (1 - \nu) \chi_{x'y'} \quad \text{with} \quad D = \frac{E t^3}{12(1-\nu^2)} \ .$$

E and t are respectively the modulus of elasticity and plate thickness. Considering the assumptions used in the analysis that E and t are both unit values and that $\nu = 0.333$ the curvature values χ can be directly used to evaluate the moments for these analytical models by substituting for $D = \frac{(1)(1)^3}{12(1-0.333^2)} = 0.09375$ k-ft (assuming units of kips for load and feet for length). For slabs with the same width-to-span aspect ratios as those analysed but with a load of q k/ft^2 and a span length of L ft the additional conversion factor for the moments evaluated by the above indicated procedure is qL^2.

Tables 5.1, 5.2 and 5.3 present, for each of the two-span plates studies the moments $m_{x'}$, $m_{y'}$ and $m_{x'y'}$ along the section at mid-span of

the loaded span for both load cases 1 and 2. It should be noted immediately that the computed m_x, moments along this section for $\beta = 0°$, are in excellent agreement with the corresponding average moments of $0.0625\ qL^2$ and $0.09375\ qL^2$ respectively for cases 1 and 2 as derived from statics. The average moments along this section are graphically represented, in Figure 5.19. It is interesting to note that the m_x, moments reduce rapidly under increasing angle of skew. This reduction is basically due to the reduction in the gross moments at mid-span because of the shorter normal-span length between supports as compared to the skew span along the free edge. Since this phenomenon will be more effective for a wide plate (aspect ratio 2.0) than for a narrow plate (aspect ratio 0.5) the minimum reduction is most pronounced for a plate with a 2.0 aspect ratio. This is clearly illustrated by the m_x, graphs in Figure 5.19.

While the m_x, moments show a considerable variation with varying angle of skew, the m_y, moments remain relatively constant. As expected from the fact that in general, the transverse moments in a plate with increasing width increase due to the predominant influence of the longitudinal curvature through a Poisson's ratio effect, the calculated m_y, moments are indeed larger for the plate with a 2.0 aspect ratio than for the plate with a 0.5 aspect ratio. The magnitude of the m_y, moments under increasing width and uniform in load are therefore greatly influenced by the magnitude of ν. For a zero value of ν the average transverse moment, contrary to the results shown in Figure 5.19, would decrease for increasing width.

The average twisting moments, at mid-span, are becoming relatively significant under increasing angle of skew. For an angle of skew of 30°

Table 5.1 Moments $m_{x'}$, $m_{y'}$, $m_{x'y'}$ at Midspan, Loaded Span, Load Cases 1 and 2
Width-to-Span Ratio 2.0

$\beta = 0°$

	Load Case 1						Load Case 2					
	$\chi_{x'}$	$\chi_{y'}$	$\chi_{x'y'}$	$m_{x'}$	$m_{y'}$	$m_{x'y'}$	$\chi_{x'}$	$\chi_{y'}$	$\chi_{x'y'}$	$m_{x'}$	$m_{y'}$	$m_{x'y'}$
	10^{-3}	10^{-3}	10^{-3}	10^{-4}lb	10^{-4}lb	10^{-4}lb	10^{-3}	10^{-3}	10^{-3}	10^{-4}lb	10^{-4}lb	10^{-4}lb
A	-795	+265	-	+662	0	-	-1200	+400	-	+1000	0	-
B	-665	+ 42	-	+610	+169	-	-1010	+ 75	-	+ 923	+246	-
C	-655	+ 04	-	+613	+201	-	- 980	+ 10	-	+ 915	+297	-
D	-655	+ 04	-	+613	+201	-	- 980	+ 10	-	+ 915	+297	-
E	-665	+ 42	-	+610	+169	-	-1010	+ 75	-	+ 923	+246	-
F	-795	+265	-	+662	0	-	-1200	+400	-	+1000	0	-

$\beta = 30°$

A	-860	+287	-225	+715	0	+141	-980	+326	-285	+815	0	+178
B	-575	-025	-308	+546	+204	+192	-713	-070	-388	+690	+288	+242
C	-435	-106	-268	+440	+235	+167	-610	-168	-358	+625	+348	+223
D	-380	-125	-228	+396	+236	+142	-575	-178	-335	+594	+347	+209
E	-350	-095	-174	+358	+199	+108	-590	-110	-327	+587	+287	+204
F	-290	+ 97	+030	+241	0	- 19	-680	+227	-180	+567	0	+112

$\beta = 45°$

A	-615	+205	-244	+513	0	+152	-635	+212	-265	+560	0	+165
B	-345	-105	-340	+356	+206	+212	-382	-155	-390	+406	+264	+243
C	-205	-183	-242	+249	+235	+151	-282	-260	-303	+346	+332	+189
D	-175	-175	-190	+218	+218	+118	-250	-250	-270	+312	+312	+168
E	-180	-128	-150	+209	+176	+ 94	-288	-175	-282	+324	+252	+176
F	-125	+ 42	+ 50	+105	0	- 31	-350	+117	-125	+292	0	+ 78

Table 5.2 Moments $m_{x'}$, $m_{y'}$, $m_{x'y'}$ at Midspan, Loaded Span, Load Cases 1 and 2
Width-to-Span Ratio 1.0

$\beta = 0°$

	Load Case 1						Load Case 2					
	$X_{x'}$	$X_{y'}$	$X_{x'y'}$	$m_{x'}$	$m_{y'}$	$m_{x'y'}$	$X_{x'}$	$X_{y'}$	$X_{x'y'}$	$m_{x'}$	$m_{y'}$	$m_{x'y'}$
	10^{-3}	10^{-3}	10^{-3}	10^{-4} lb	10^{-4} lb	10^{-4} lb	10^{-3}	10^{-3}	10^{-3}	10^{-4} lb	10^{-4} lb	10^{-4} lb
A	-792	+264	-	+660	0	-	-1185	+395	-	+988	0	-
B	-705	+107	-	+626	+120	-	-1060	+180	-	+937	+162	-
C	-665	+ 52	-	+607	+159	-	-1012	+ 98	-	+916	+225	-
D	-665	+ 52	-	+607	+159	-	-1012	+ 98	-	+916	+225	-
E	-705	+107	-	+626	+120	-	-1060	+180	-	+937	+162	-
F	-792	+264	-	+660	0	-	-1185	+395	-	+988	0	-

$\beta = 30°$

A	-838	+279	-212	+698	0	+132	-950	+317	-262	+790	0	+164
B	-685	+ 75	-276	+618	+143	+172	-807	+ 75	-360	+733	+182	+225
C	-550	- 23	-280	+524	+193	+175	-695	- 50	-388	+667	+264	+242
D	-460	- 50	-240	+447	+190	+150	-655	- 62	-373	+635	+262	+233
E	-410	- 5	-153	+386	+133	+ 96	-675	+ 37	-322	+622	+176	+201
F	-340	+113	0	+283	0	0	-714	+238	-196	+595	0	+122

$\beta = 45°$

A	-600	+200	-220	+500	0	+137	-620	+207	-245	+516	0	+153
B	-492	+ 22	-330	+455	+133	+206	-520	0	-376	+487	+162	+235
C	-335	-100	-336	+345	+199	+210	-370	-145	-410	+382	+251	+256
D	-262	-127	-267	+285	+201	+167	-338	-170	-375	+370	+265	+234
E	-230	- 56	-158	+234	+125	+ 99	-387	- 45	-310	+377	+163	+194
F	-150	+ 50	+ 25	+125	0	- 16	-378	+126	-145	+315	0	- 90

Table 5.3 Moments $m_{x'}$, $m_{y'}$, $m_{x'y'}$ at Midspan, Loaded Span, Load Cases 1 and 2

Width-to-Span Ratio 0.5

$\beta = 0°$

	Load Case 1						Load Case 2					
	$\chi_{x'}$	$\chi_{y'}$	$\chi_{x'y'}$	$m_{x'}$	$m_{y'}$	$m_{x'y'}$	$\chi_{x'}$	$\chi_{y'}$	$\chi_{x'y'}$	$m_{x'}$	$m_{y'}$	$m_{x'y'}$
	10^{-3}	10^{-3}	10^{-3}	10^{-4} lb	10^{-4} lb	10^{-4} lb	10^{-3}	10^{-3}	10^{-3}	10^{-4} lb	10^{-4} lb	10^{-4} lb
A	-750	+250	-	+635	0	-	-1150	+383	-	+958	0	-
B	-700	+178	-	+600	+52	-	-1087	+283	-	+930	+ 74	-
C	-685	+140	-	+599	+83	-	-1060	+237	-	+920	+109	-
D	-685	+140	-	+599	+83	-	-1060	+237	-	+920	+109	-
E	-700	+178	-	+600	+52	-	-1087	+283	-	+930	+ 74	-
F	-750	+250	-	+635	0	-	-1150	+383	-	+958	0	-

$\beta = 30°$

A	-790	+263	-190	+658	0	+119	-945	+315	-278	+788	0	+174
B	-720	+164	-220	+623	+71	+138	-887	+206	-330	+767	+ 84	+206
C	-655	+115	-225	+578	+97	+141	-845	+157	-360	+744	+117	+225
D	-590	+100	-200	+522	+91	+125	-800	+158	-355	+700	+102	+222
E	-535	+120	-145	+465	+54	+ 91	-780	+182	-313	+673	+ 73	+195
F	-470	+157	- 65	+392	0	+ 41	-760	+253	-250	+634	0	+156

$\beta = 45°$

A	-690	+230	-254	+575	0	+159	-725	+242	-338	+604	0	+211
B	-645	+ 75	-320	+581	+131	+200	-700	+148	-432	+610	+ 81	+270
C	-575	+ 74	-355	+515	+110	+222	-670	+110	-493	+594	+106	+308
D	-490	+100	-330	+428	+ 59	+206	-630	+102	-493	+558	+101	+308
E	-395	+145	-250	+325	- 12	+156	-590	+126	-422	+514	+ 67	+264
F	-300	+100	-130	+250	0	+ 81	-545	+182	-310	+454	0	+194

the $m_{x,y}$, moments average approximately 25% of the m_x, moments. With β reaching 45° this percentage approaches approximately 50%.

The above observations indicate the complexity of the moment distribution in skew continuous plates. However the results clearly illustrate the fundamental behavior of such plates as affected by the geometry and subsequent preferential load transferring response.

An observation of the χ_x, curvature values for the lane loads (cases 3 to 6) in comparison with the curvature value for the full-width loads (cases 1 and 2) distinctly show the effective transverse load distributing capacity of the skew slab.

5.3 EXPERIMENTAL STUDIES

The objective of the experimental study was to determine the accuracy of the formulation of the mathematical model and the method of analysis employed in evaluating the curvature and moment distribution in these skew continuous slabs under the given loads.

5.3.1 Method of Experimental Analysis

The experimental procedure used to evaluate the plate curvatures and subsequently the plate moments is the so-called Moiré effect method [40] [41]. This method incorporates in general a plastic sheet as model material. The actual plate model is placed in a horizontal position, see figure 5.20.a, with a reflective surface facing down. By using a black plexiglass sheet the model surface is automatically reflective. Observing the unloaded model through a camera the photographic plate records through reflection from the model surface and mirror an image of the ruled screen.

Figure 5.20.b illustrates this phenomenon where, by observing point A of the model surface, an image of the screen at point B will be recorded on the photographic plate at C. Observing the entire model plate the camera will record a reflective image of the ruled screen. When the model subsequently deflects under load the plate surface will reflect into the camera another image of the ruled screen then previously recorded for the unloaded case. Using the first - unloaded model - image as a reference grid and super imposing on the same photographic plate the distorted grid image, reflected from the loaded model, one obtains through interference of the two grid images a so-called moiré - pattern in which each line represents a contour line of constant slope ($\partial\omega/\partial x'$ or $\partial\omega/\partial y'$). The closer these lines are spaced the greater the curvature values are. For a pattern of $\partial\omega/\partial x'$ contour lines the curvature $\partial^2\omega/\partial x'^2$ or $\chi_{x'}$ is inversely proportional to the distance between lines measured perpendicular to the initial reference grid lines. The distance between lines measured along these reference grid lines is inversely proportional to the angle of twist $\partial^2\omega/\partial x'\partial y'$ or $\chi_{x'y'}$. By rotating the ruled screen 90° the photographic procedures repeated. The moiré - line picture thus obtained shows $\partial\omega/\partial y'$ contour lines. Again the distances between these lines, measured perpendicular and parallel to the reference grid lines are inversely proportional to the curvature values $\partial^2\omega/\partial y'^2$ (or $\chi_{y'}$) and $\partial^2\omega/\partial x\partial y'$ (or $\chi_{x'y'}$) respectively. An example of two such photographic images are presented in Figures 5.21 and 5.22, each showing the slope contour lines $\partial\omega/\partial x'$ and $\partial\omega/\partial y'$ for a uniformly distributed load over the entire two-span skew plate.

5.4 COMPARATIVE ANALYTICAL-EXPERIMENTAL STUDIES

To evaluate the accuracy of the analytical results in comparison with the experimental values obtained by use of the moiré - effect method two continuous slabs are studied under uniformly distributed loads on both spans (case 1) and on a single span (case 2). The selected slabs have respectively an angle of skew of $\beta = 30°$ and a width-to-span aspect ratio of 1.0, and an angle of skew of $\beta = 45°$ and an aspect ratio of 0.5. For each case the curvature values χ_x, are compared along the longitudinal sections A, B, C, D, E and F.

For the 30° and 45° skew, fully loaded, bridge slabs the results along sections A, B, and C are presented in Figures 5.23 and 5.24 respectively. For the 30° skew slab with a uniformly distributed load on one span only (load case 2) the theoretical and experimental curvature values χ_x, along sections A, B, C, and D, E, F, are presented in Figures 5.25 and 5.26 respectively. Similarly the results for the 45° skew slab under load case 2 are presented in Figures 5.27 and 5.28 respectively.

A general comparison of these results show an excellent agreement between the theoretical and experimental values. Considering the fact that the accuracy of the moiré - method has been proven to be within 1%, the comparative results of the study presented in this chapter clearly indicate that the FEASAP computer program is an excellent tool to analyze accurately the moment distribution in skew isotropic slabs.

CHAPTER 6

BEHAVIOR OF SKEW DECK SLAB PANELS

6.1 PANELS STUDIED

Because of the unusual behavior of complete bridges on skew supports, it is of interest to study individual deck slab panels which are supported by skew girders and diaphragms.

For this study, a deck slab has been idealized as a solid isotropic plate which is continuous over rigid line supports, representing the girders and diaphragms. That is, it is assumed that the concrete slab can be idealized as a thin isotropic plate, that the girders and diaphragms are sufficiently narrow to be represented as line supports, that the effects of composite action are not significant for the study proposed, and that the relative deflections of the girders and diaphragms do not significantly affect the slab. It is further assumed that a wheel load can be represented as a point load on the plate. Although these assumptions might not be justified if a detailed analysis of an actual deck slab were required, they are satisfactory for the purposes of a parameter study.

The plate which has been analyzed, and the finite element subdivision used, are shown in Figs. 6.1 and 6.2. The supports parallel to the y axis have been assumed to represent girders, and those parallel to the x axis to represent diaphragms. The angle of skew is 40°, as shown. The thickness is 6 in., and E and ν are respectively 5,000 ksi and 0.15. The following analyses have been carried out, using the FEASAP program.

1. With supports at both the girder and diaphragm lines:
    a. load in the middle of the center panel;
    b. load in the middle of an edge panel;
    c. load in the middle of an obtuse corner panel.
2. With supports at the girder lines only:
    a. load near the edge, away from the corners;
    b. load near an obtuse corner.

In addition, a similar plate with zero skew and with supports along both the girder and diaphragm lines has been analyzed for comparison.

In all cases a point load of 16 k has been applied, and the principal bending moments in the plate have been calculated. The results are shown in Figs. 6.3 through 6.8. The double line in each case represents the negative plate bending moment (tension on the top of the slab) and the single line the positive moment. The lengths of the lines represent the moment magnitudes, in k. in./in. The directions of the lines indicate the "directions" of the moments in the sense that they indicate the strips of slab on which the moments act. That is, the lines are not moment vectors, but are drawn normal to the moment vectors.

6.2 DISCUSSION OF RESULTS

6.2.1 Support by Girders and Diaphragms

Fig. 6.3 shows the principal moment pattern for a load at the middle of a skew panel which is continuous on all four sides. The tendency is clearly for the plate to span between the obtuse corners. The largest moment is the positive moment under the load.

Fig. 6.4 shows the pattern for the load at the middle of an edge panel. Here again the tendency is for the plate to span between the obtuse corner, and the largest moment is under the load. This moment is of virtually the same magnitude as that in the previous case. However, the negative moments at the discontinuous edge are significantly larger than the previous negative moments.

Fig. 6.5 shows the pattern for the load at the middle of a corner panel. The plate again spans between the corners, and the positive moment under the load is of essentially the same magnitude as in the two previous cases. However, the largest moment is now the negative moment in the obtuse corner.

For the purposes of comparison, Fig. 6.6 shows the moment pattern for the load in the corner panel of a plate with no skew. It can be seen that the negative moment in the discontinuous corner is now much smaller than the positive moment under the load. The large corner moment in the skew case is therefore due to the shape of the plate.

The question which is of importance to the designer is whether the large negative moment in the obtuse corner can lead to serious cracking of the deck slab. As was done in Chapter 4, it is possible to modify the support conditions in the finite element analysis, in order to permit free rotation of the system at the corner support, while still preventing this support from deflecting. The effect of making this modification is startling, as the negative moment in the corner changes from -8.29 k.in./in. to +1.93 k. in./in. Of equal importance, however, is the fact that the positive moment under the load increases by only a very small amount, from 3.88 k.in./in. to 3.89 k.in./in., and the deflection under the load also increases only very slightly. This demonstrates that the strain energy released when corner rotations are permitted is very small, and hence

that the large negative moments occur over only a small region of the plate. Further, if the rotations at the corners are examined, it is found that they are so small that they would correspond to a crack width of only .00017 inches at the surface of the plate. That is, the large negative moments are so localized and have so little strain energy associated with them, that it would require a negligible amount of cracking in a concrete slab to eliminate these moments completely. It appears, therefore, that there is no need to provide reinforcement to resist these moments, and that any cracking associated with them will be unimportant.

From the results of thin plate theory, similar conclusions can be drawn about corner effects in complete bridges. However, it is dangerous to draw conclusions about the behavior of particular details of a bridge from the results of a thin plate analysis, because the thin plate idealization is inadequate. Rather, if the behavior of the corner regions of skew bridges is to be studied analytically, a refined model such as the ribbed plate model should be used. An investigation of this aspect of skew bridge behavior will be presented in a future report. In particular, the membrane shearing behavior in the deck slab near obtuse corners will be studied, to determine whether the distortions are sufficient to lead to significant cracking of a concrete structure.

6.2.2 Support by Girders Only

Fig. 6.7 shows the principal moment pattern for a load applied to an elongated slab panel supported at all of the girder lines but at only the two end diaphragm lines. With this type of geometry,

one-way slab behavior is expected, and indeed this type of behavior is essentially predicted. However, these results show a tendency for the slab to span towards the obtuse corners, rather than directly between supports, and the principal moments under the load are inclined at 13° to the supports.

Fig. 6.8 shows the moment pattern for a load applied near the obtuse corner. The behavior in this case is rather similar to that in Fig. 6.5, with a large negative moment in the obtuse corner, and as before it can be concluded that this large moment is actually unimportant in practice.

6.2.3 Positive Moment Magnitudes

The magnitudes of the maximum positive principal moments under the loads for each of the cases in Figs. 6.3 through 6.8 are shown in the following table.

TABLE 6.1

Maximum Positive Plate Moments Under Load	
Figure No.	Positive Moment (k.in./in.)
6.3	3.65
6.4	3.75
6.5	3.88
6.6	3.87
6.7	4.40
6.8	4.21

It is interesting to note that the moment values from Figs. 6.3 through 6.5 are all very similar. The moment in the corner panel, which

is discontinuous on two edges, is only 6% larger than the moment in the fully continuous panel. The result from Fig. 6.6 also indicates that the maximum positive moment may not be greatly affected by the angle of skew.

The maximum positive moments from Figs. 6.7 and 6.8 are 17% and 9% higher, respectively, than for the corresponding load positions with support at the diaphragm lines. Because of the added corner constraint, the moment in Fig. 6.8 is slightly lower than that in Fig. 6.7.

6.3 CONCLUSIONS

The results of this investigation may be of importance in the design of concrete deck slabs on skew supports. The conclusions which can be drawn are as follows:

1. Although thin plate theory predicts negative moments of high intensity at discontinuous obtuse corners, these moments are very local, and are eliminated by very slight cracking of the concrete.
2. For skew slabs which are of approximately rhomboidal shape the largest positive and negative bending moments act essentially parallel to lines joining the obtuse corners. In the design of such slabs it may therefore be desirable to align the reinforcement in this direction. However, this should be determined by test.
3. For skew slabs which are very long, one-way slab behavior occurs for loads applied away from the ends. However, if the load is applied near the end the largest positive moment is inclined

substantially to a line normal to the supports. It may be desirable to align the reinforcement in this direction, but again this must be determined by test.

REFERENCES

1. "Finite Element Analysis of Skew Composite Girder Bridges",
   M. Mehrain, Structures and Material Research,
   Department of Civil Engineering, University of California,
   Berkeley, Report No. 67-28, November 1967.

2. "Concrete Bridge Design" and Supplement,
   R. E. Rowe, C. R. Books Limited, London, 1962.

3. "Calcul des ponts larges à poutres multiples solidarisseés par des entretoises"
   Y. Guyon, Annales des Ponts et Chaussees
   No. 24, September - October 1946.

4. "Method of Calculation of bridges with several longitudinal beams taking into consideration their torsional resistance"
   C. Massonet, Publications, International Association for Bridge and Structural Engineering, Zurich, Vol. 10, 1950.

5. "Design Curves for the Effects of Concentrated Loads on Bridge Decks"
   P. B. Morice, G. Little, and R. E. Rowe, Publication Cement and Concrete Association, London, No. Db 11a, July 1956.

6. "Theory of Plates and Shells"
   S. P. Timoshenko and S. Woinowsky-Kreiger, McGraw-Hill Book Co.,
   Second Edition, 1959.

7. "Die Berechnung der ebenen Flächentragwerke mit Hilfe der Theorie der orthogonal-anisotropen Platte"
   W. Cornelius, Der Stahlbau, Nos 2,3 and 4, 1952.

8. "Theory and Design of Cylindrical Shell Structures"
   Privately published by Ore Arup and Partners, London, 1947.

9. "Use of Orthotropic Plate Theory in Bridge Design"
   K. H. Chu and G. Krishnamoorthy, Journal Structural Division
   ASCE, Vol. 88, No.ST3, June 1962.

10. "Die Grundgleichungen für die orthotrope Platte mit exzentrischen Steifen"
    E. Giencke, Der Stahlbau, No.6, June 1955.

11. "Die Berechnung von durchlaufenden Fahrbahnplatten"
    E. Giencke, Der Stahlbau No.9, September 1958.

12. "The Solution of Continuous Orthotropic Plates on Flexible Supports as Applied to Bridge Structures"
    C. P. Heins and C. T. G. Looney, Civil Engineering Department, University of Maryland, College Park, Maryland, Vols. I and II, March 1966.

13. "Bridge Analysis Using Orthotropic Plate Theory"
C.P. Heins and C. T. G. Looney, Journal Structural Division, ASCE, Vol. 94, No. ST2, February, 1968.

14. "Finite Strip Method Analysis of Elastic Slabs"
Y. K. Cheung, Journal Applied Mechanics Division, ASCE, Vol. 94, No. EM6, December 1968.

15. "Analysis of Orthotropic Steel Plate Bridge Decks"
G. H. Powell and W. Ogden, to be published Journal Structural Division, ASCE.

16. "Die Stahlfahrbahn, Berechnung und Konstruktion"
(Steel Decks, Analysis and Construction)
W. Pelikan and M. Esslinger, M.A.N. Forschung sheft, No. 7, 1957.

17. "Design Manual for Orthotropic Steel Plate Deck Bridges"
American Institute of Steel Constructution, New York, 1963.

18. "Analysis for Skew Slabs"
V. P. Jensen, University of Illinois, Engineering Experiment Station, Bulletin 332, 1941.

19. "Moments in I-Beam Bridges"
N. M. Newmark and C. P. Siess, University of Illinois Engineering Experiment Station, Bulletin 336, 1942.

20. "Moments in Simply Supported Skew I-Beam Bridges"
T. Y. Chen, C. P. Siess and N. M. Newmark, University of Illinois, Engineering Experiment Station, Bulletin 439, Vol. 54, No. 37, January 1957.

21. "Design of I-Beam Bridges"
N. M. Newmark, Proceedings ASCE, Vol.74, No. 3, March 1948.

22. "An Analytical Study of Eight Different Types of Highway Bridge Structures"
C. P. Heins and C. T. G. Looney, Civil Engineering Department, University of Maryland, College Park, Maryland, September 1966.

23. "Analytical and Experimental Study of a Through Truss Bridge"
R. A. Svotelis, C. P. Heins and C. T. G. Looney, Civil Engineering Department, University of Maryland, College Park, Maryland, June 1967.

24. "On the Analysis of a Skew Bridge by the Theory of Orthotropic Parallelogram Plates"
M. Naruoka and H. Ohmura, Publications International Association for Bridge and Structural Engineering, Zurich, Vol. 19, 1959.

25. "The Analysis of Grid Frameworks and Related Structures"
A. W. Hendry and L. G. Jaeger, Chatto and Windus, London, 1958.

26. "The Analysis of Grid Frameworks and Floor Systems by Electronic Computer"
E. Lightfoot and F. Sawko, The Structural Engineer, Vol. 38, No. 3, March 1960.

27. "Structural Behavior of an Orthotropic Steel Deck Bridge"
J. G. Bouwkamp and G. H. Powell, Structures and Materials Research, Department of Civil Engineering, University of California, Berkeley, Report No. 67-27, November 1967.

28. "Beitrag zur Berechnung orthogonal anisotroper Rechteckplatten"
K. Trenks, Der Bavingenieur, Vol. 29, No. 10, October 1954.

29. "Die Orthotrope Platte mit Hohlsteifen"
A. Pfluger, Osterreichisches Ingenieur, Archiv Vol. 2, 1955.

30. "Analysis of Composite Beam Bridges by Orthotropic Plate Theory"
V. Vitols, R. J. Clifton and T. Au, Journal Structural Division, ASCE, Vol. 89, No. ST4, August 1963.

31. "Plaques et coques cylindriques orthotropes à nervures dissymétriqus" (Orthotropic Plates and Orthotropic Cylindrical Shells with Asymmetic Ribs)
C. Massonnet, Publications International Association for Bridge and Structural Engineering, Zurich, Vol. 19, 1959.

32. "Analysis of Skewed Composite Girder Bridges"
W. C. Gustafson and R. N. Wright, Journal Structural Division, ASCE, Vol. 94, No. ST4, April 1968.

33. "Wheel Load Distribution in Concrete Box Girder Bridges"
A. C. Scordelis and C. Meyer, Structures and Materials Research, Department of Civil Engineering, University of California, Berkeley Report No. 69-1, January 1969.

34. "Analysis of Multibeam Bridges with Beam Elements of Slab and Box Section"
R. B. Pool, A. S. Arya, A. R. Robinson, and N. Khachaturian, University of Illinois, Engineering Experiment Station, Bulletin 483, Vol. 62, No. 106, July 1965.

35. "Analysis of Multibeam Bridges"
G. H. Powell, A. Ghose and I. G. Buckle,
Journal Structural Division, ASCE, September 1969.

36. "Bridge Deck Analysis"
I. G. Buckle, Ph.D Dissertation, University of Auckland, New Zealand, 1967.

37. "Analysis of Orthotropic Plate Bridges"
R. J. Clifton, J. C. L. Chang and T. Au, Journal Structural Division, ASCE, Vol. 89, No. ST5, October 1963.

38. "Einflussfelder der Momente Schiefwinkliger Platten"
E. h. Hubert RÜsch and Arnfrid Hergenröder, Materialprüfungsamt für das Bauwesen der Technischen Hochschule, München, 1961.

39. "Continua and Discontinua"
J. H. Argyris Proceedings Conference Matrix Methods in Structural Mechanics, Wright Patterson Air Force Base, Ohio, October, 1965.

40. "The Moiré Method"
F. K. Ligtenberg, Proceedings Society Experimental Stress Analysis, Vol. 12, No. 2, 1955.

41. "The Moiré Method and the Evaluation of Principal - Moment and Stress Directions" J. G. Bouwkamp, Experimental Mechanics, May 1964.

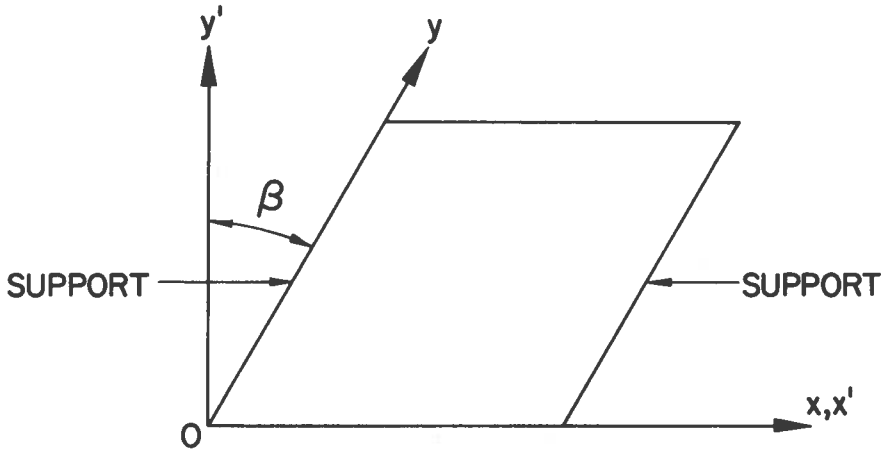

FIG. 3.1 BRIDGE AXES

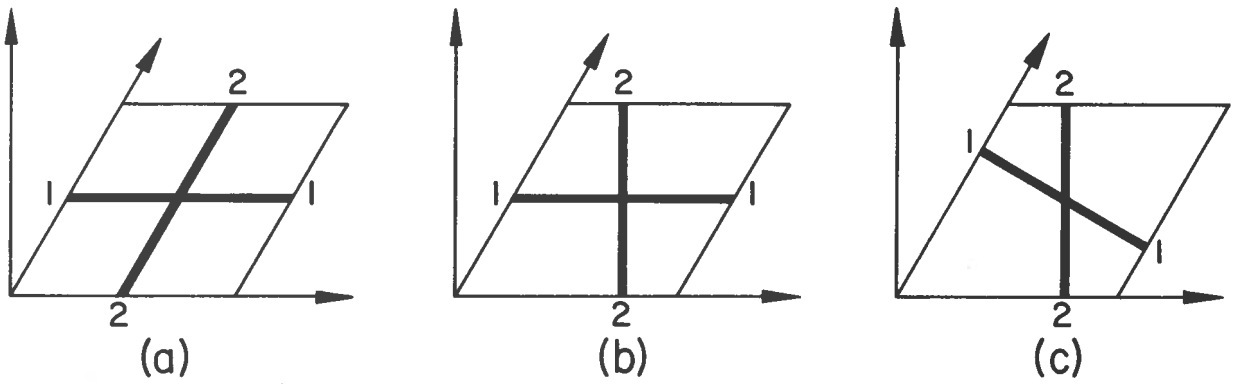

FIG. 3.2 BEAM SYSTEMS

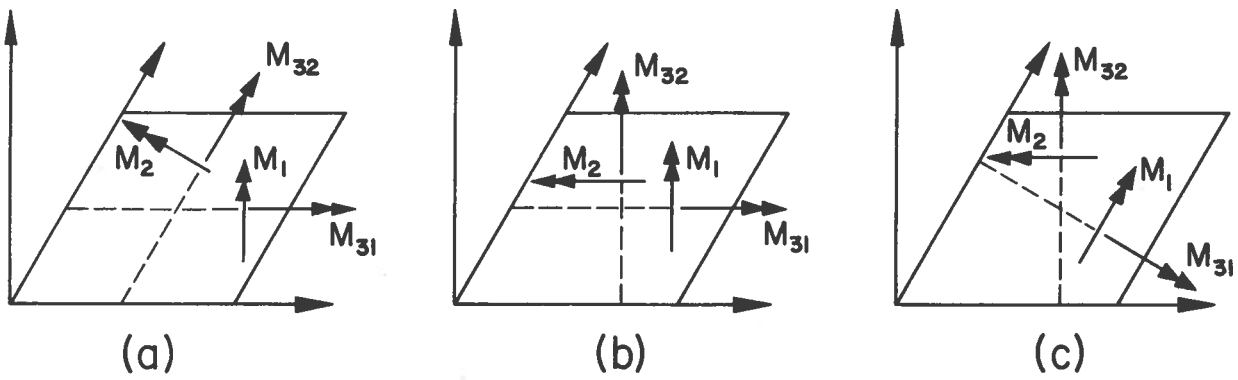

FIG. 3.3 BEAM MOMENTS

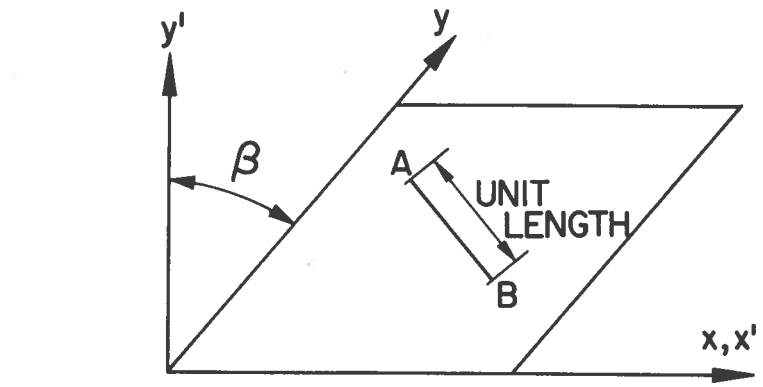

(a)

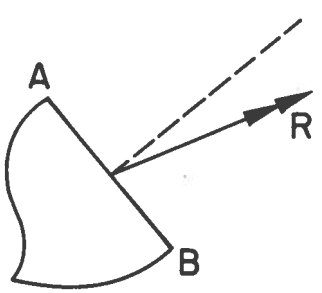

(b)

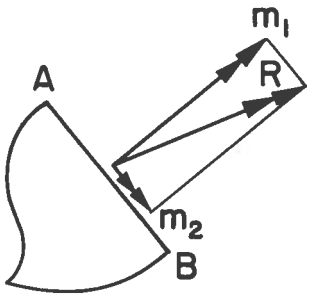

(c)

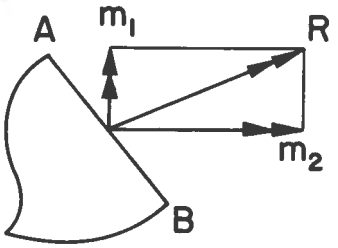

(d)

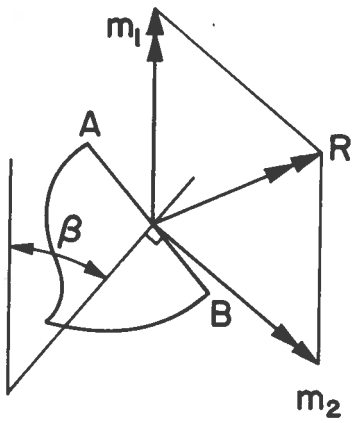

(e)

FIG. 3.4 PLATE MOMENT COMPONENTS

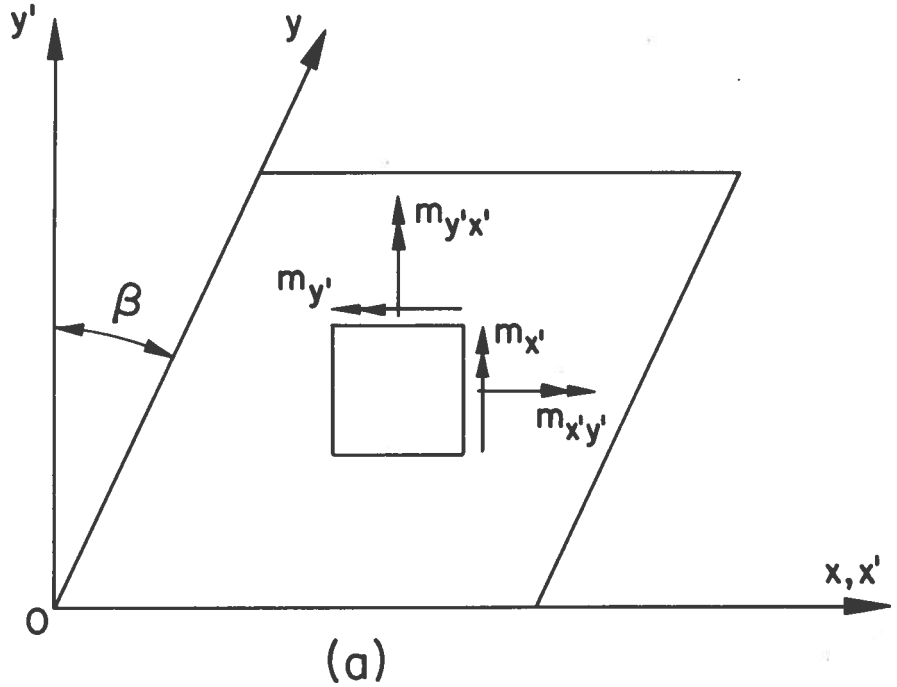

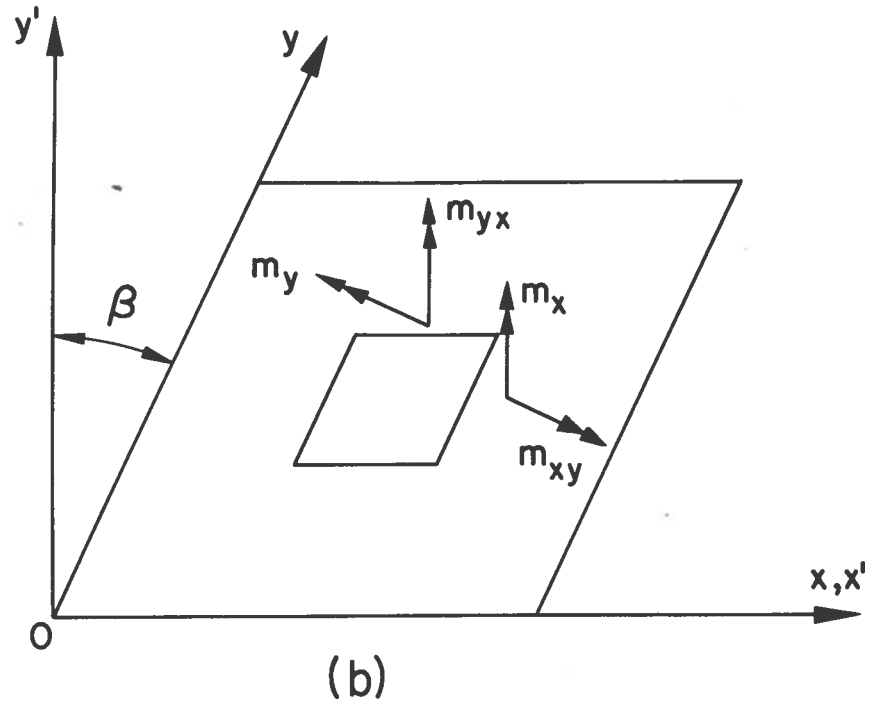

FIG. 3.5 RECTANGULAR AND SKEW PLATE MOMENTS

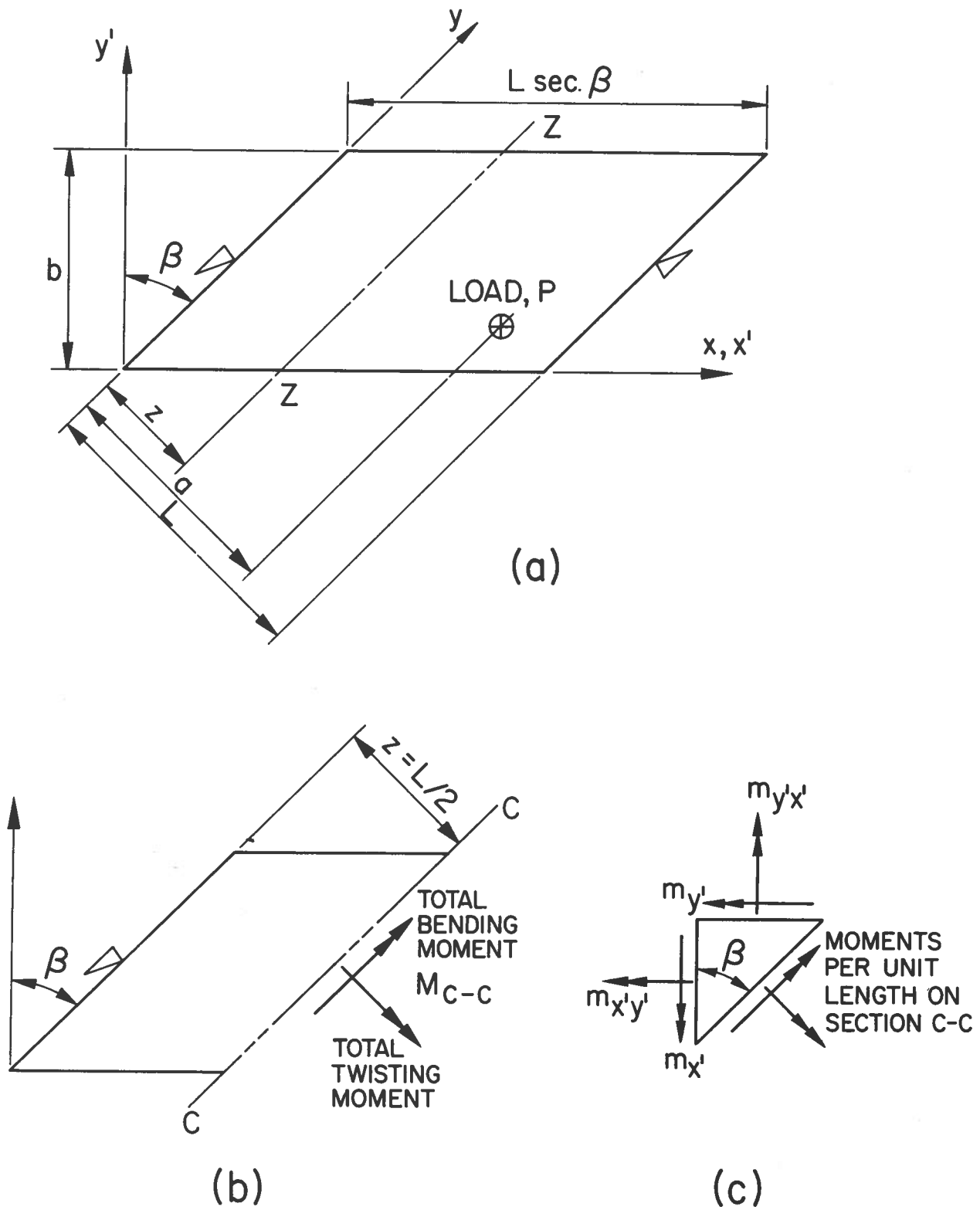

FIG. 3.6 EQUILIBRIUM IN SKEW PLATES

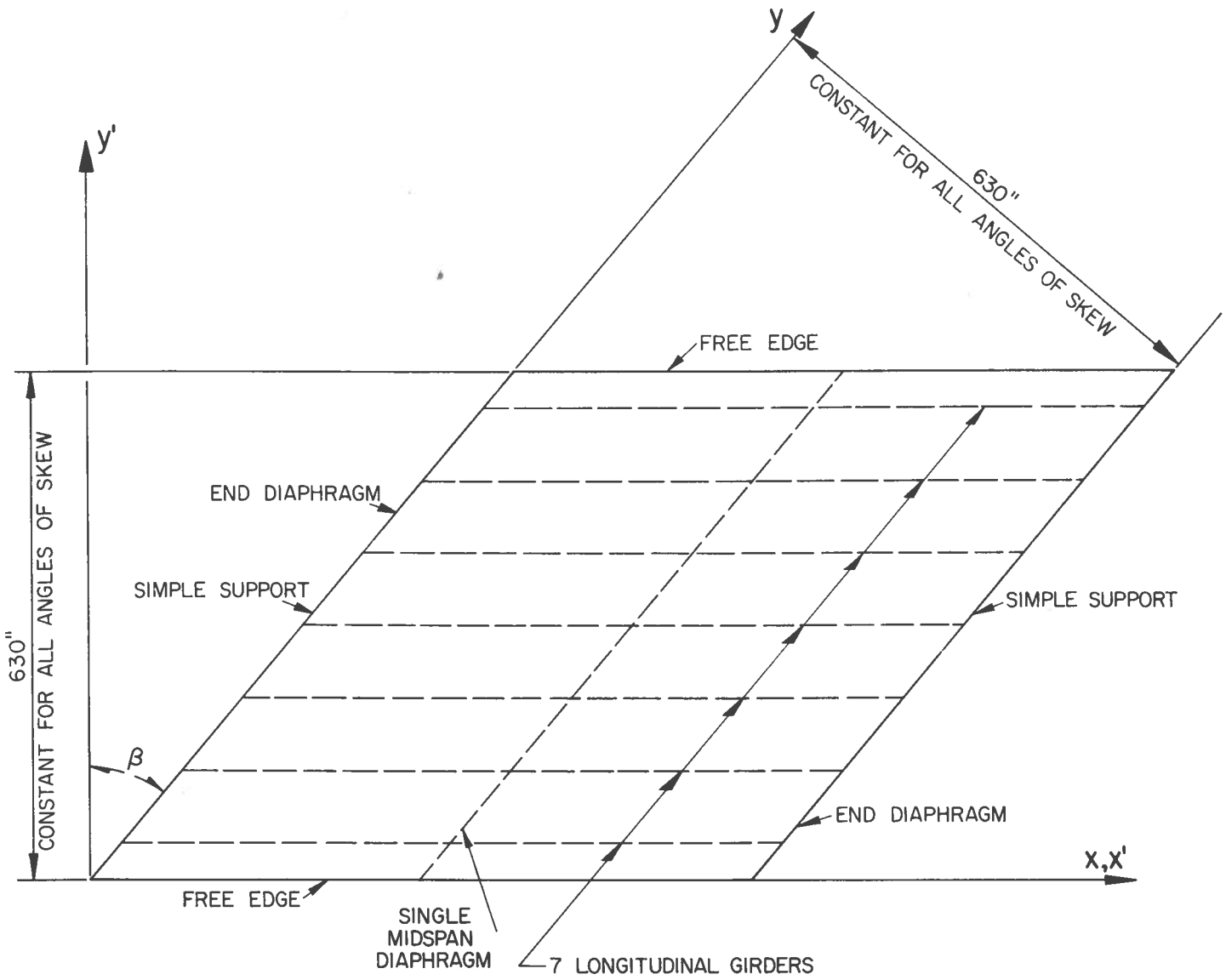

FIG. 4.1 PLAN VIEW OF DECK SELECTED FOR PARAMETER STUDY

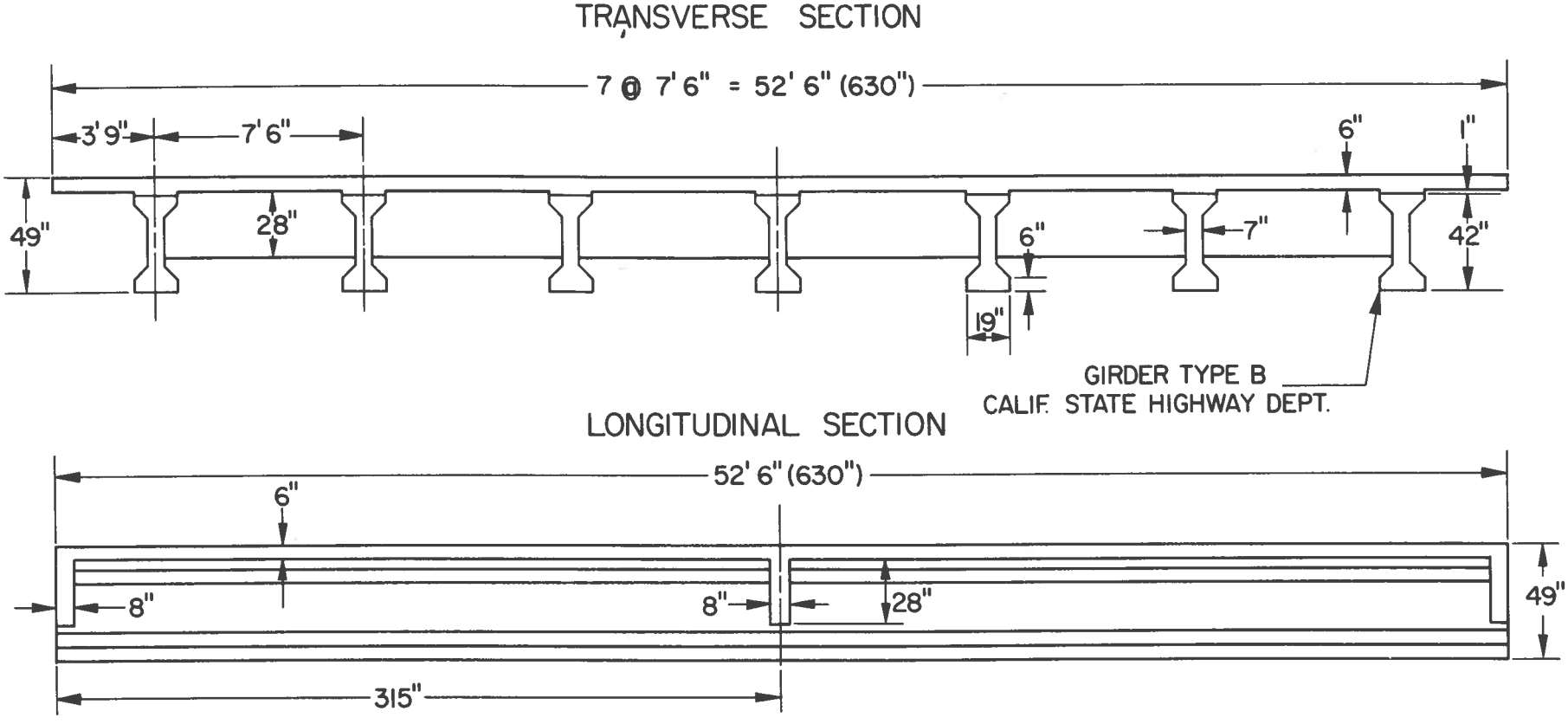

FIG. 4.2 TYPICAL SECTIONS OF DECK SELECTED FOR PARAMETER STUDY

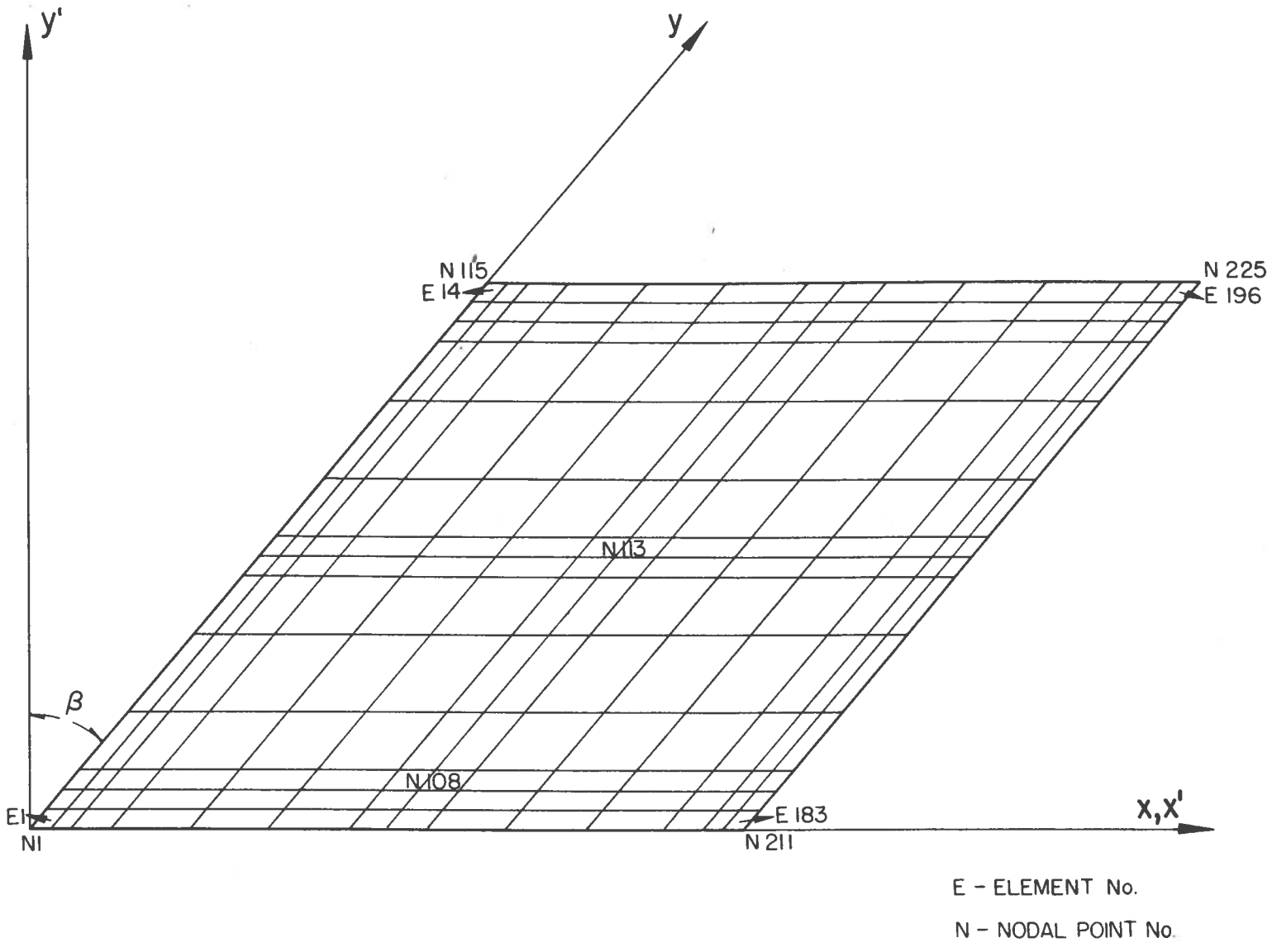

FIG. 4.3 FINITE ELEMENT MESH LAYOUT

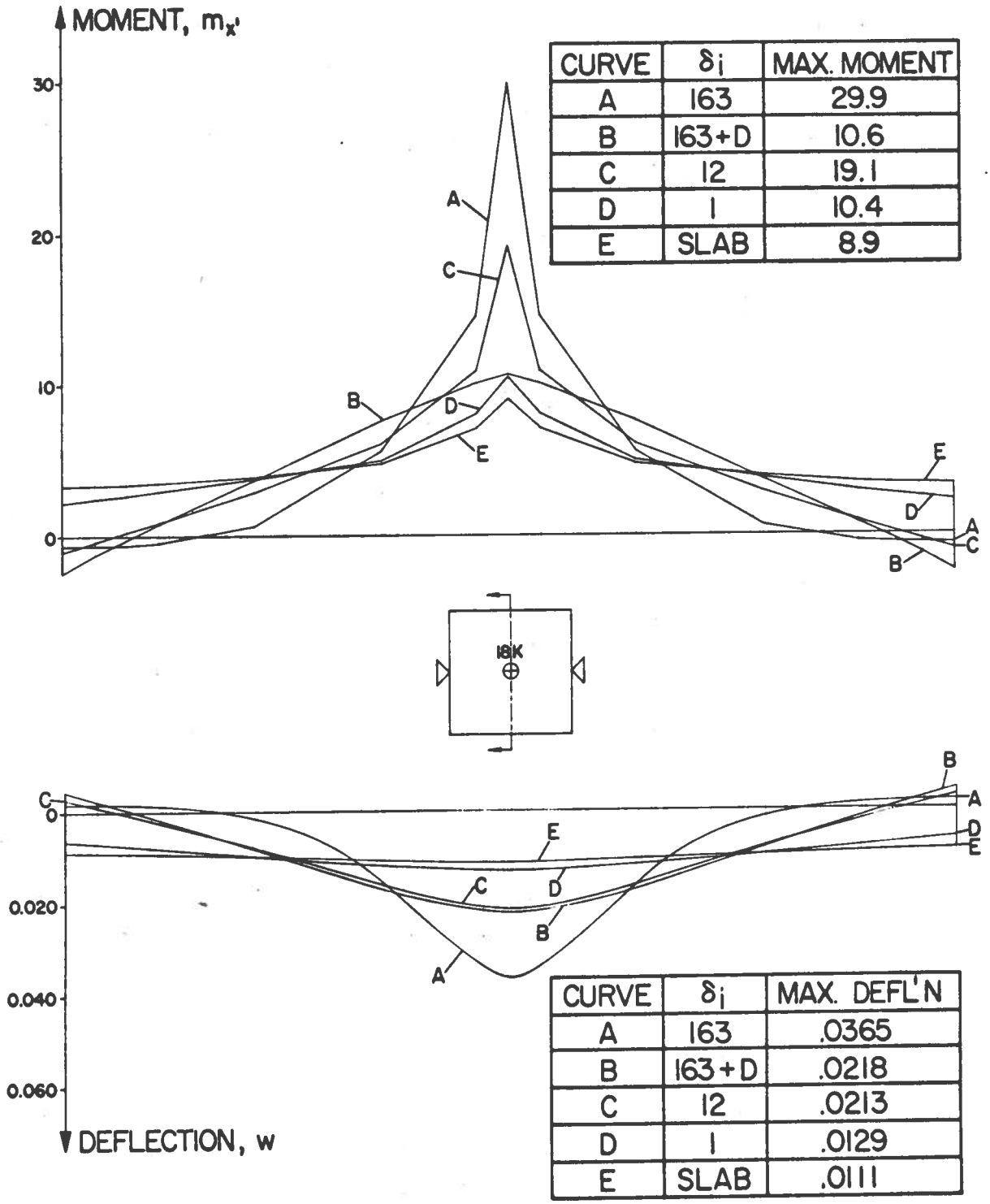

CURVE	δ_i	MAX. MOMENT
A	163	29.9
B	163+D	10.6
C	12	19.1
D	1	10.4
E	SLAB	8.9

CURVE	δ_i	MAX. DEFL'N
A	163	.0365
B	163+D	.0218
C	12	.0213
D	1	.0129
E	SLAB	.0111

FIG. 4.4 MIDSPAN TRANSVERSE PROFILES OF MOMENT AND DEFLECTION FOR VARIOUS ANISOTROPIC RATIOS, δ_i CENTER LOAD, ANGLE OF SKEW = 0°

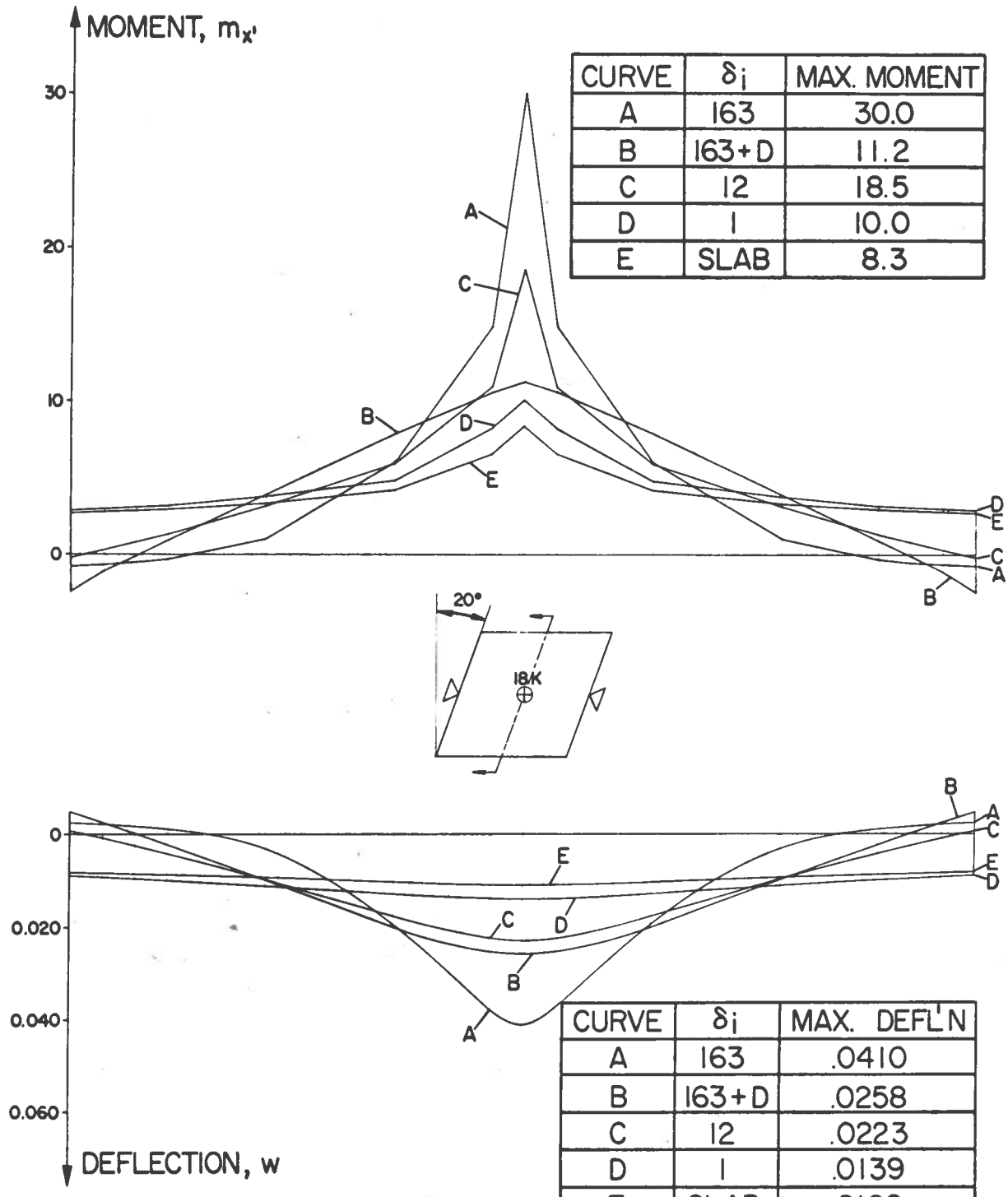

CURVE	δ_i	MAX. MOMENT
A	163	30.0
B	163+D	11.2
C	12	18.5
D	1	10.0
E	SLAB	8.3

CURVE	δ_i	MAX. DEFL'N
A	163	.0410
B	163+D	.0258
C	12	.0223
D	1	.0139
E	SLAB	.0109

FIG. 4.5 MIDSPAN TRANSVERSE PROFILES OF MOMENT AND DEFLECTION FOR VARIOUS ANISOTROPIC RATIOS, δ_i CENTER LOAD, ANGLE OF SKEW=20°

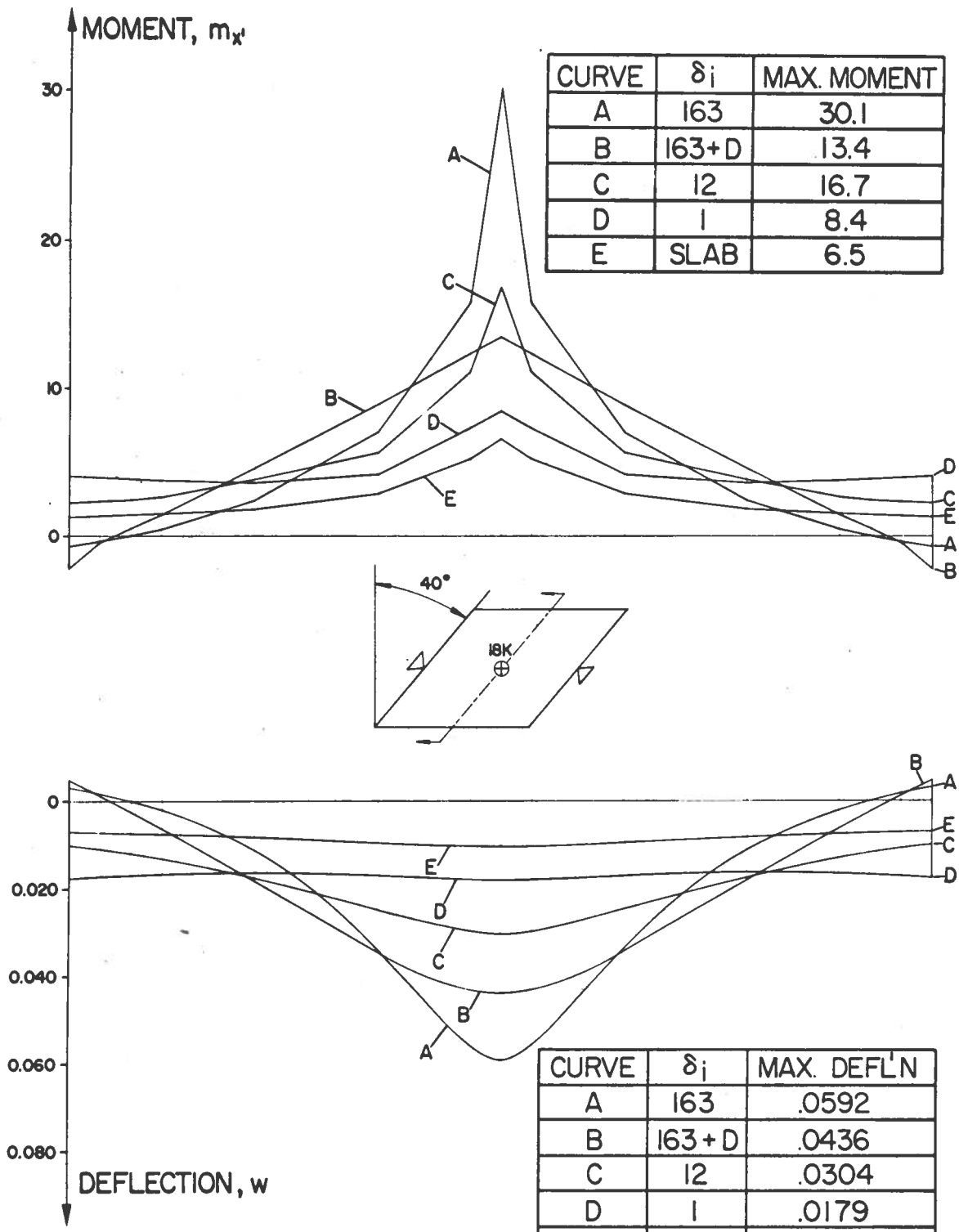

CURVE	δ_i	MAX. MOMENT
A	163	30.1
B	163+D	13.4
C	12	16.7
D	1	8.4
E	SLAB	6.5

CURVE	δ_i	MAX. DEFL'N
A	163	.0592
B	163+D	.0436
C	12	.0304
D	1	.0179
E	SLAB	.0104

FIG. 4.6 MIDSPAN TRANSVERSE PROFILES OF MOMENT AND DEFLECTION FOR VARIOUS ANISOTROPIC RATIOS, δ_i CENTER LOAD, ANGLE OF SKEW=40°

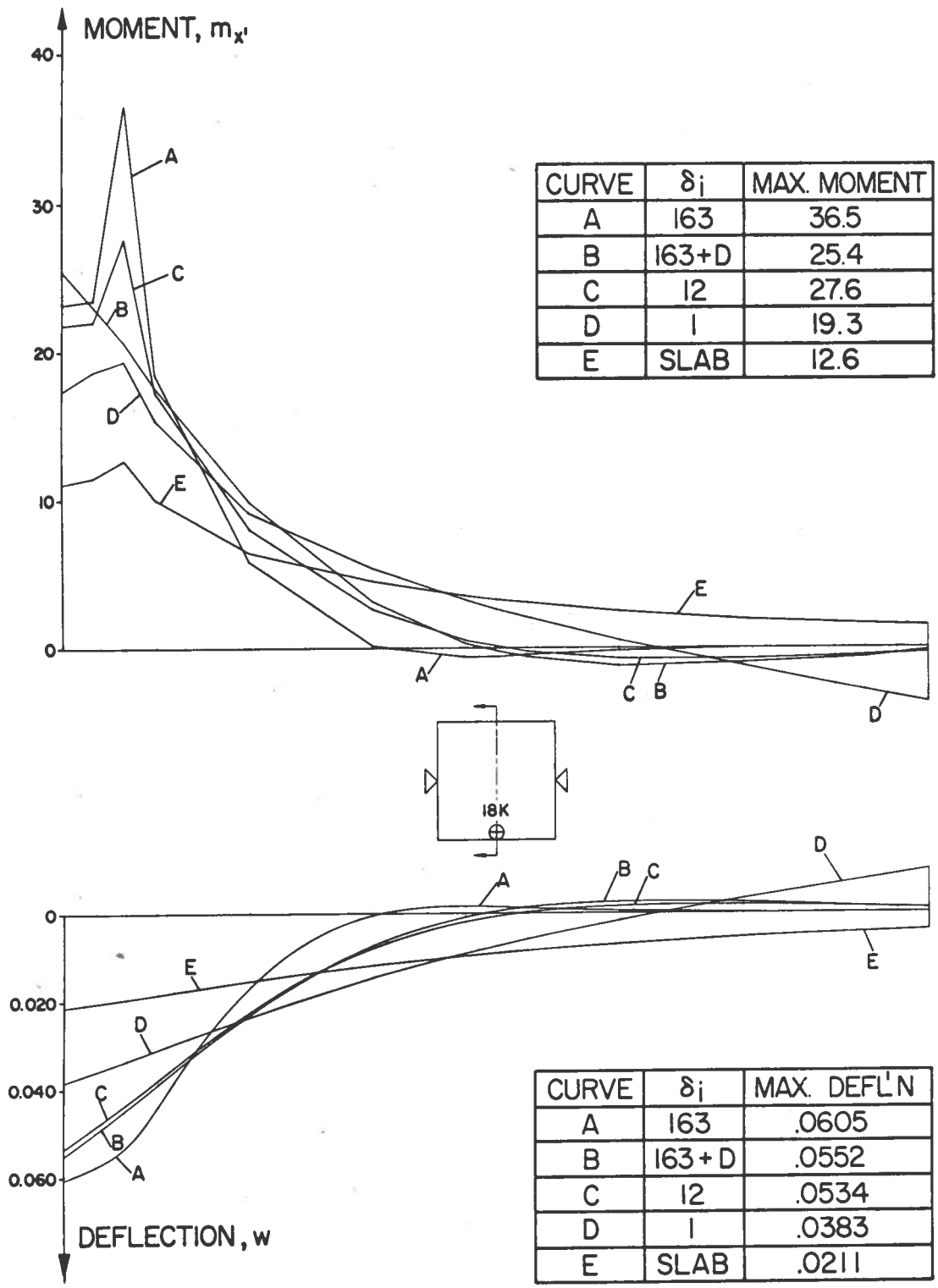

CURVE	δ_i	MAX. MOMENT
A	163	36.5
B	163+D	25.4
C	12	27.6
D	1	19.3
E	SLAB	12.6

CURVE	δ_i	MAX. DEFL'N
A	163	.0605
B	163+D	.0552
C	12	.0534
D	1	.0383
E	SLAB	.0211

FIG. 4.7 MIDSPAN TRANSVERSE PROFILES OF MOMENT AND DEFLECTION FOR VARIOUS ANISOTROPIC RATIOS, δ_i EDGE LOAD, ANGLE OF SKEW = 0°

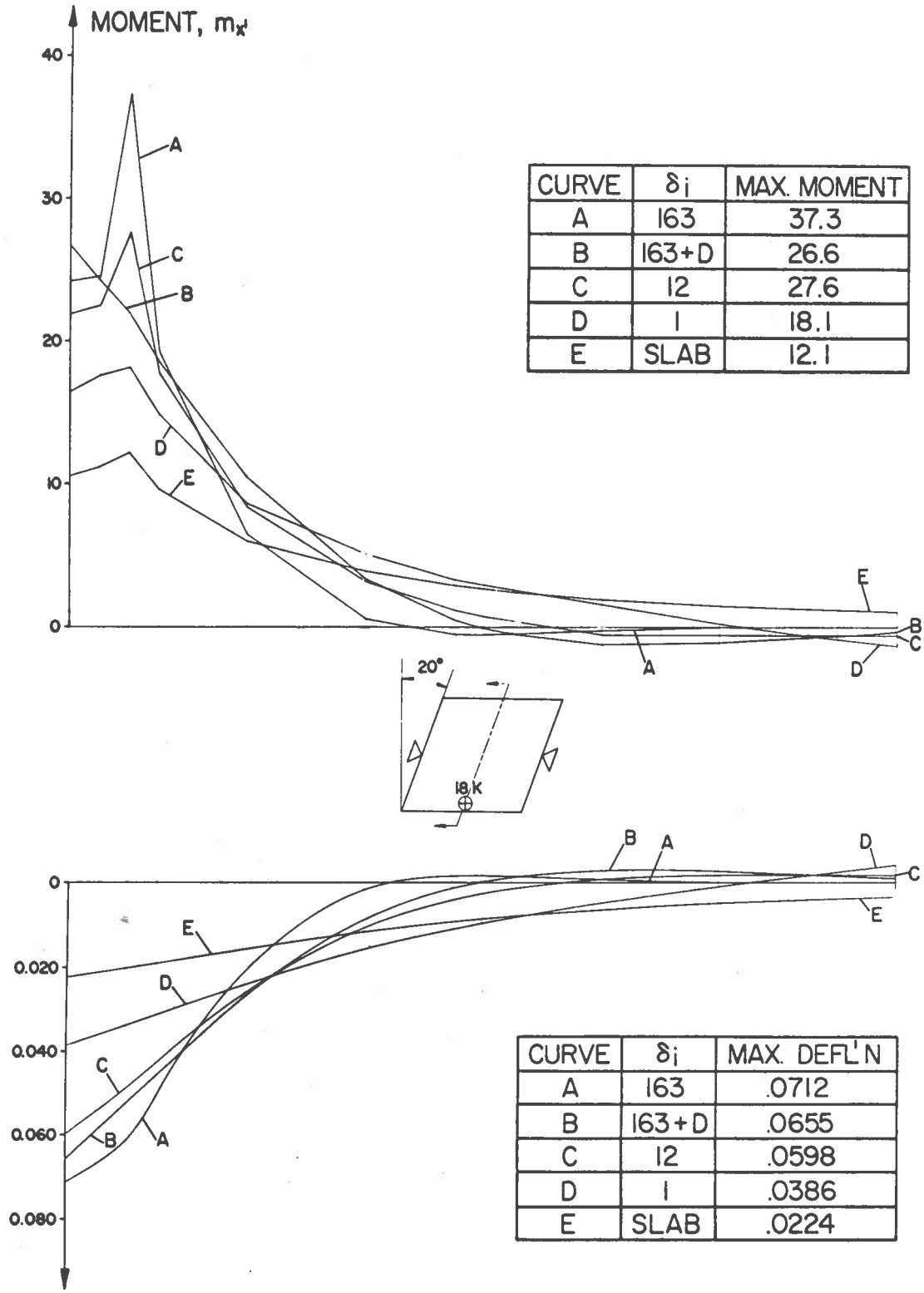

CURVE	δ_i	MAX. MOMENT
A	163	37.3
B	163+D	26.6
C	12	27.6
D	1	18.1
E	SLAB	12.1

CURVE	δ_i	MAX. DEFL'N
A	163	.0712
B	163+D	.0655
C	12	.0598
D	1	.0386
E	SLAB	.0224

FIG. 4.8 MIDSPAN TRANSVERSE PROFILES OF MOMENT AND DEFLECTION FOR VARIOUS ANISOTROPIC RATIOS, δ_i EDGE LOAD, ANGLE OF SKEW=20°

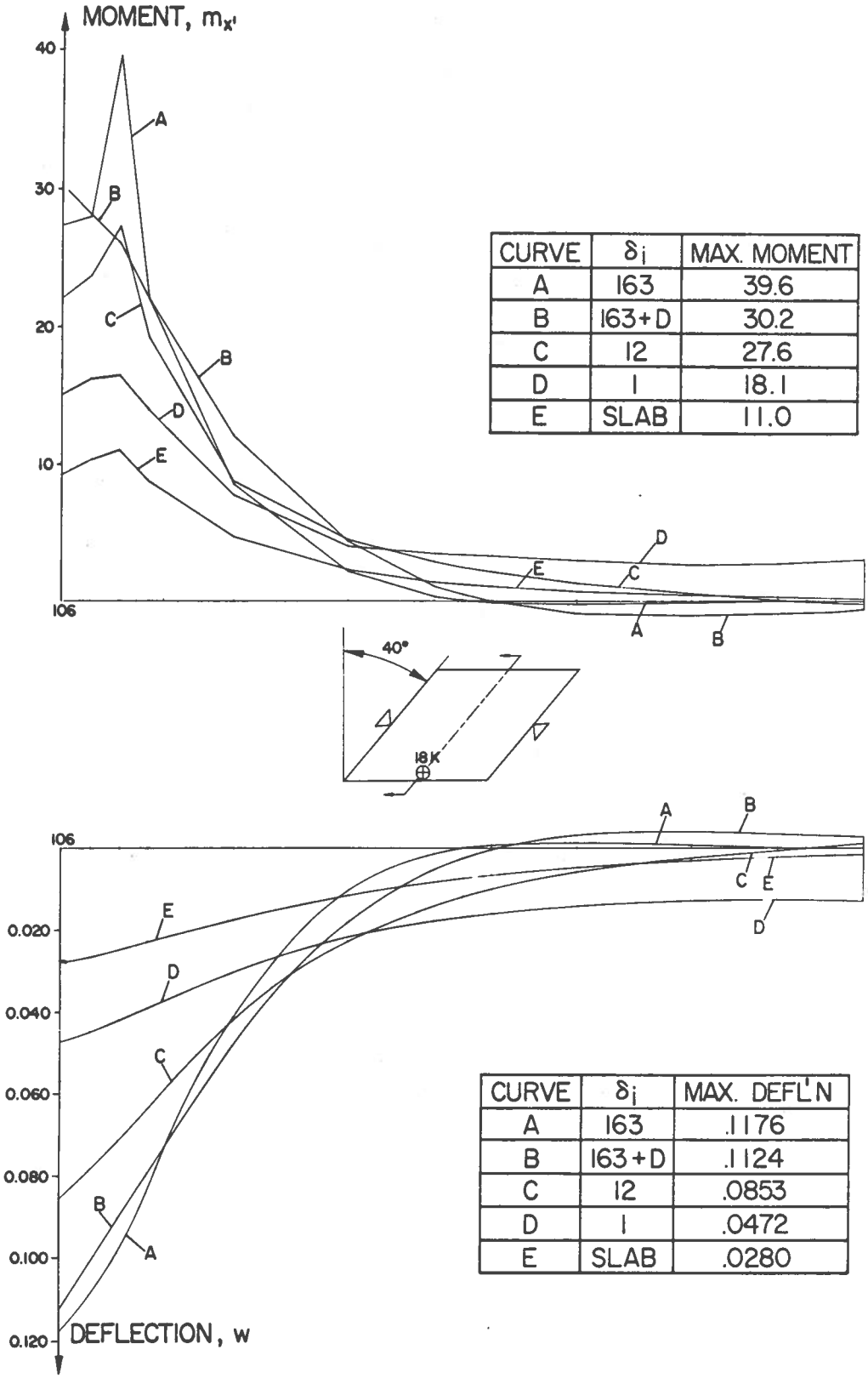

CURVE	δ_i	MAX. MOMENT
A	163	39.6
B	163+D	30.2
C	12	27.6
D	1	18.1
E	SLAB	11.0

CURVE	δ_i	MAX. DEFL'N
A	163	.1176
B	163+D	.1124
C	12	.0853
D	1	.0472
E	SLAB	.0280

FIG. 4.9 MIDSPAN TRANSVERSE PROFILES OF MOMENT AND DEFLECTION FOR VARIOUS ANISOTROPIC RATIOS, δ_i EDGE LOAD, ANGLE OF SKEW = 40°

CURVE	δ_i	MAX. MOMENT
A	163	22.05
B	163+D	22.2
C	12	21.8
D	1	22.05
E	SLAB	21.8

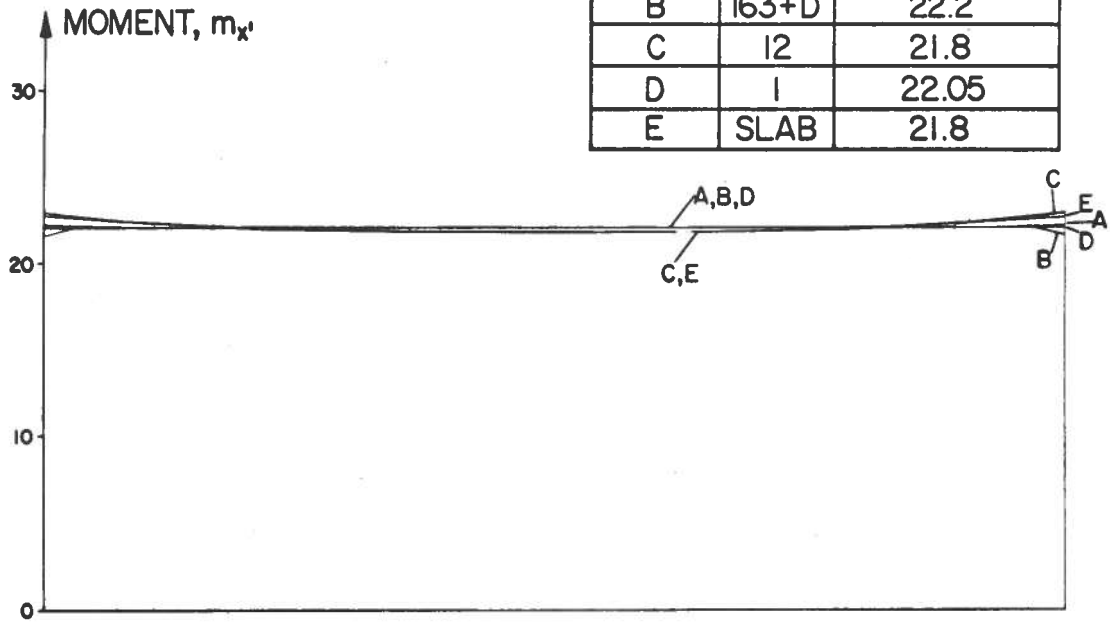

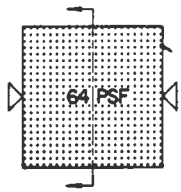

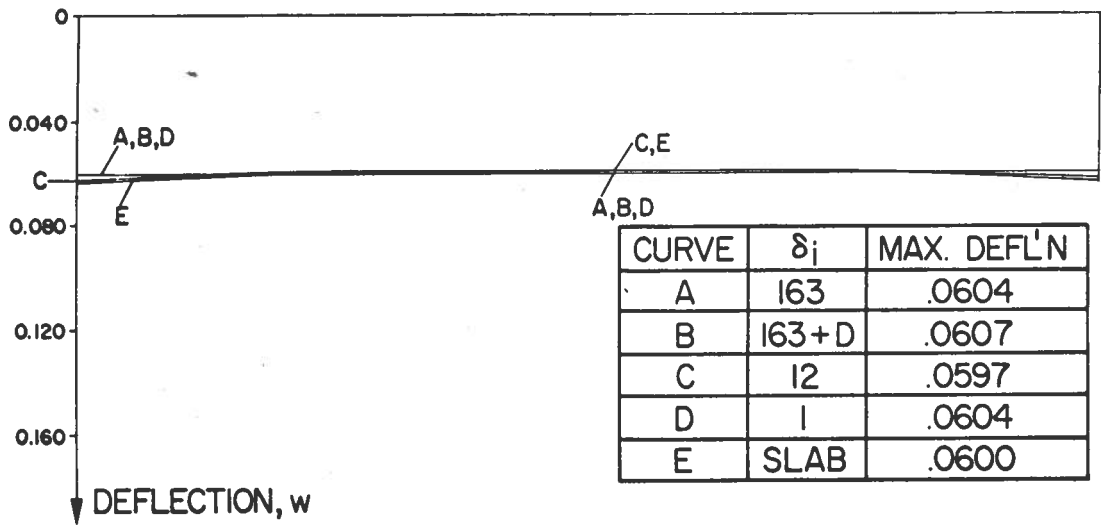

CURVE	δ_i	MAX. DEFL'N
A	163	.0604
B	163+D	.0607
C	12	.0597
D	1	.0604
E	SLAB	.0600

FIG. 4.10 MIDSPAN TRANSVERSE PROFILES OF MOMENT AND DEFLECTION FOR VARIOUS ANISOTROPIC RATIOS, δ_i UNIFORM LOAD. ANGLE OF SKEW=0°

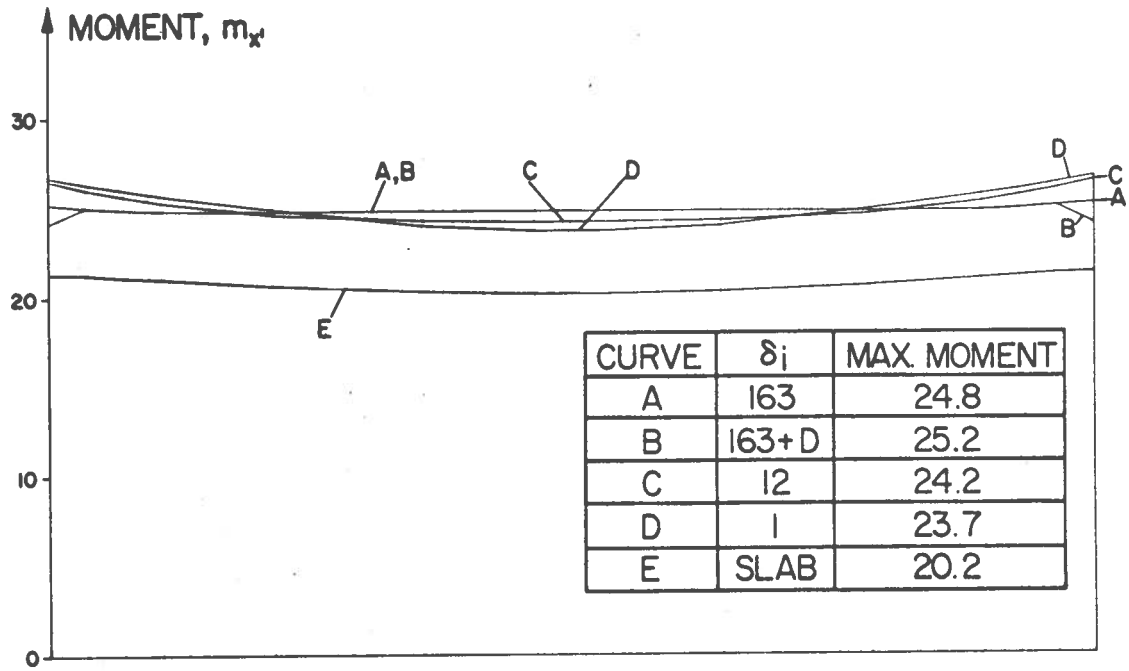

CURVE	δ_i	MAX. MOMENT
A	163	24.8
B	163+D	25.2
C	12	24.2
D	1	23.7
E	SLAB	20.2

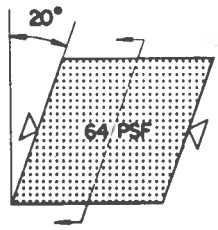

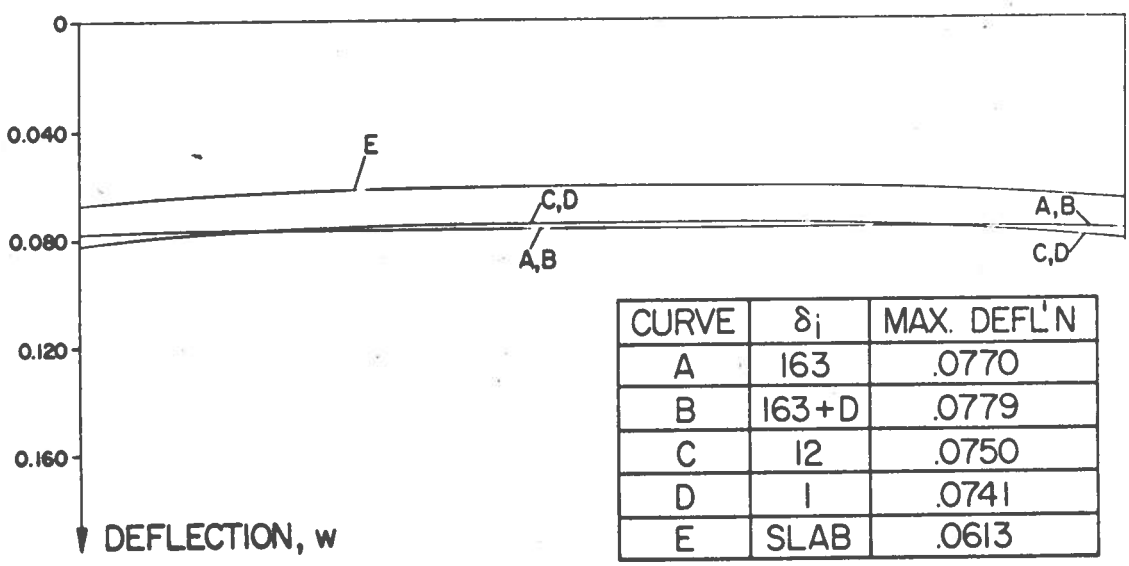

CURVE	δ_i	MAX. DEFL'N
A	163	.0770
B	163+D	.0779
C	12	.0750
D	1	.0741
E	SLAB	.0613

FIG. 4.11 MIDSPAN TRANSVERSE PROFILES OF MOMENT AND DEFLECTION FOR VARIOUS ANISOTROPIC RATIOS, δ_i UNIFORM LOAD, ANGLE OF SKEW=20°

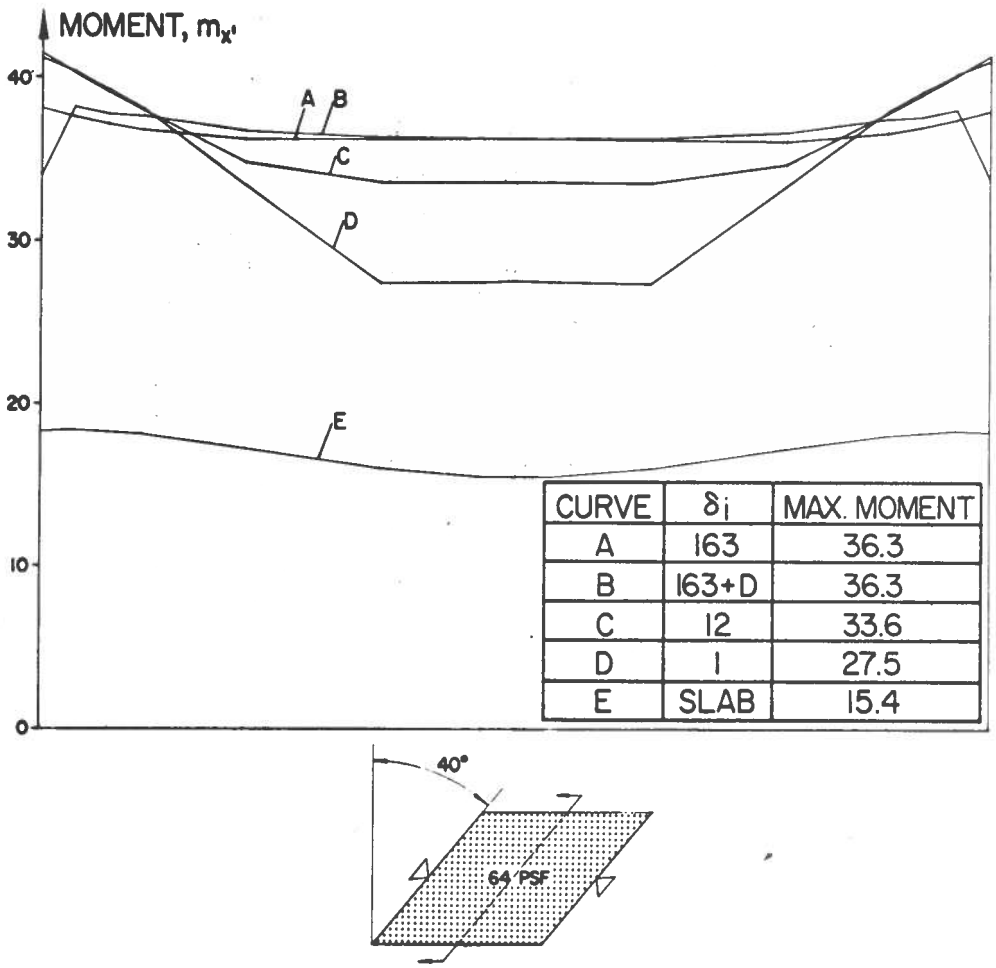

CURVE	δ_i	MAX. MOMENT
A	163	36.3
B	163+D	36.3
C	12	33.6
D	1	27.5
E	SLAB	15.4

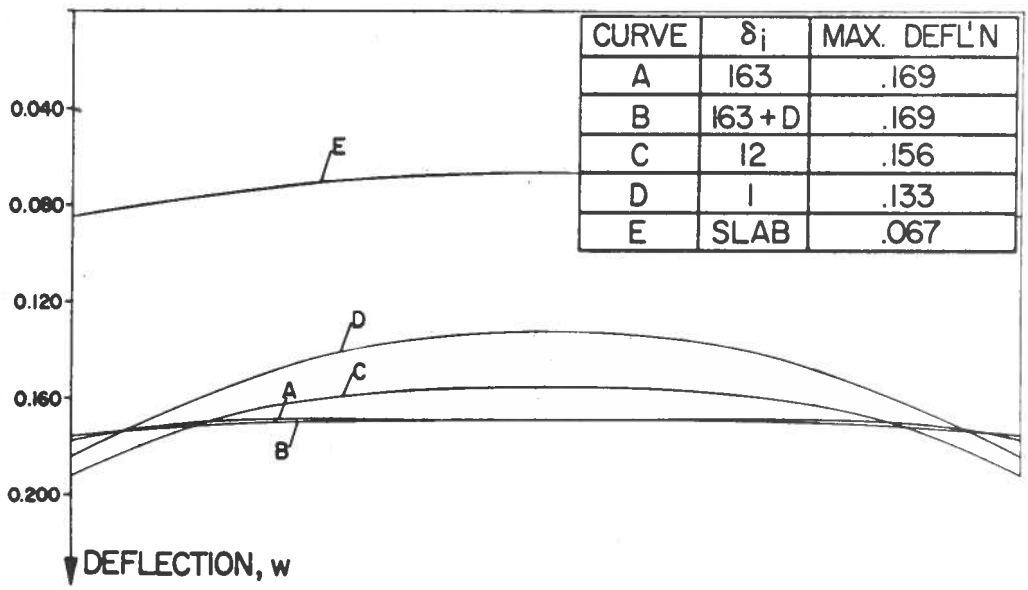

CURVE	δ_i	MAX. DEFL'N
A	163	.169
B	163+D	.169
C	12	.156
D	1	.133
E	SLAB	.067

FIG. 4.12 MIDSPAN TRANSVERSE PROFILES OF MOMENT AND DEFLECTION FOR VARIOUS ANISOTROPIC RATIOS, δ_i UNIFORM LOAD, ANGLE OF SKEW=40°

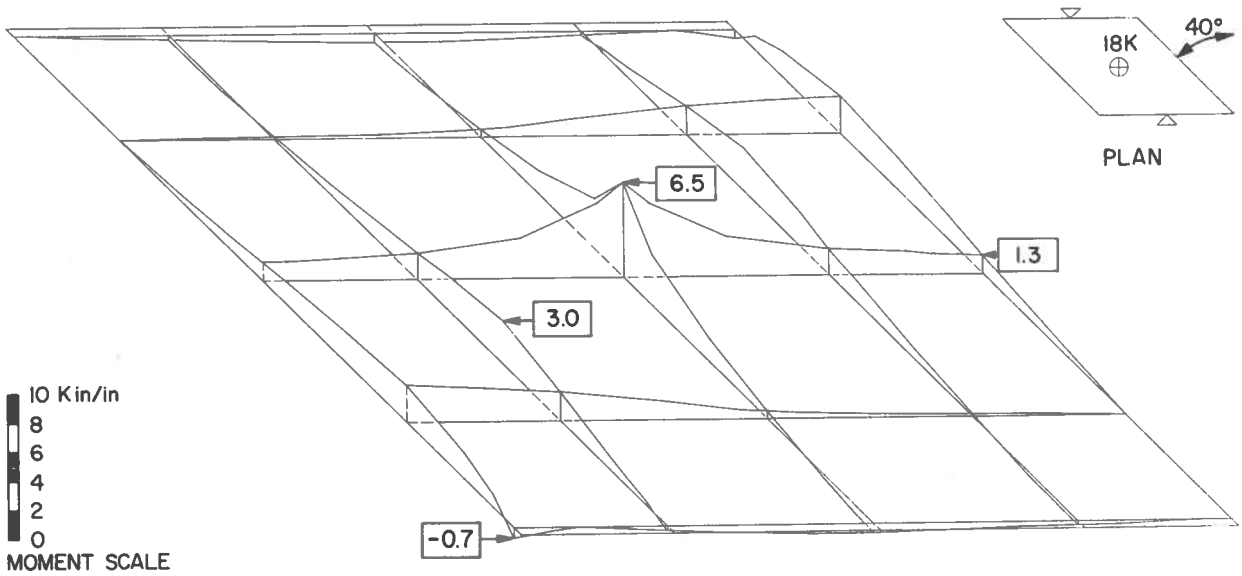

FIG. 4.13 MOMENT SURFACE, $m_{x'}$ CENTER LOAD

δ_i	SLAB
β	40°

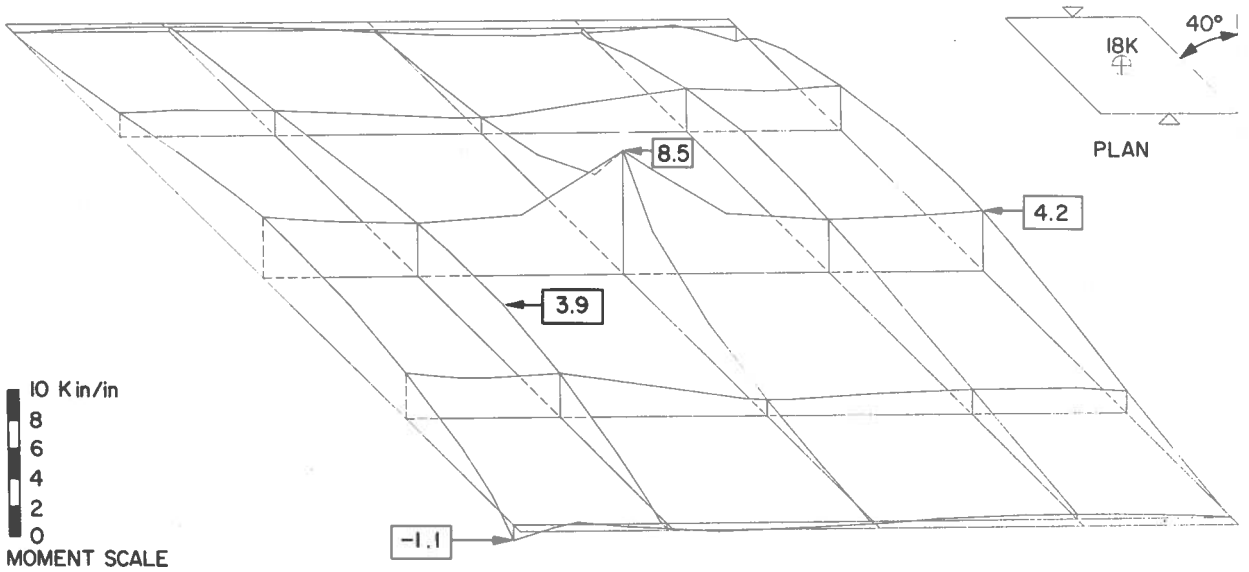

FIG. 4.14 MOMENT SURFACE, $m_{x'}$ CENTER LOAD

δ_i	1
β	40°

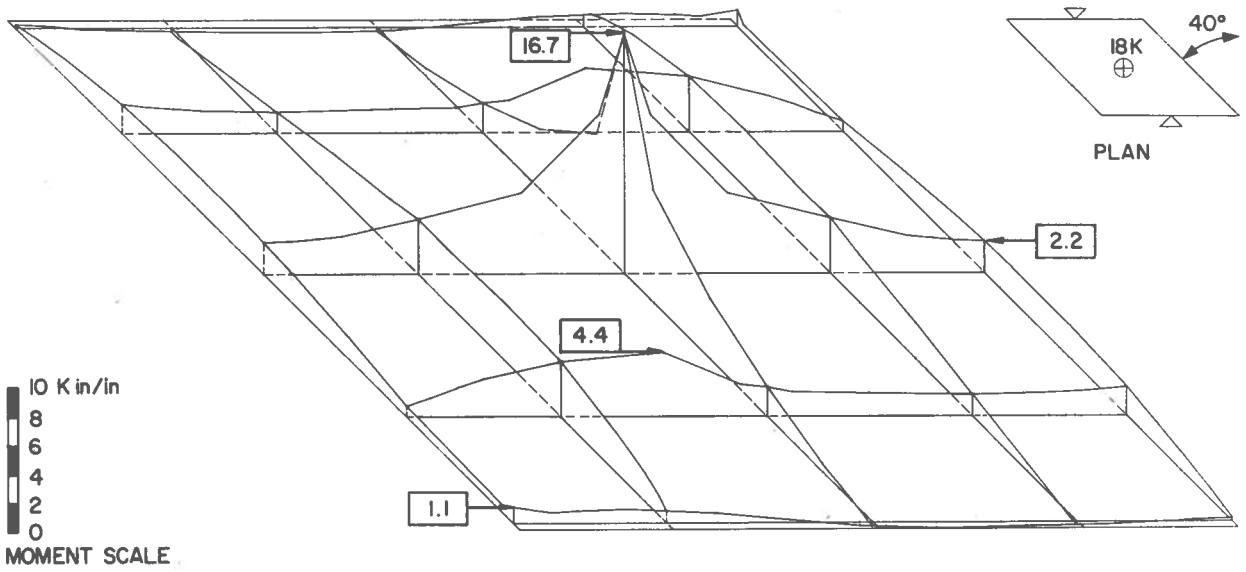

FIG. 4.15 MOMENT SURFACE, $m_{x'}$ CENTER LOAD

δ_i	12
β	40°

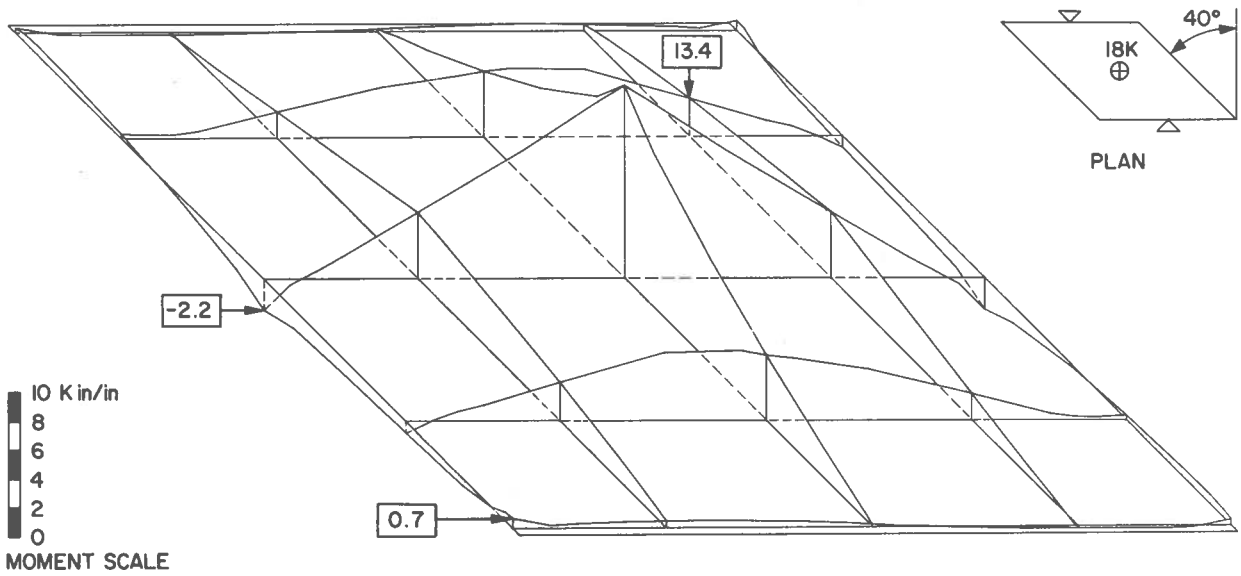

FIG. 4.16 MOMENT SURFACE, $m_{x'}$ CENTER LOAD

δ_i	163+D
β	40°

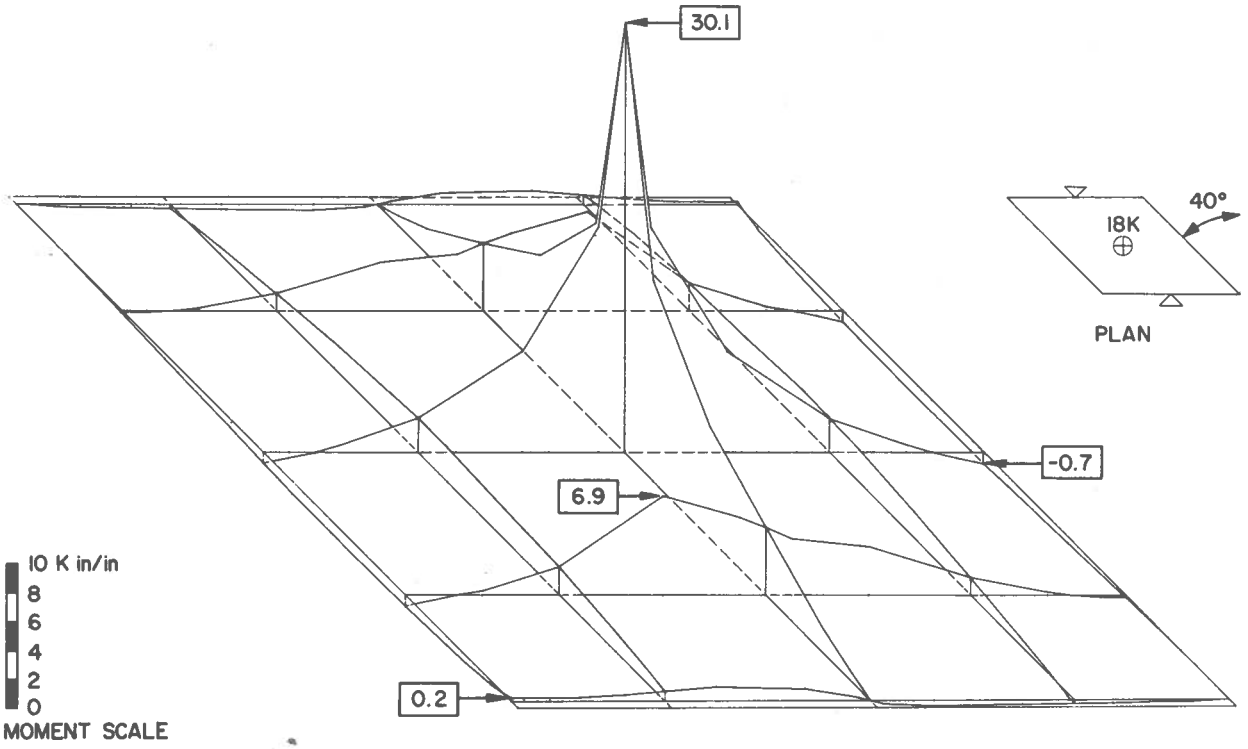

FIG. 4.17 MOMENT SURFACE, $m_{x'}$ CENTER LOAD

δ_i	163
β	40°

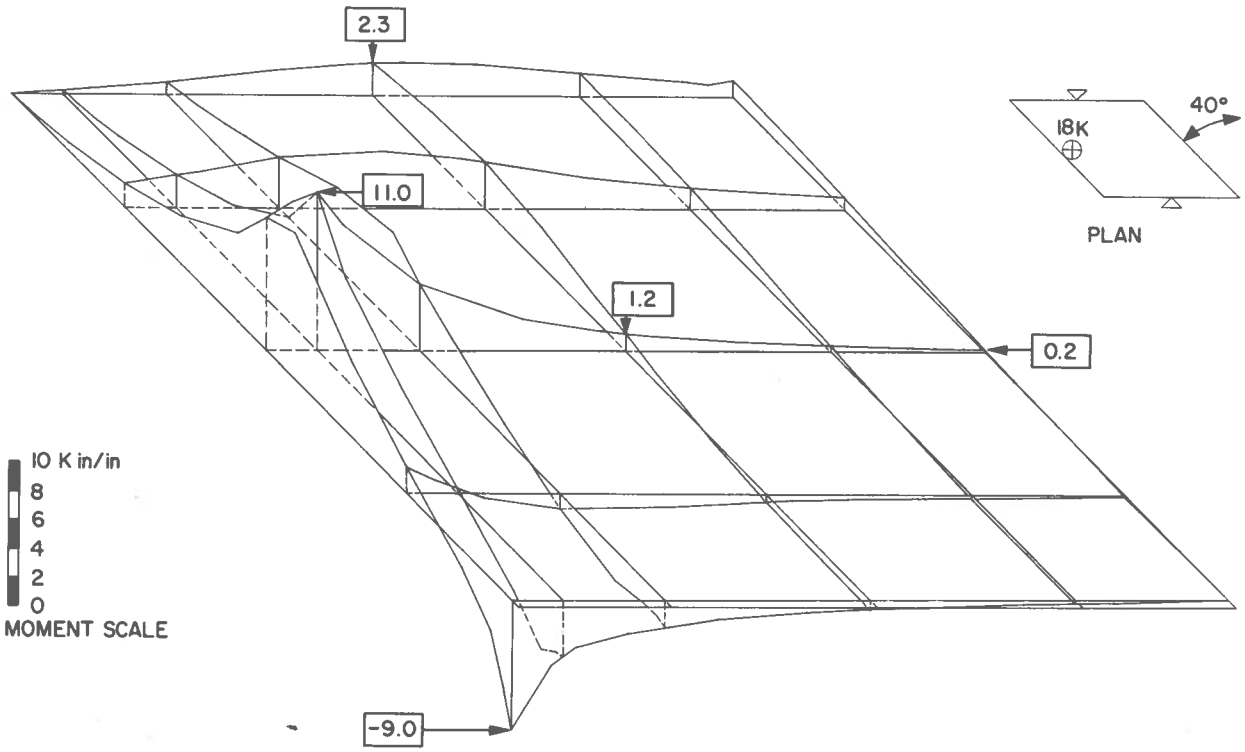

FIG. 4.18 MOMENT SURFACE, $m_{x'}$ EDGE LOAD

δ_i	SLAB
β	40°

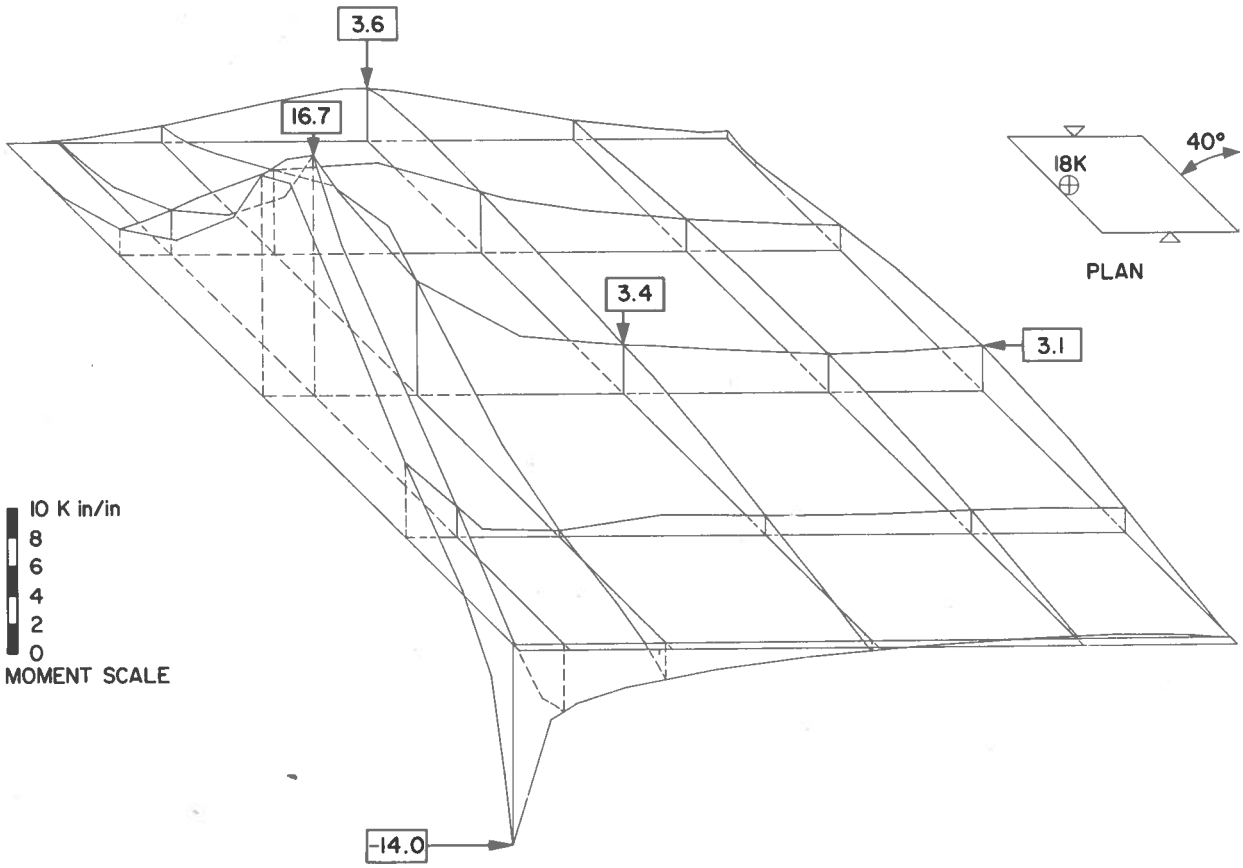

FIG. 4.19 MOMENT SURFACE, $m_{x'}$ EDGE LOAD

δ_i	1
β	40°

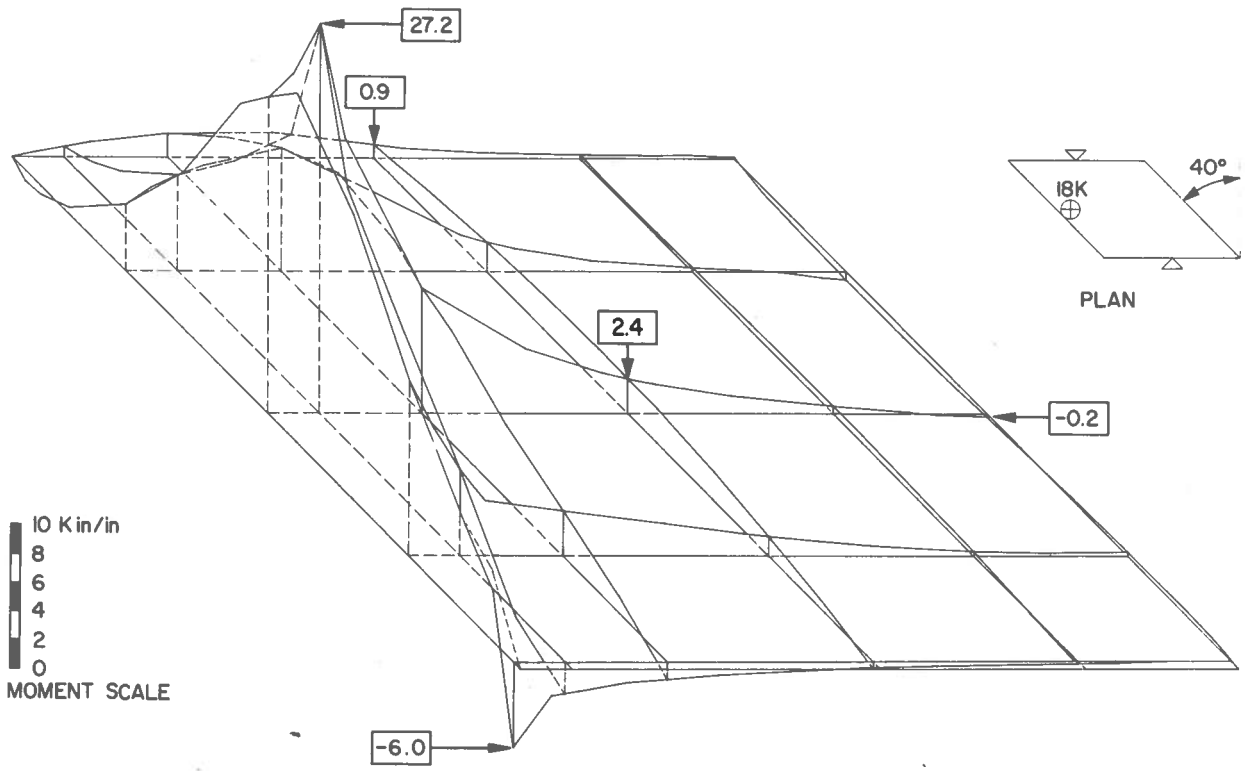

FIG. 4.20 MOMENT SURFACE, $m_{x'}$ EDGE LOAD

δ_i	12
β	40°

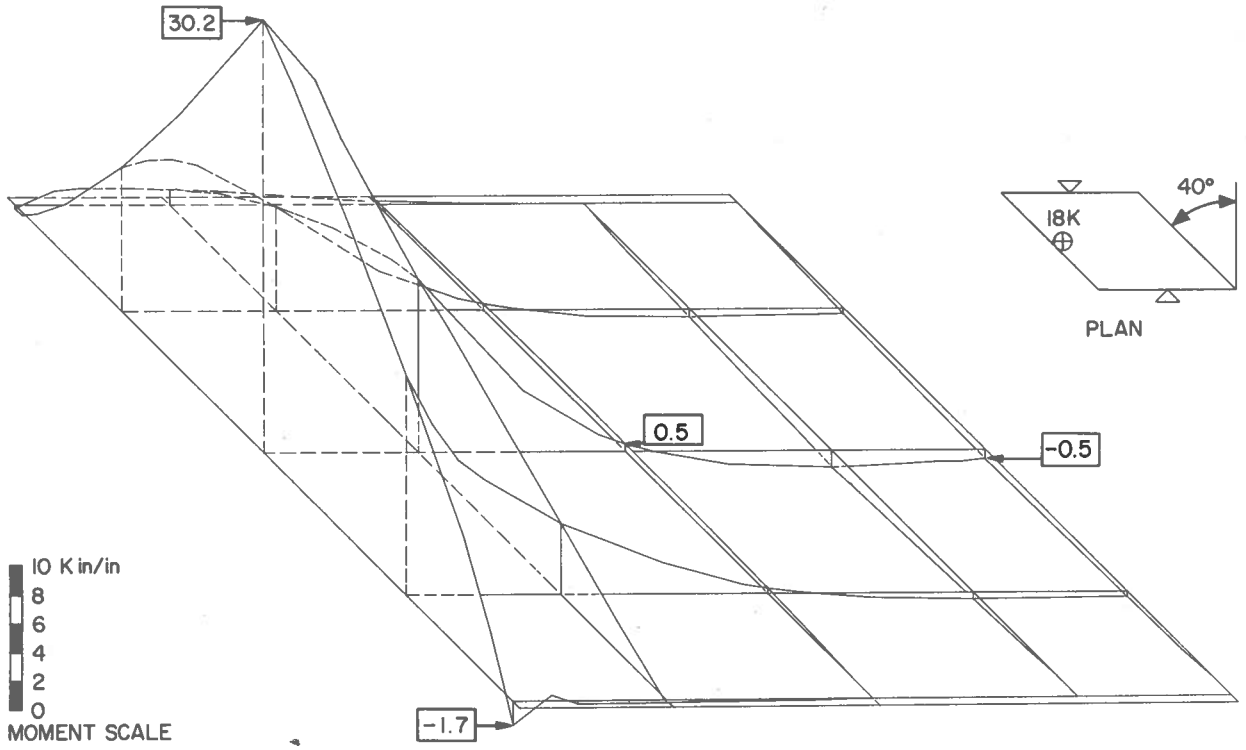

FIG. 4.21 MOMENT SURFACE, $m_{x'}$ EDGE LOAD

δ_i	163+D
β	40°

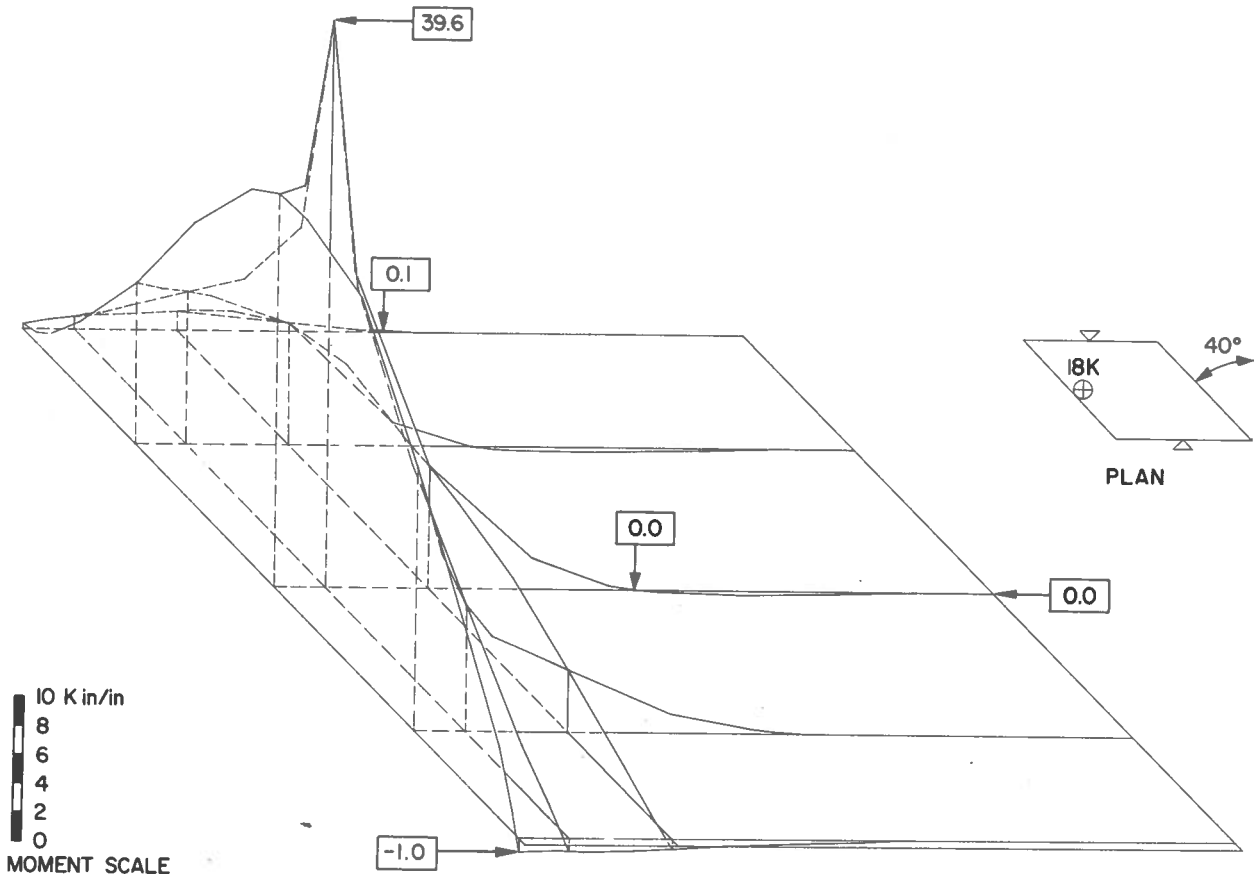

FIG. 4.22 MOMENT SURFACE, $m_{x'}$ EDGE LOAD

δ_i	163
β	40°

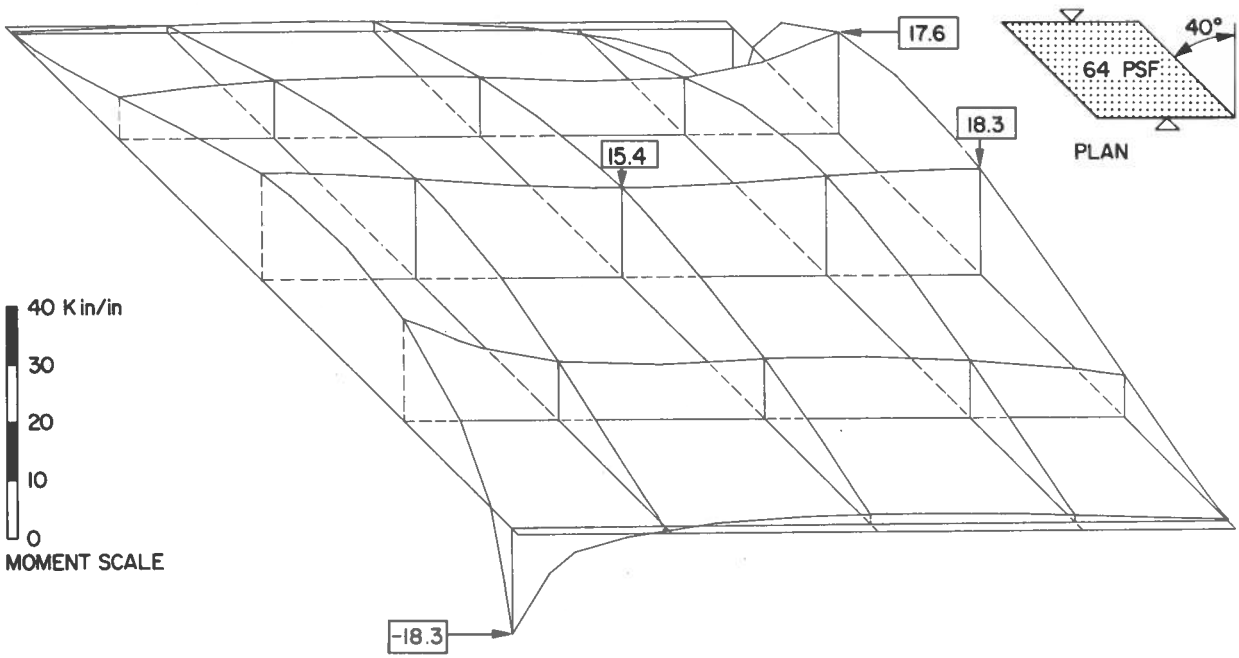

FIG. 4.23 MOMENT SURFACE, $m_{x'}$ UNIFORM LOAD

δ_i	SLAB
β	40°

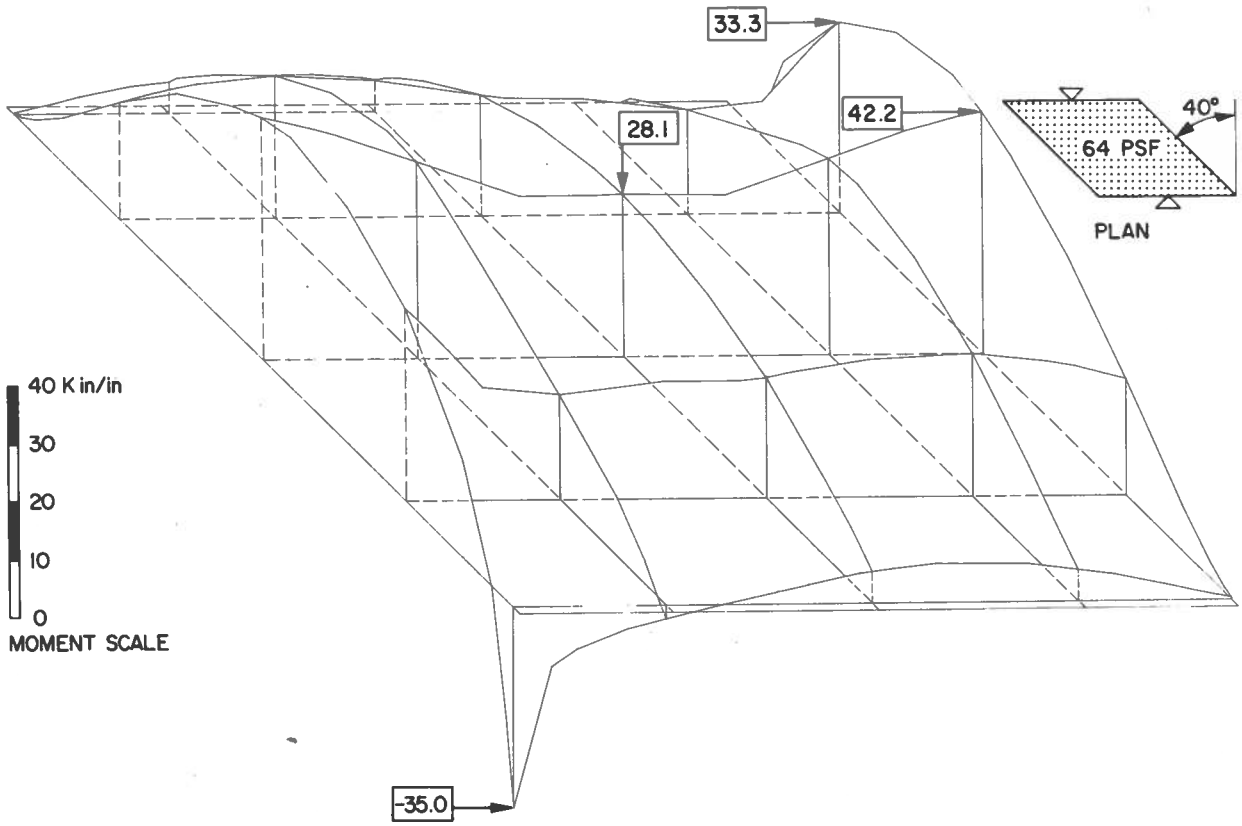

FIG. 4.24 MOMENT SURFACE, $m_{x'}$ UNIFORM LOAD

δi	1
β	40°

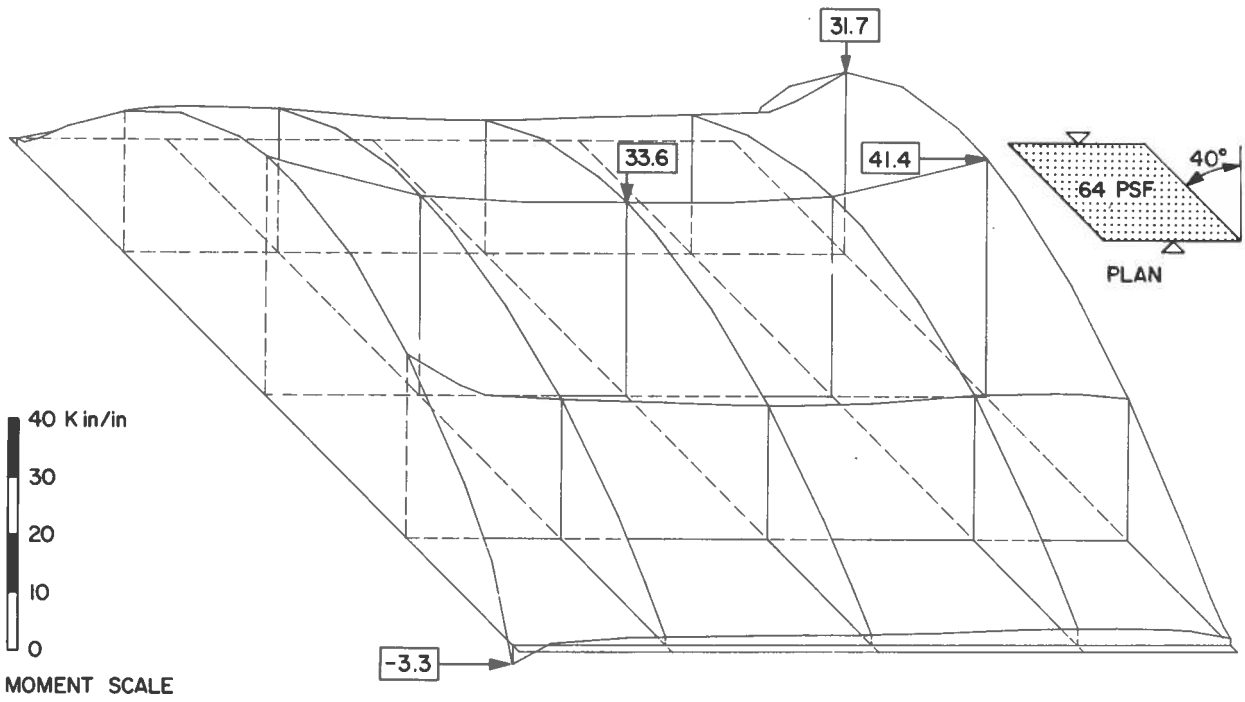

FIG. 4.25 MOMENT SURFACE, $m_{x'}$ UNIFORM LOAD

δ_i	12
β	40°

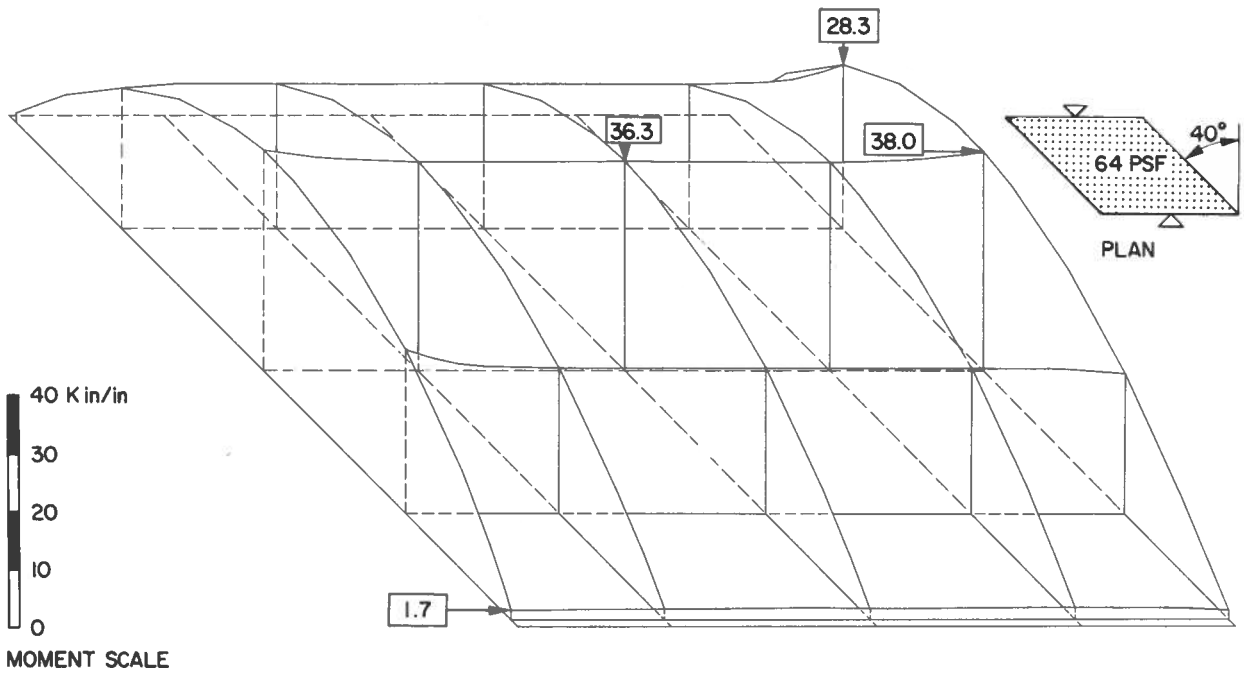

FIG. 4.26 MOMENT SURFACE, $m_{x'}$ UNIFORM LOAD

δ_i	163
β	40°

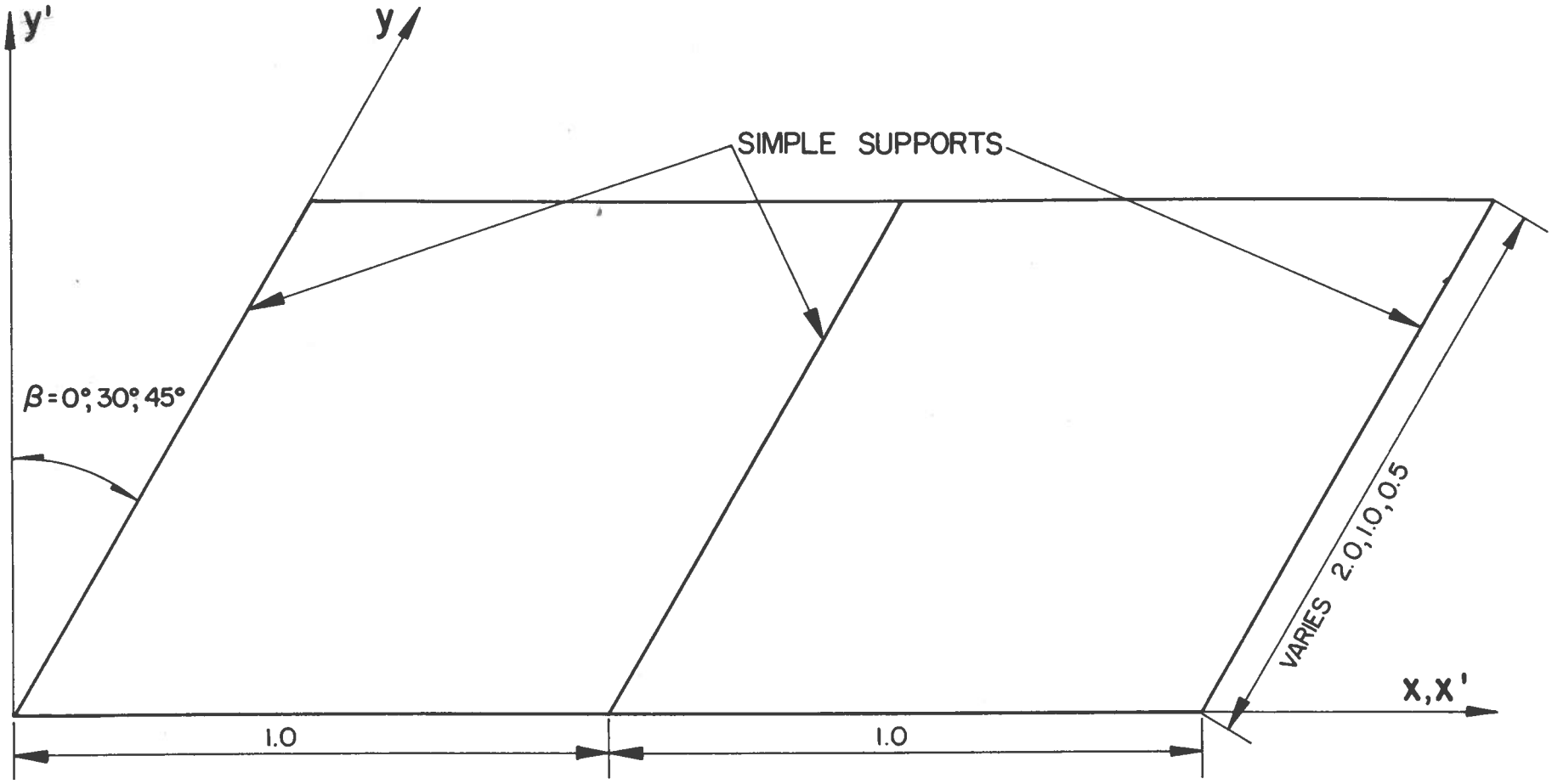

FIG. 5.1 PLAN VIEW OF CONTINUOUS SLAB

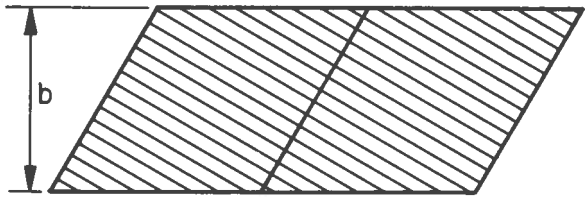

LOAD CASE 1

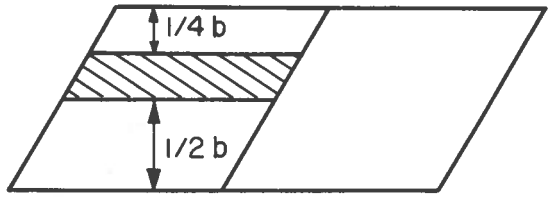

LOAD CASE 4

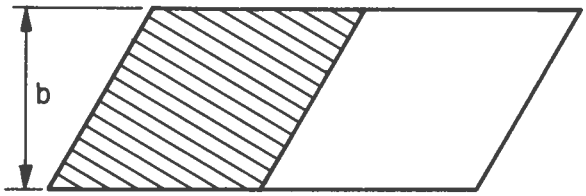

LOAD CASE 2

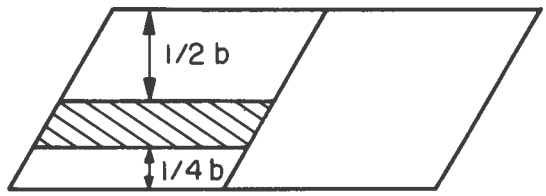

LOAD CASE 5

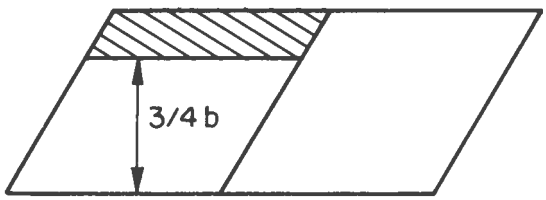

LOAD CASE 3

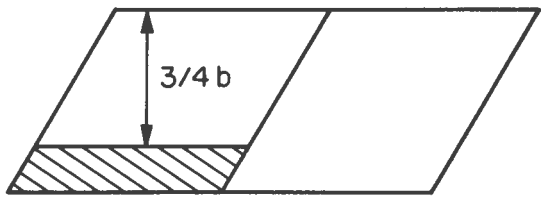

LOAD CASE 6

UNIFORM LOAD INTENSITY = 1.0

FIG. 5.2 LOAD CASES

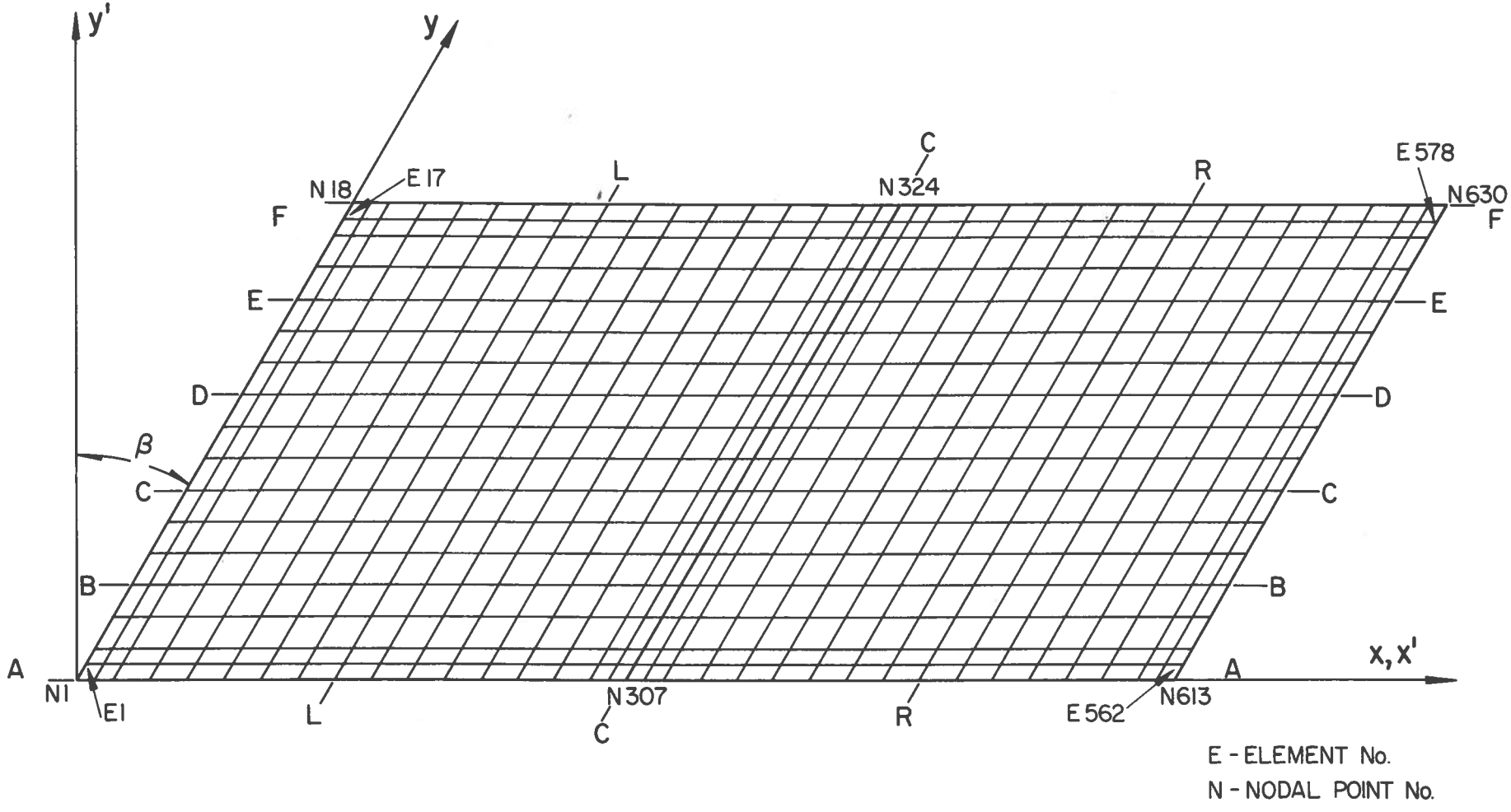

FIG. 5.3 FINITE ELEMENT MESH LAYOUT AND SECTIONS USED FOR RESULT PRESENTATION

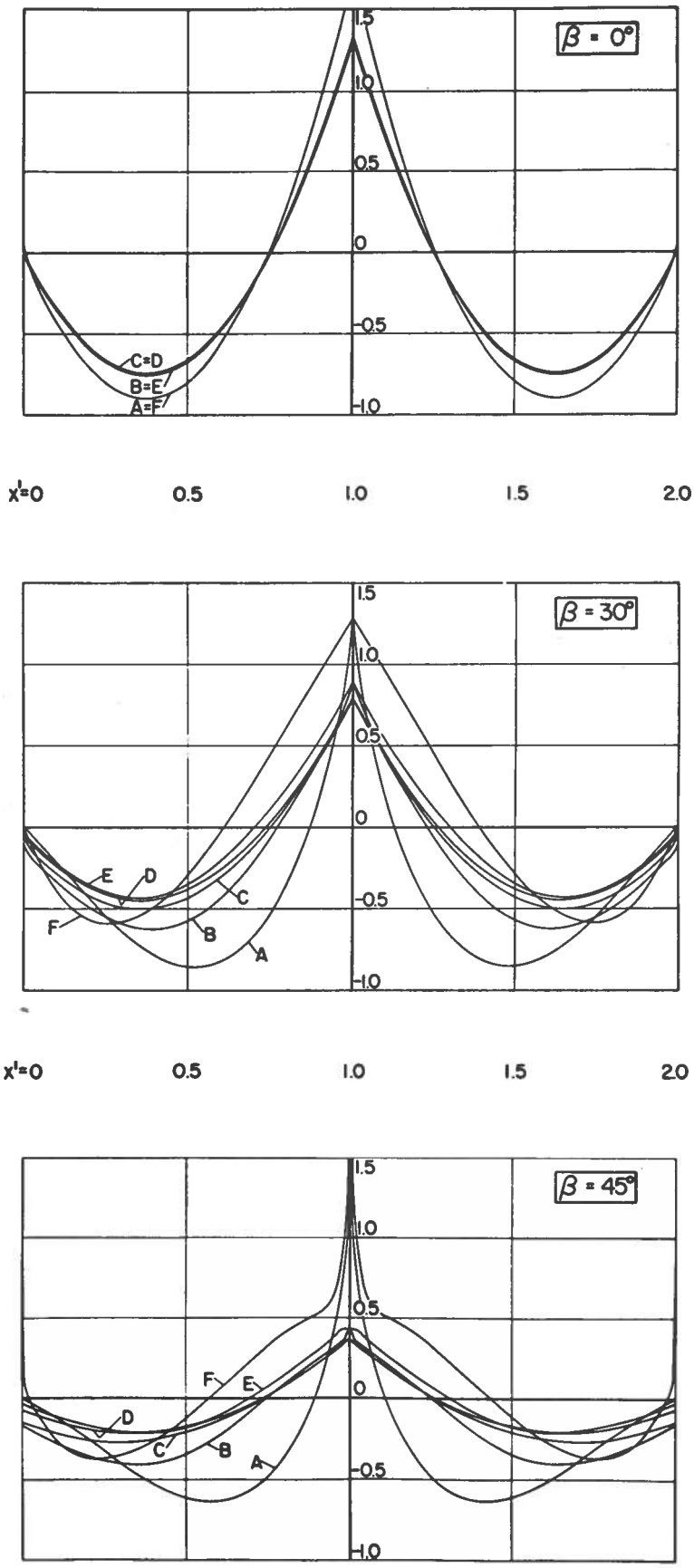

FIG. 5.4 LONGITUDINAL CURVATURE, $\chi_{x'}$ AGAINST x'
CASE 2.0 - 1

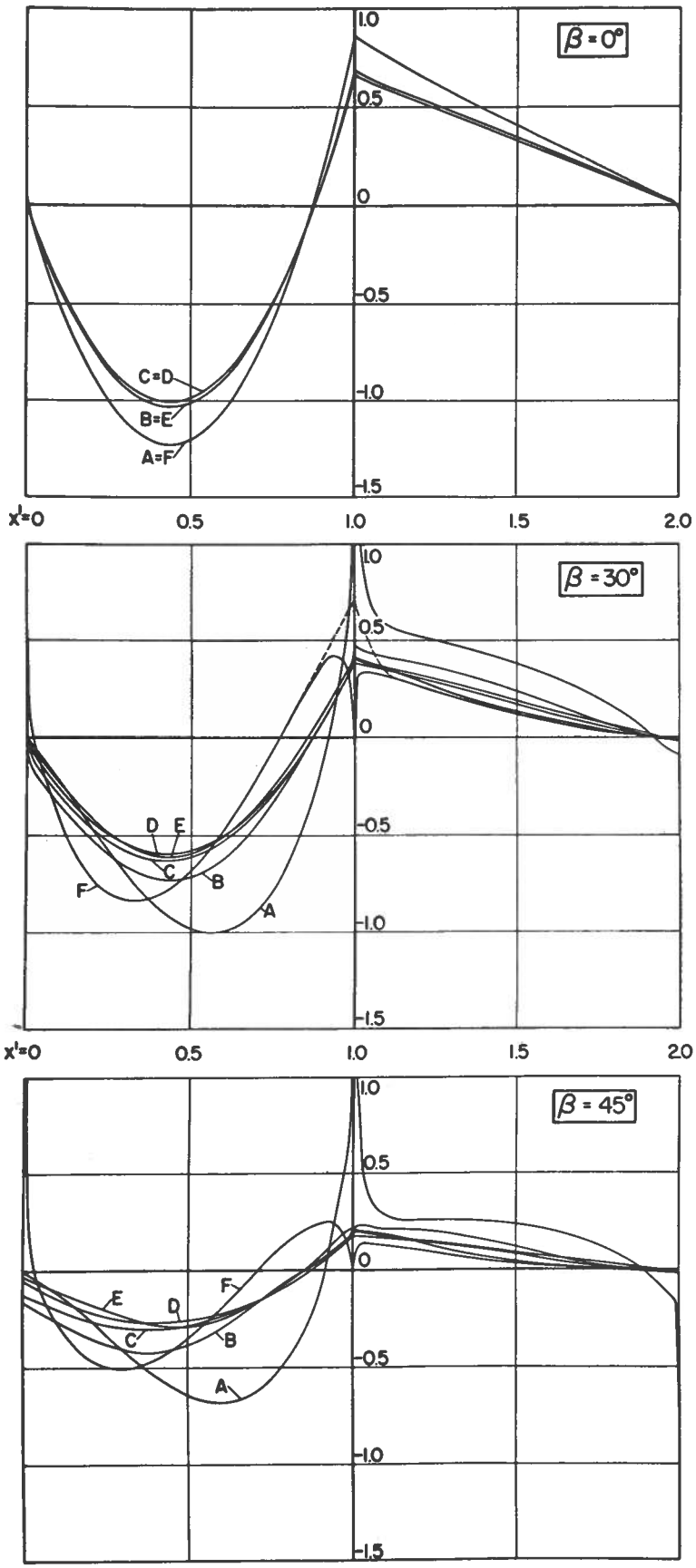

FIG. 5.5 LONGITUDINAL CURVATURE, $\chi_{x'}$ AGAINST x'
CASE 2.0 - 2

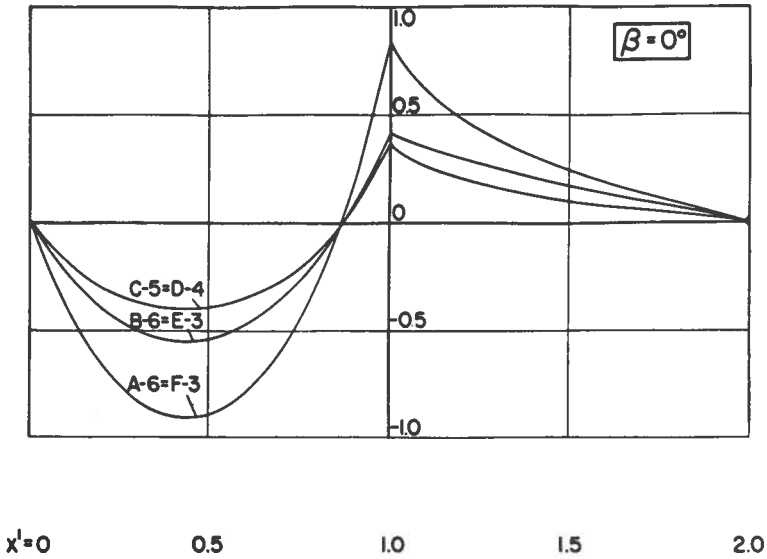

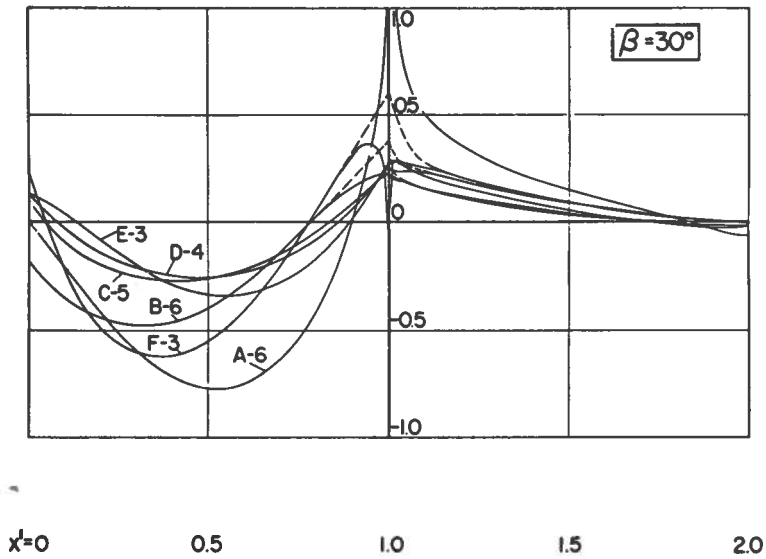

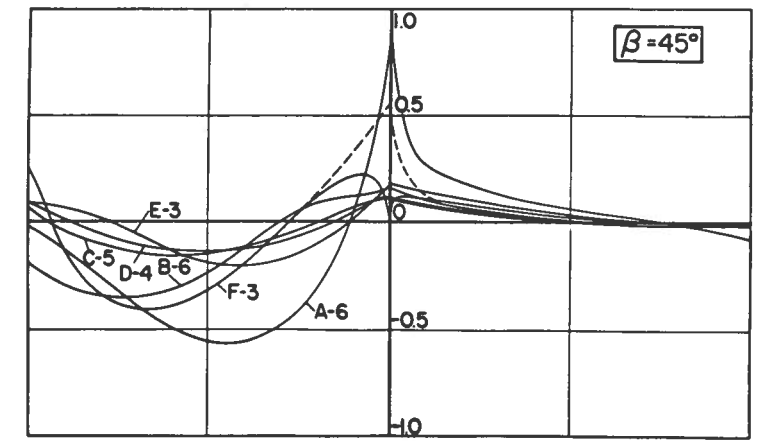

FIG. 5.6 LONGITUDINAL CURVATURE, $\chi_{x'}$ AGAINST x'
CASE 2.0 - 3,4,5,6

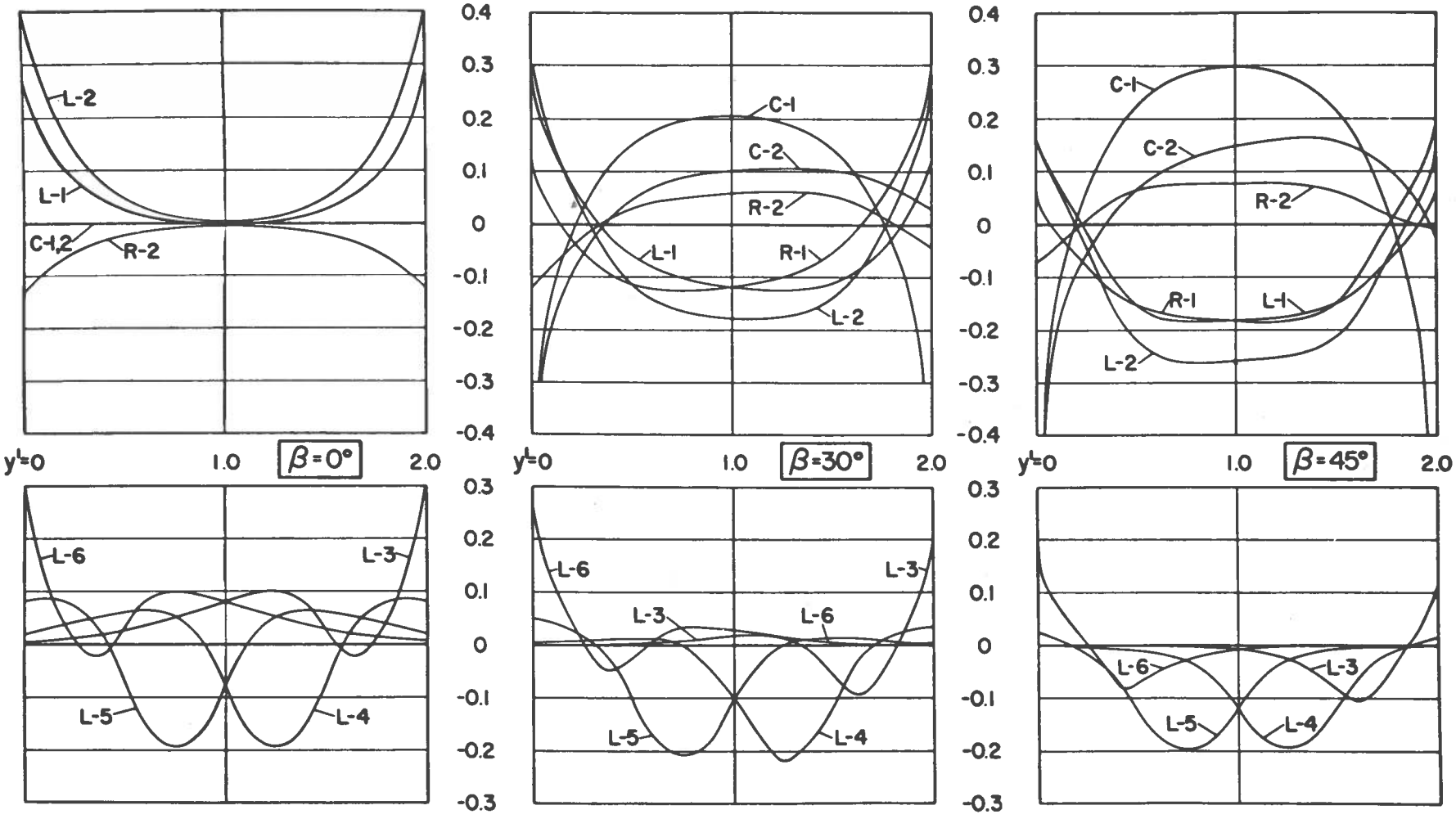

FIG. 5.7 TRANSVERSE CURVATURE, $\chi_{y'}$ AGAINST y' - CASE 2.0-1,2,3,4,5,6

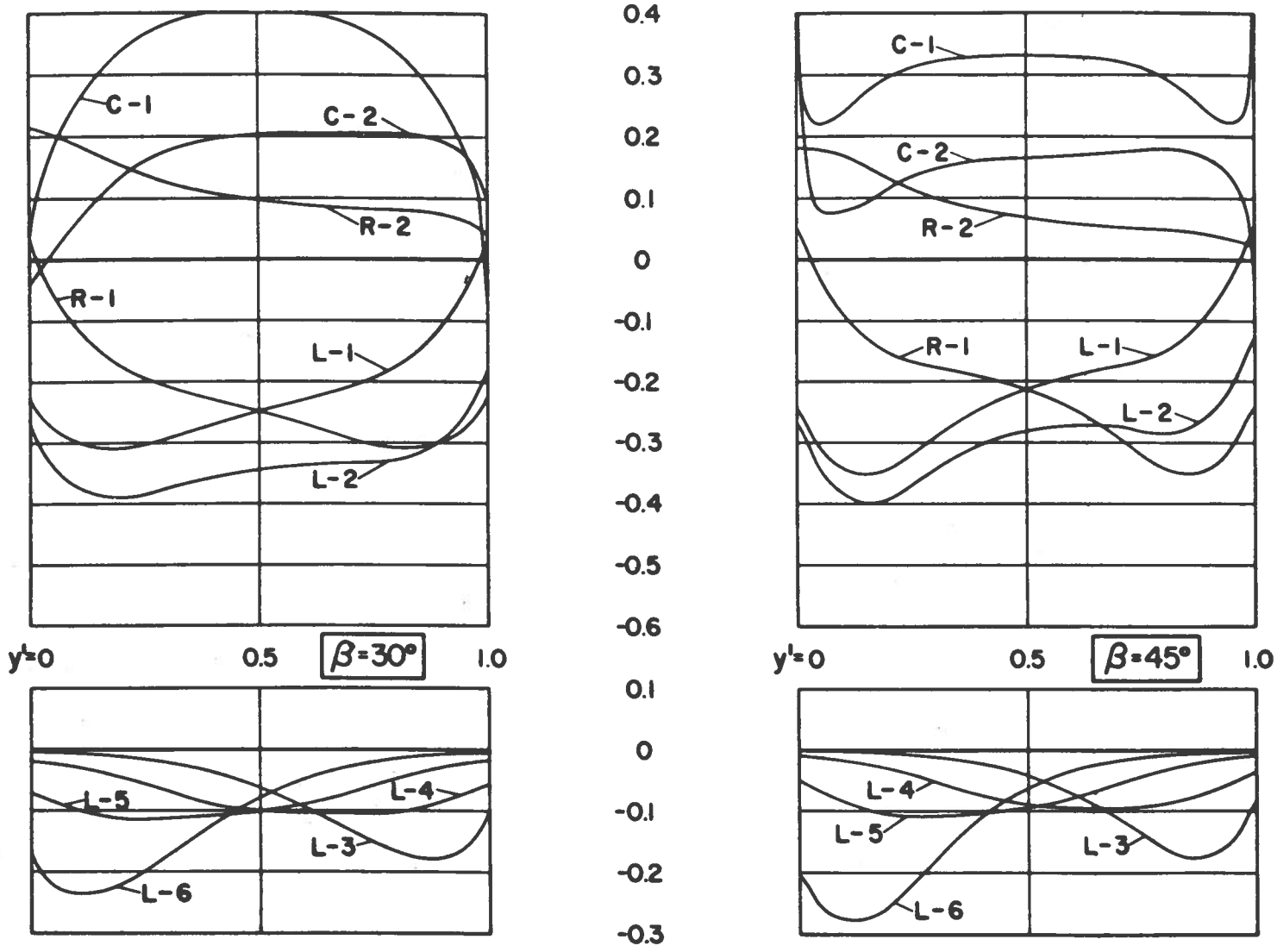

FIG. 5.8 TWIST, $\chi_{xy'}$ AGAINST y' - CASE 2.0-1,2,3,4,5,6

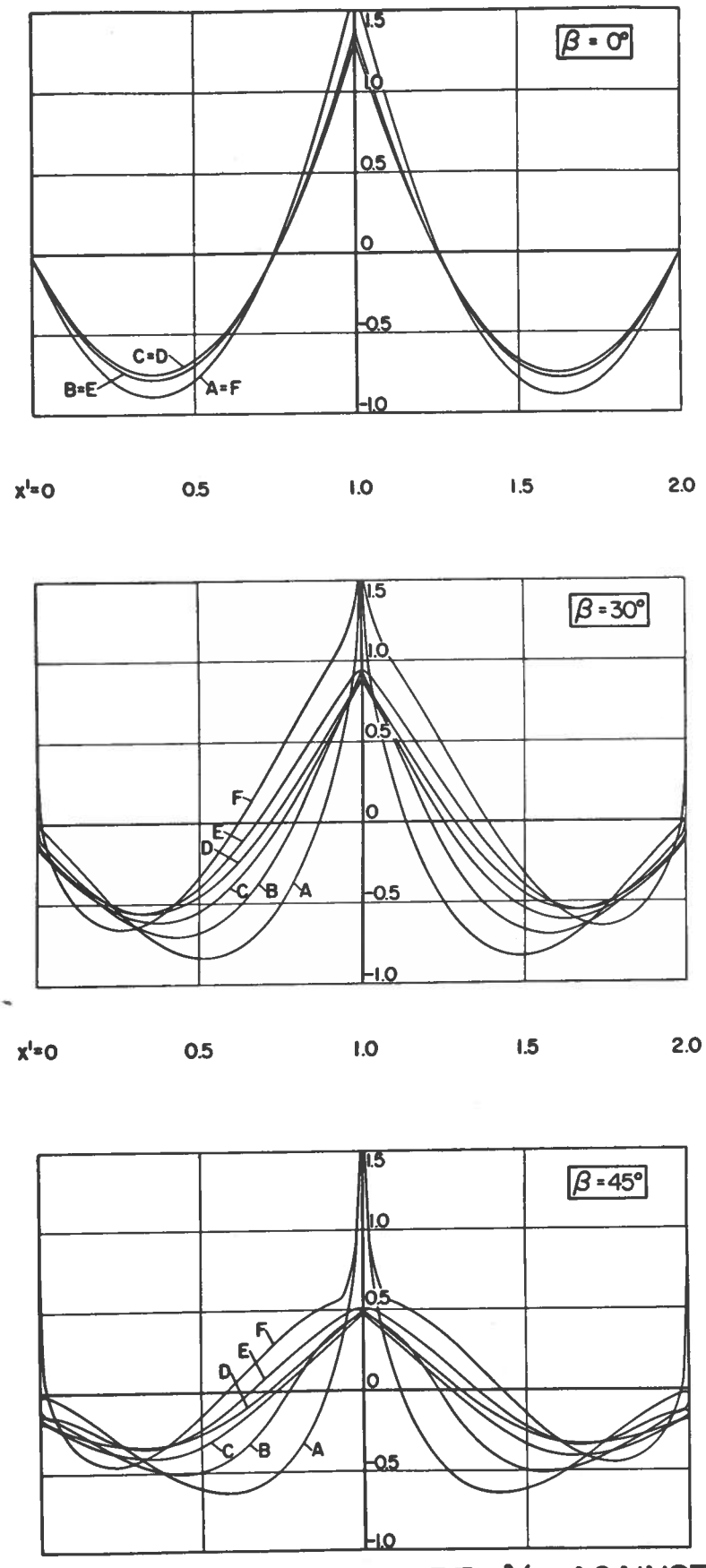

FIG. 5.9 LONGITUDINAL CURVATURE, $\chi_{x'}$ AGAINST x'
CASE 1.0 - 1

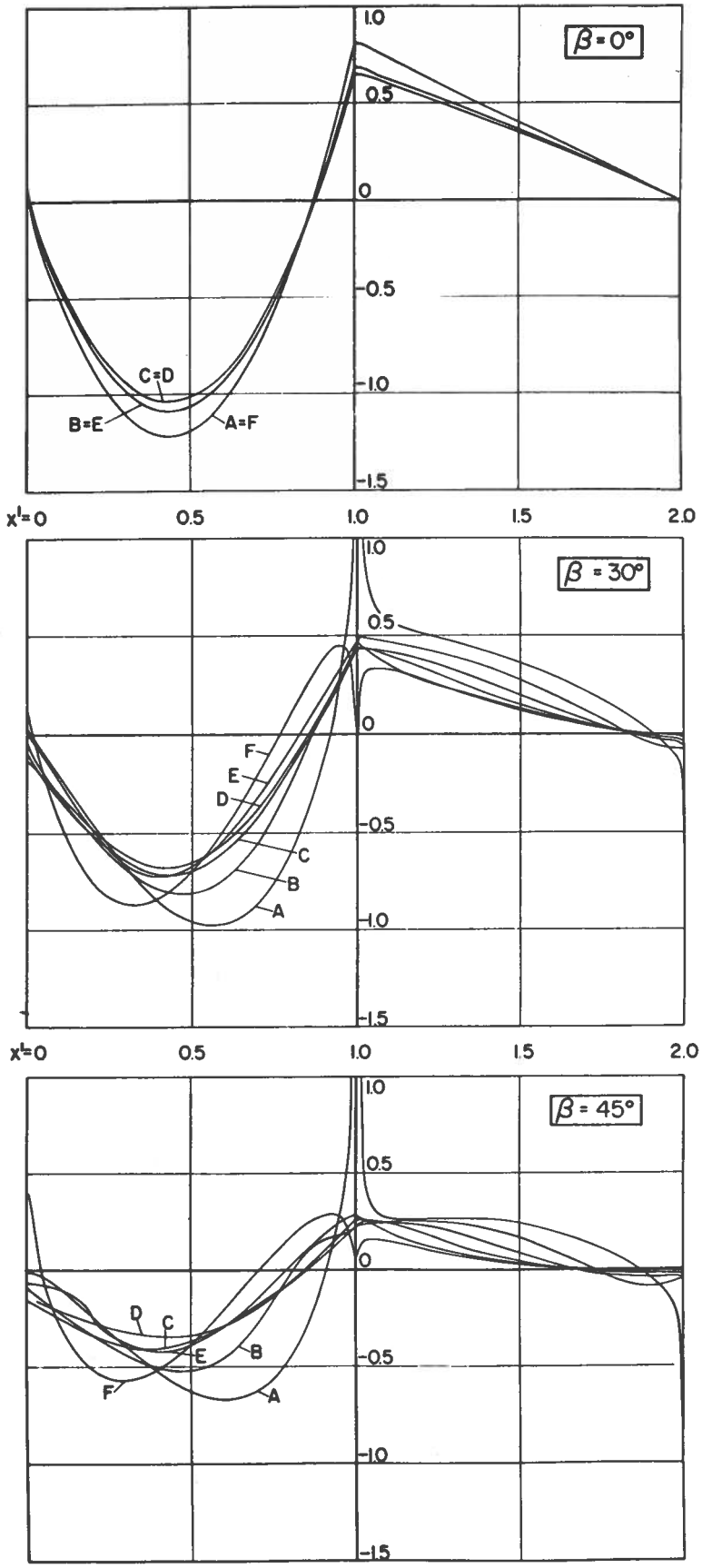

FIG. 5.10 LONGITUDINAL CURVATURE, $\chi_{x'}$ AGAINST x'
CASE 1.0 - 2

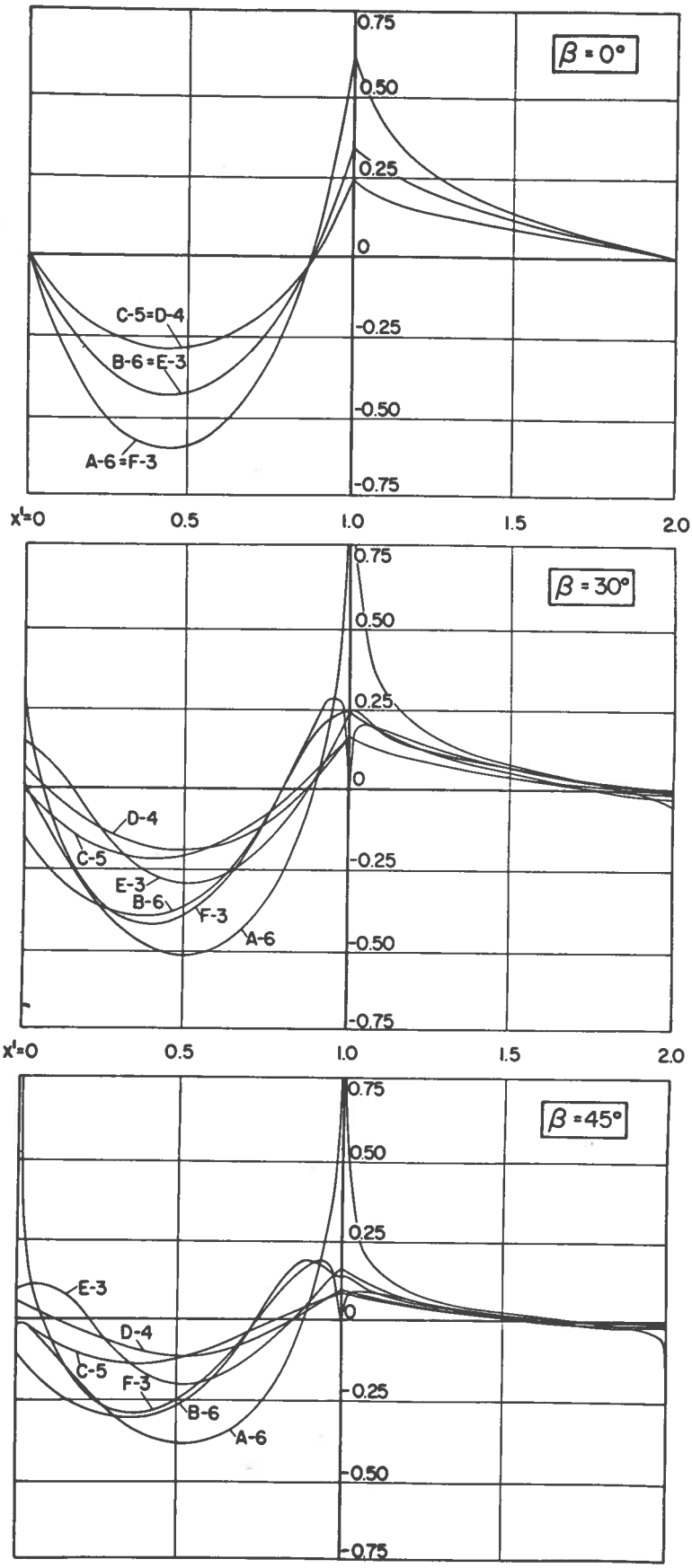

FIG. 5.11 LONGITUDINAL CURVATURE, $\chi_{x'}$ AGAINST x'
CASE 1.0 -3,4,5,6

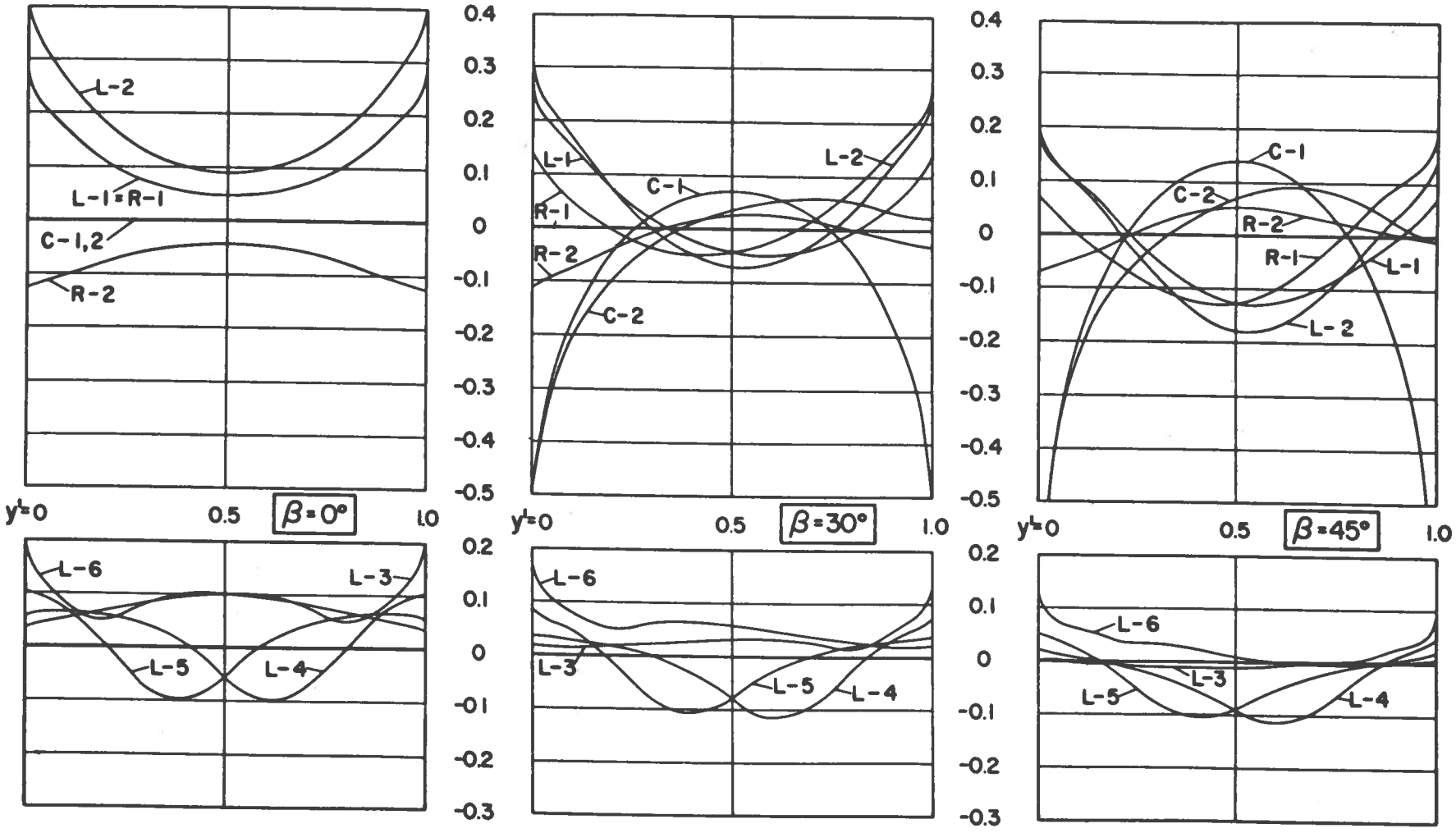

FIG. 5.12 TRANSVERSE CURVATURE, $\chi_{y'}$ AGAINST y' - CASE 1.0-1,2,3,4,5,6

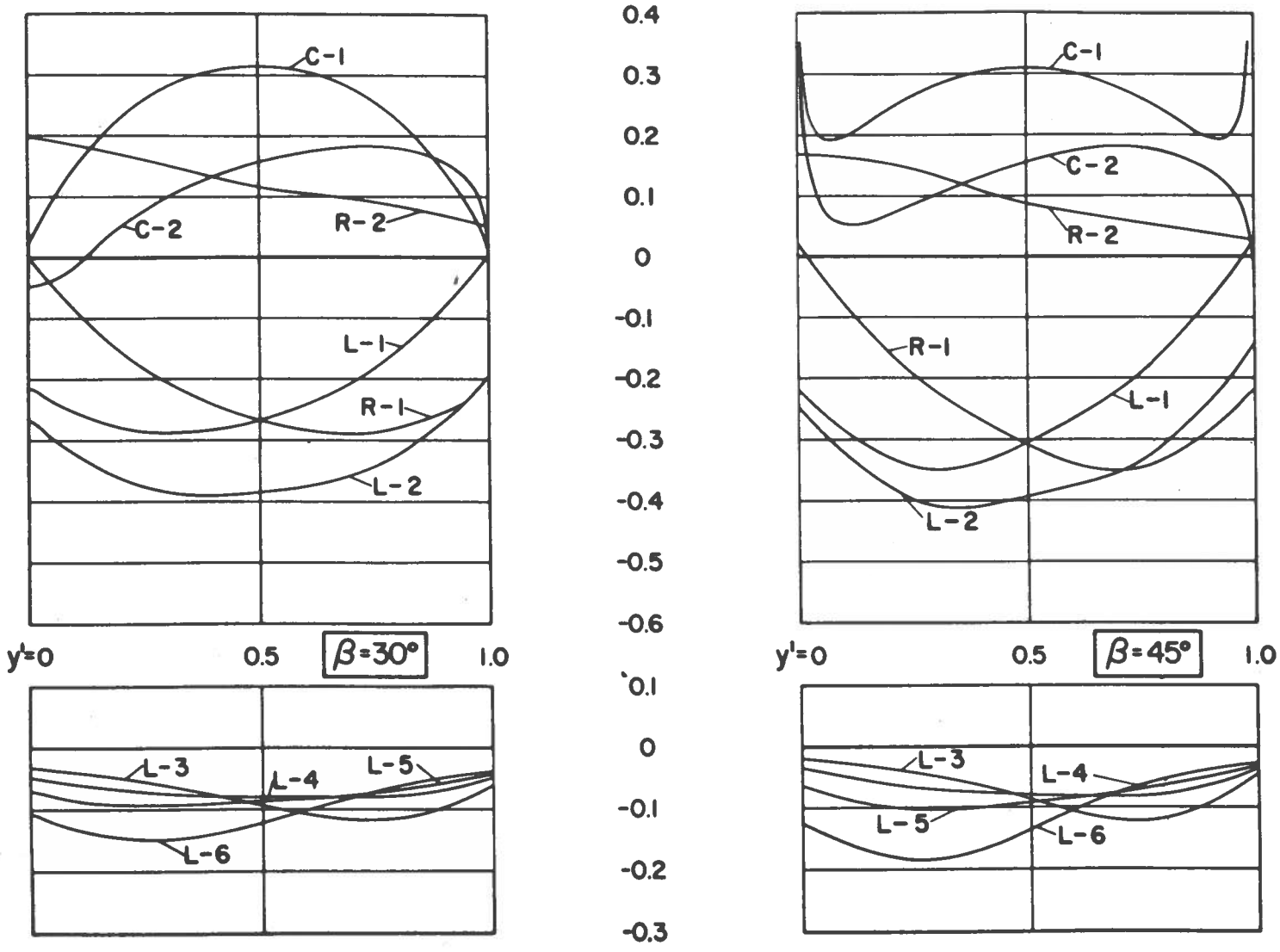

FIG. 5.13 TWIST, $\chi_{x'y'}$ AGAINST y' - CASE 1.0-1, 2, 3, 4, 5, 6

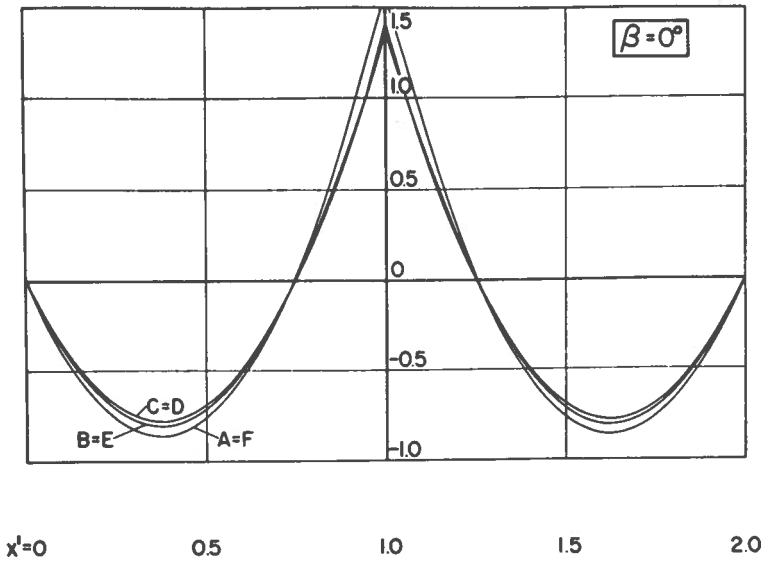

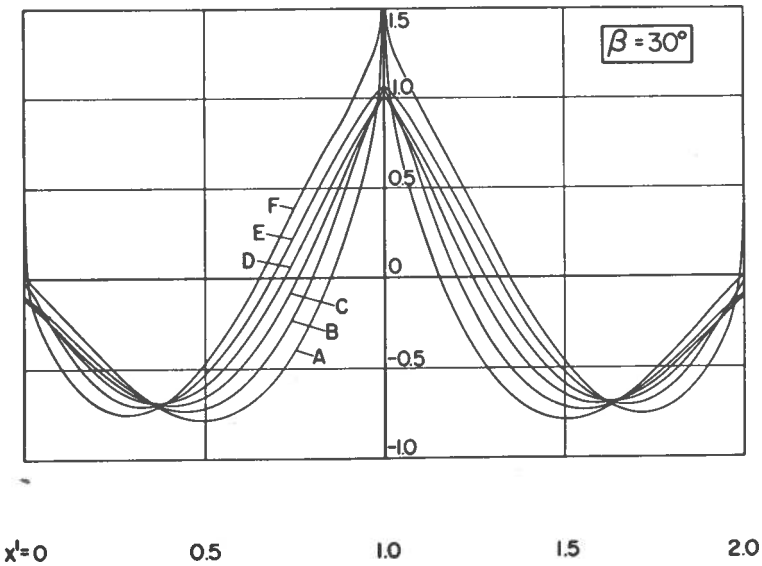

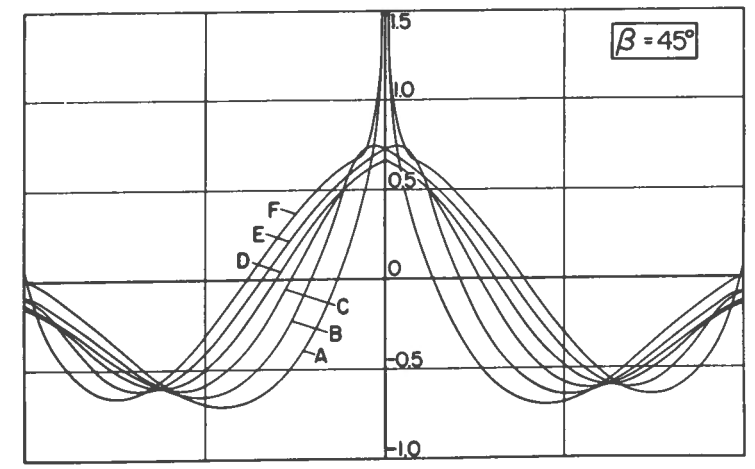

FIG. 5.14 LONGITUDINAL CURVATURE, $\chi_{x'}$ AGAINST x' CASE 0.5 - 1

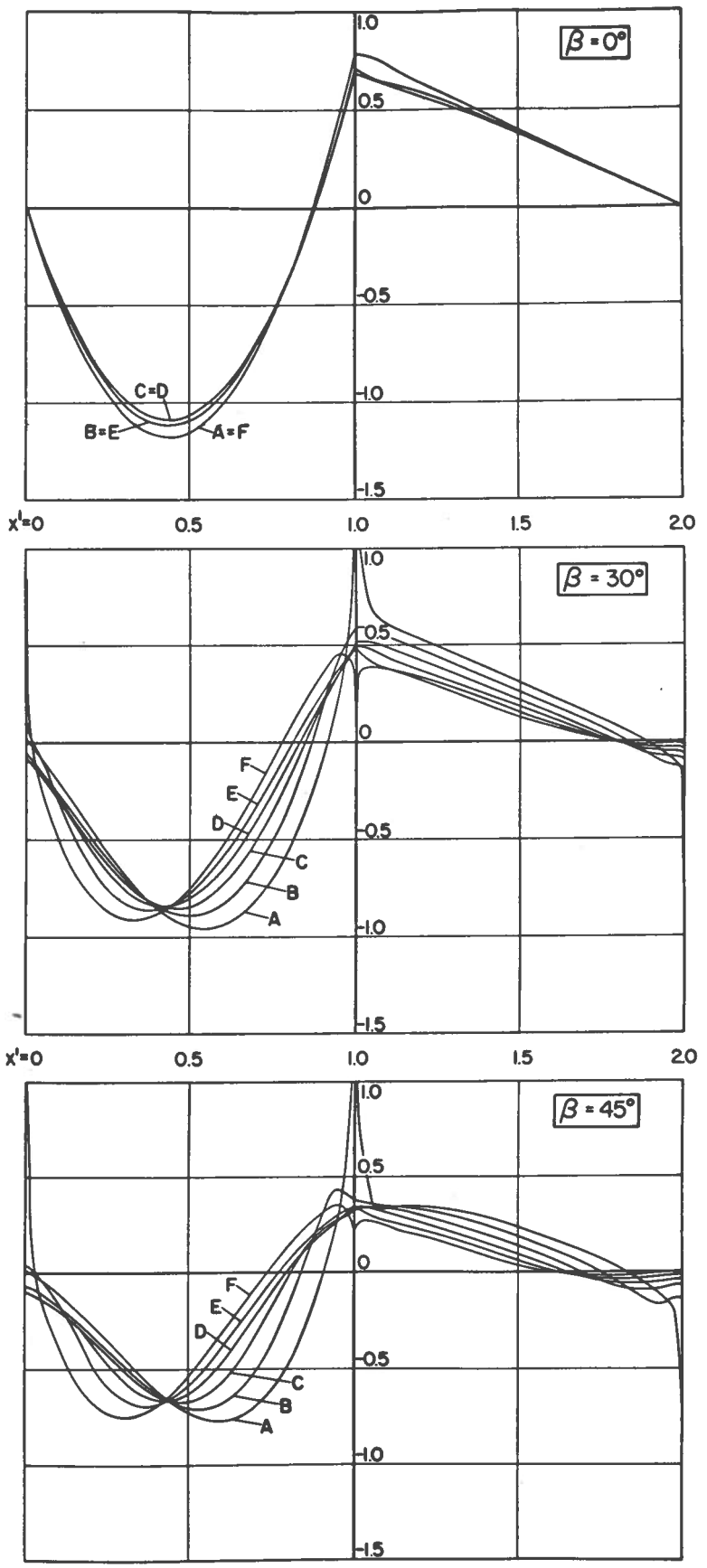

FIG. 5.15 LONGITUDINAL CURVATURE, $\chi_{x'}$ AGAINST x'
CASE 0.5 - 2

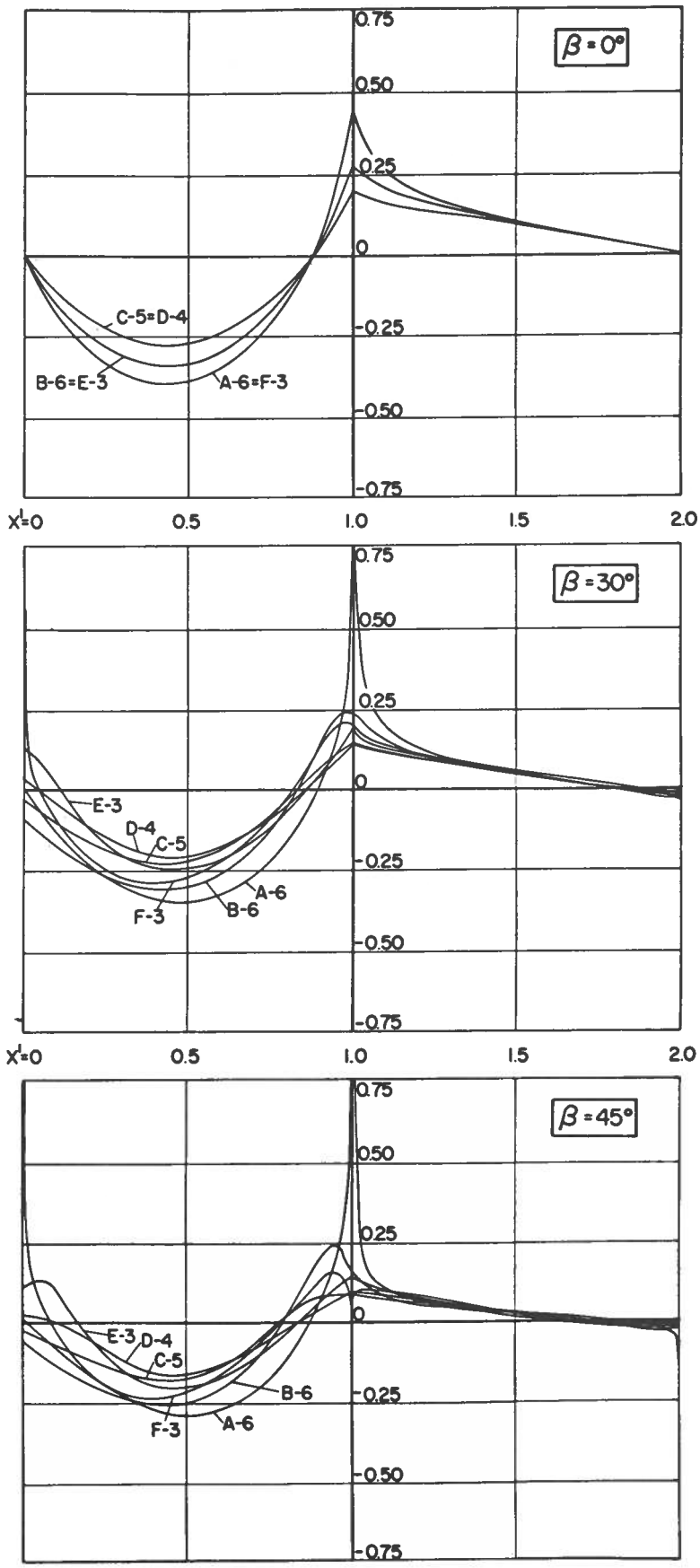

FIG. 5.16 LONGITUDINAL CURVATURE, $\chi_{x'}$ AGAINST x'
CASE 0.5 - 3, 4, 5, 6

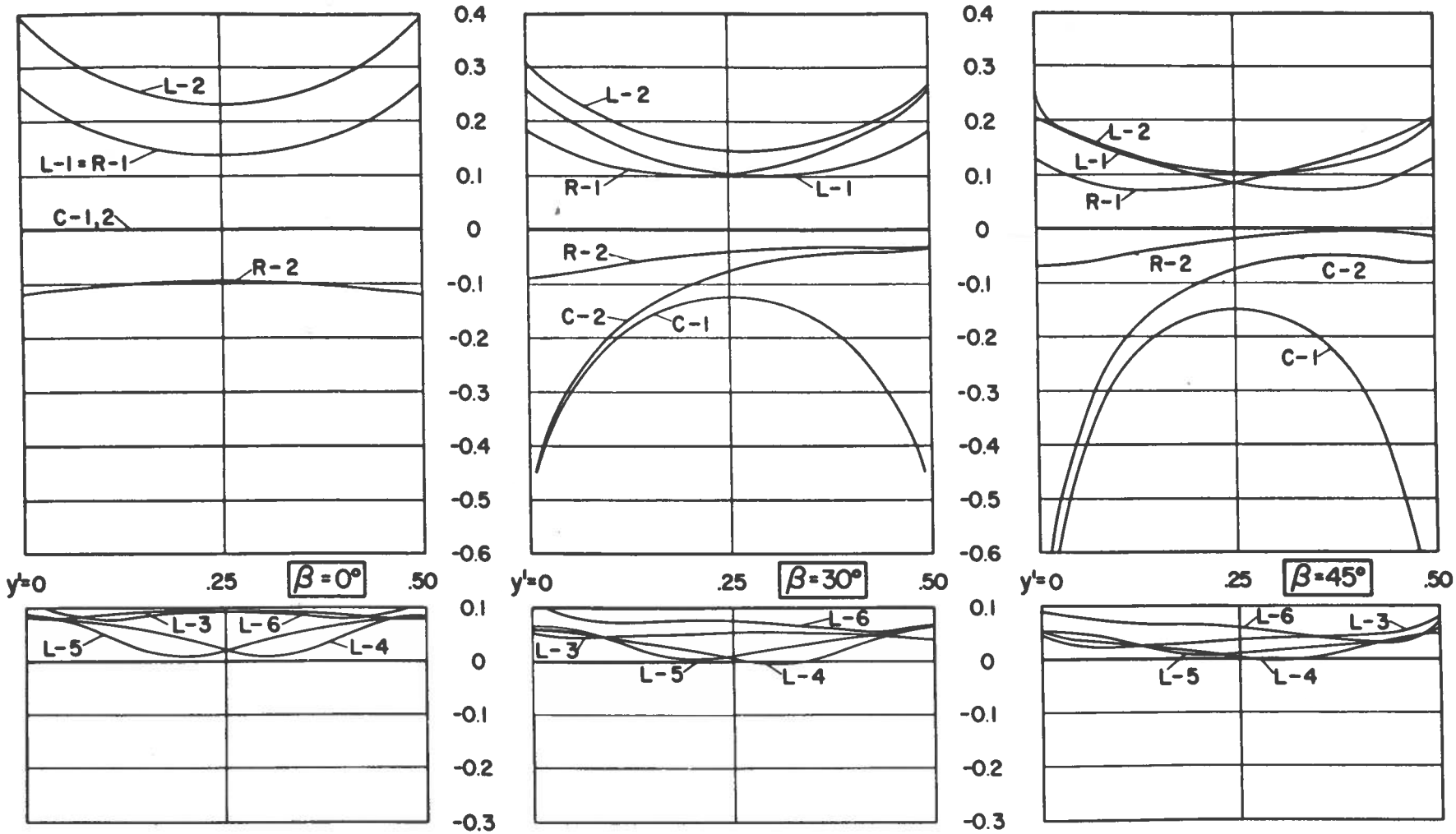

FIG. 5.17 TRANSVERSE CURVATURE, $\chi_{y'}$ AGAINST y' - CASE 0.5 - 1, 2, 3, 4, 5, 6

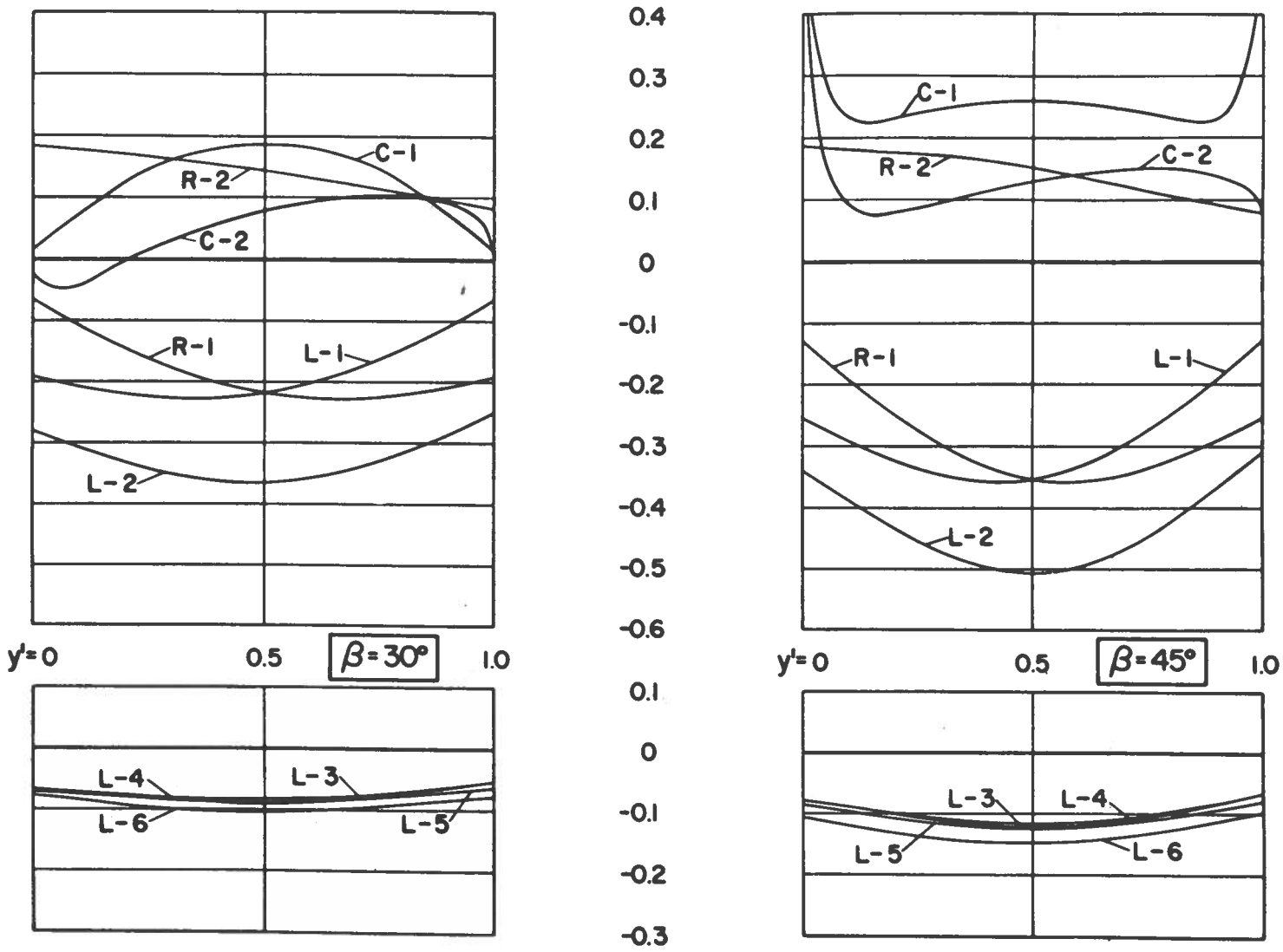

FIG. 5.18 TWIST, $\chi_{x'y'}$ AGAINST y' - CASE 0.5-1,2,3,4,5,6

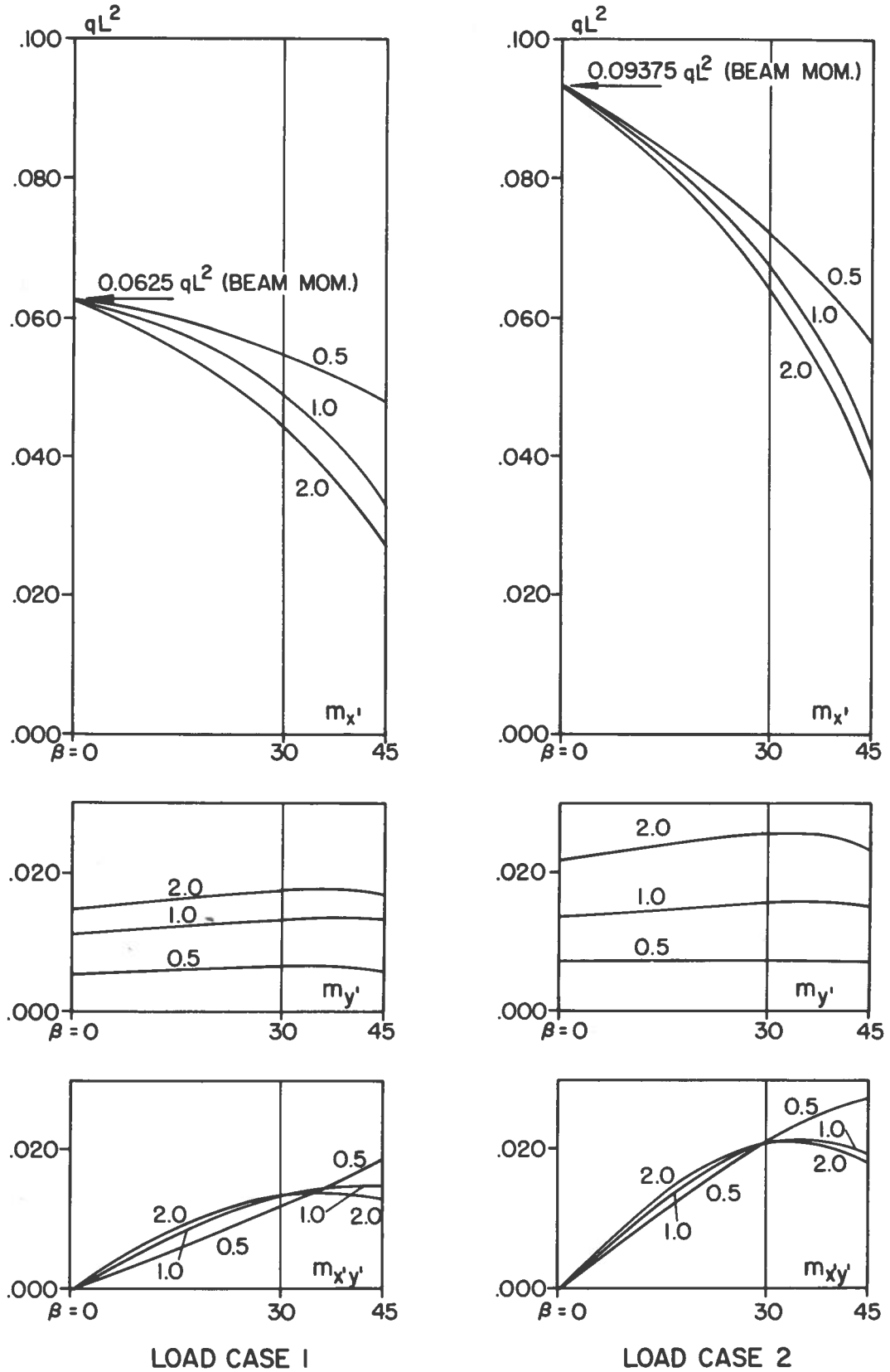

FIG. 5.19 AVERAGE MOMENTS FOR MID-SPAN SECTION, LOAD CASES 1 AND 2

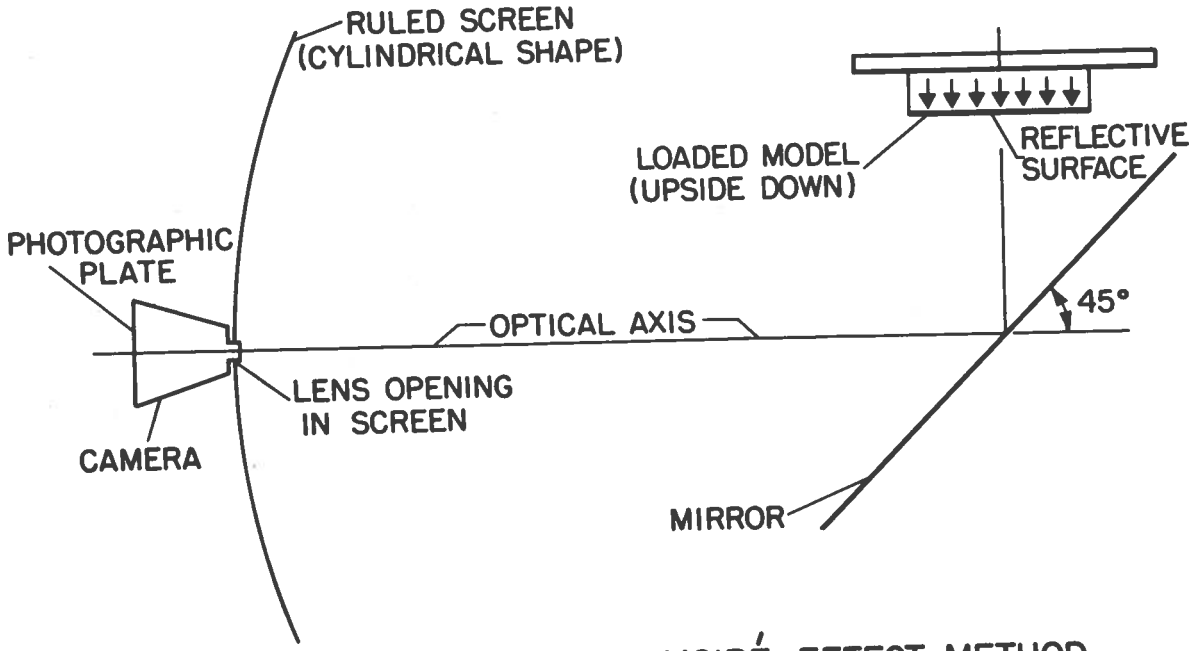

(a) BASIC ARRANGEMENT MOIRÉ-EFFECT METHOD

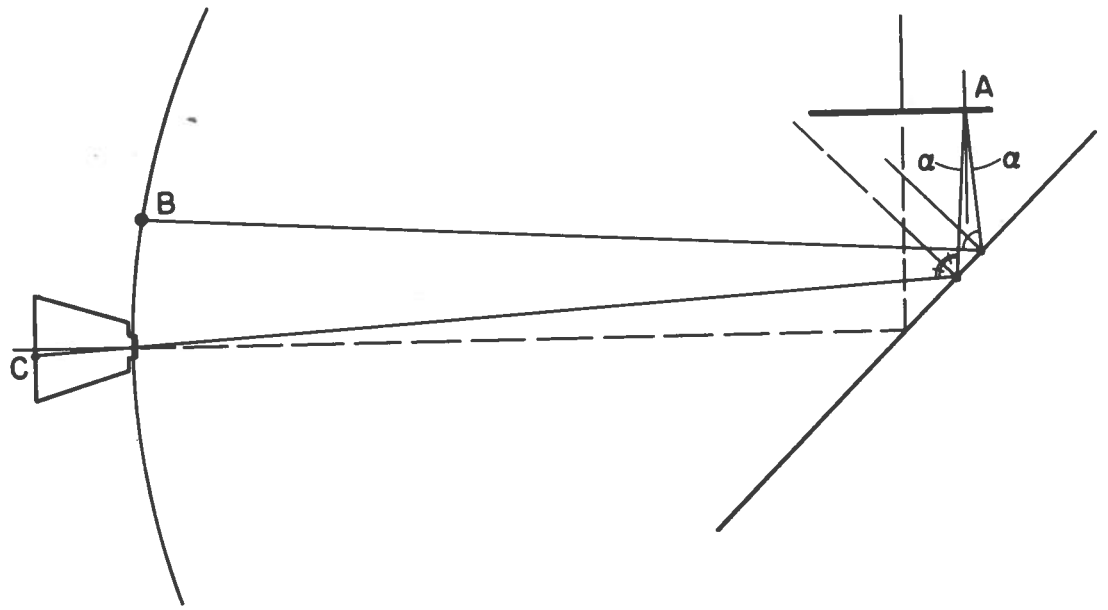

(b) OPTICAL REFLECTIVE PROCEDURE

FIG. 5.20

(a) CONTOUR LINES $\frac{\partial w}{\partial x'}$

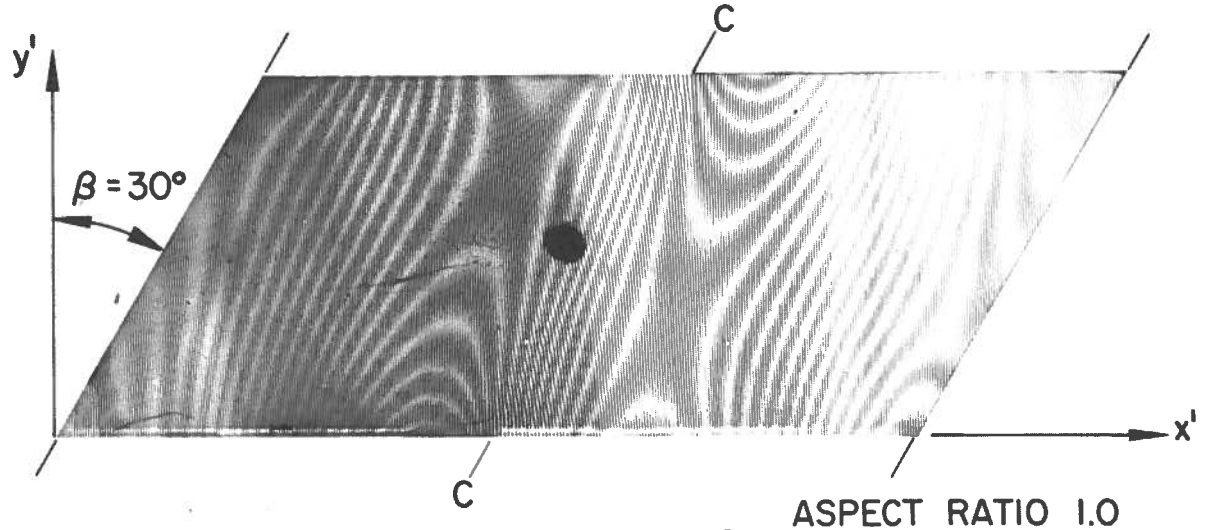

(b) CONTOUR LINES $\frac{\partial w}{\partial y'}$

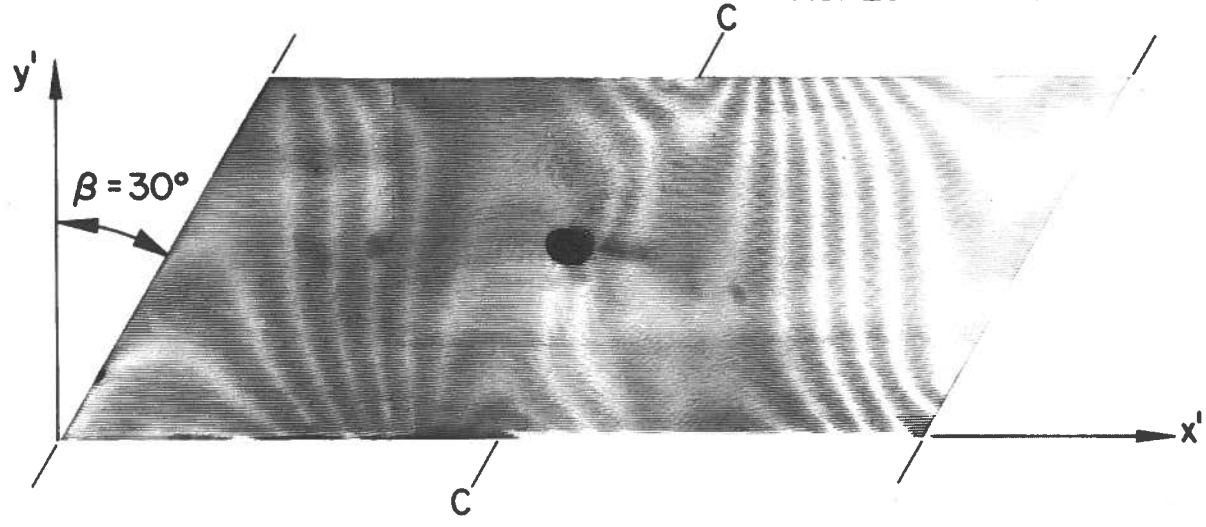

FIG. 5.21 SLOPE CONTOUR LINES FOR $\frac{\partial w}{\partial x'}$ AND $\frac{\partial w}{\partial y'}$, LOAD CASE I

(a) CONTOUR LINES $\frac{\partial w}{\partial x'}$

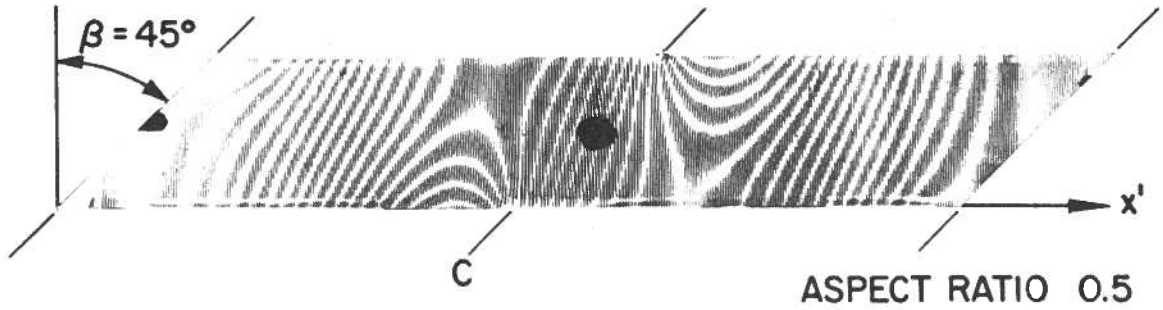

(b) CONTOUR LINES $\frac{\partial w}{\partial y'}$

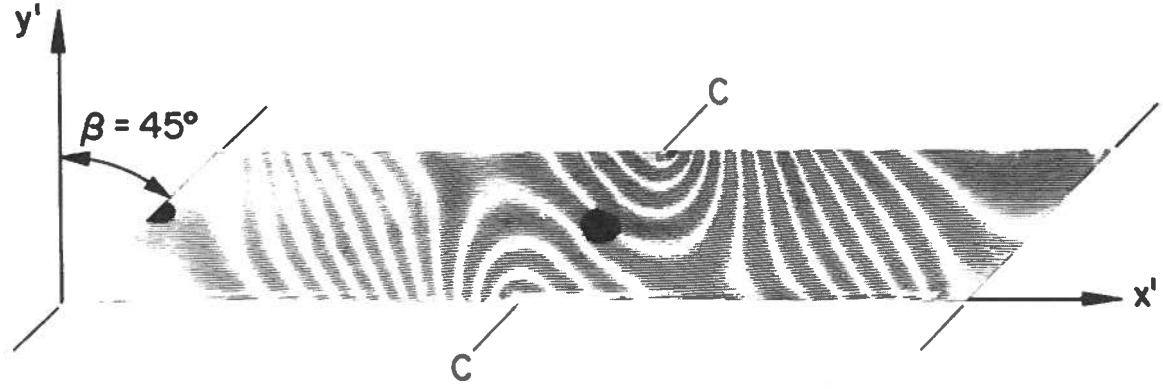

FIG. 5.22 SLOPE CONTOUR LINES FOR $\frac{\partial w}{\partial x'}$ AND $\frac{\partial w}{\partial y'}$, LOAD CASE I

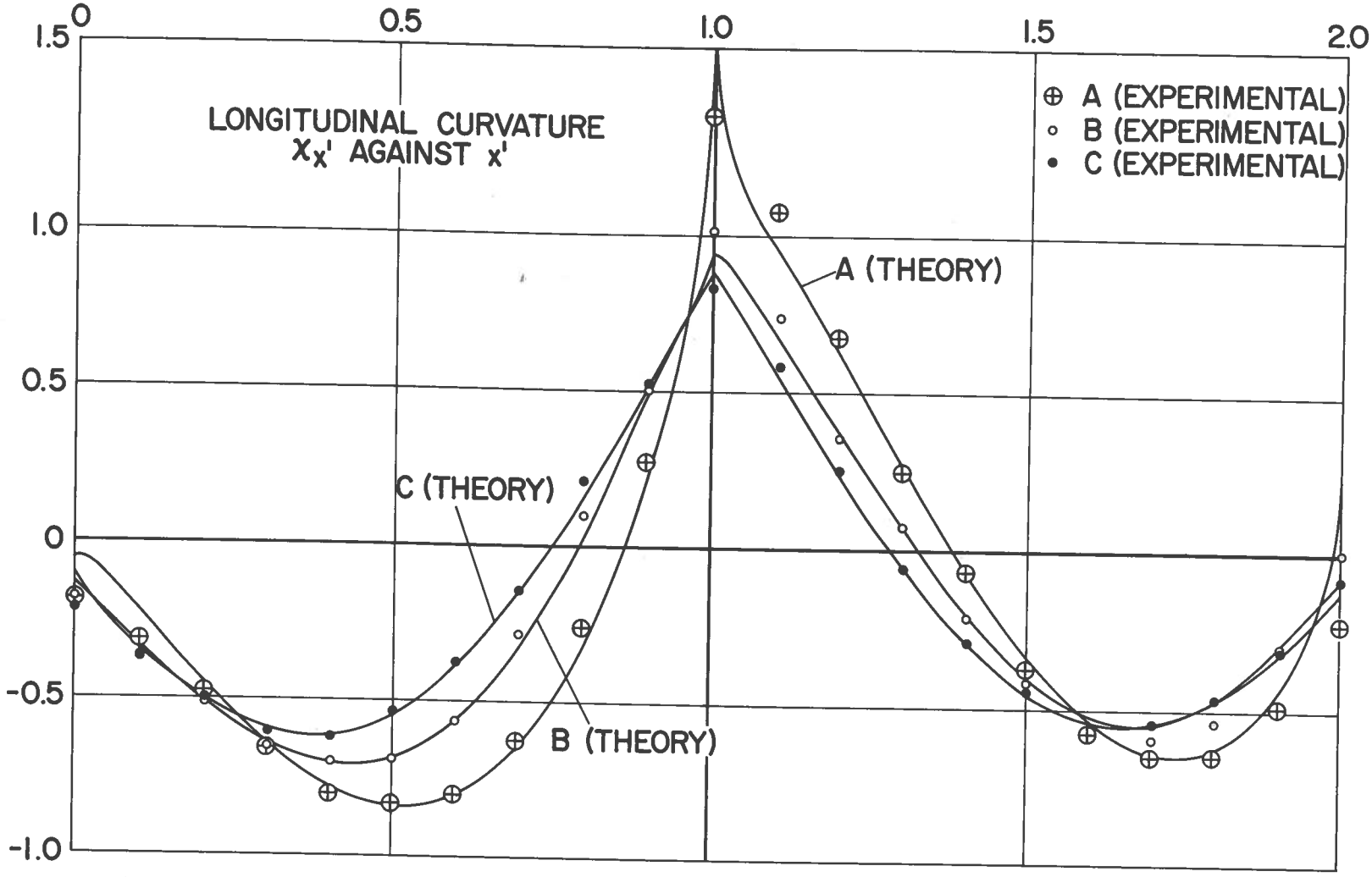

FIG. 5.23 COMPARISON OF ANALYTICAL AND EXPERIMENTAL RESULTS ALONG SECTIONS A, B, AND C
$\beta = 30°$, ASPECT RATIO = 1.0, LOAD CASE 1

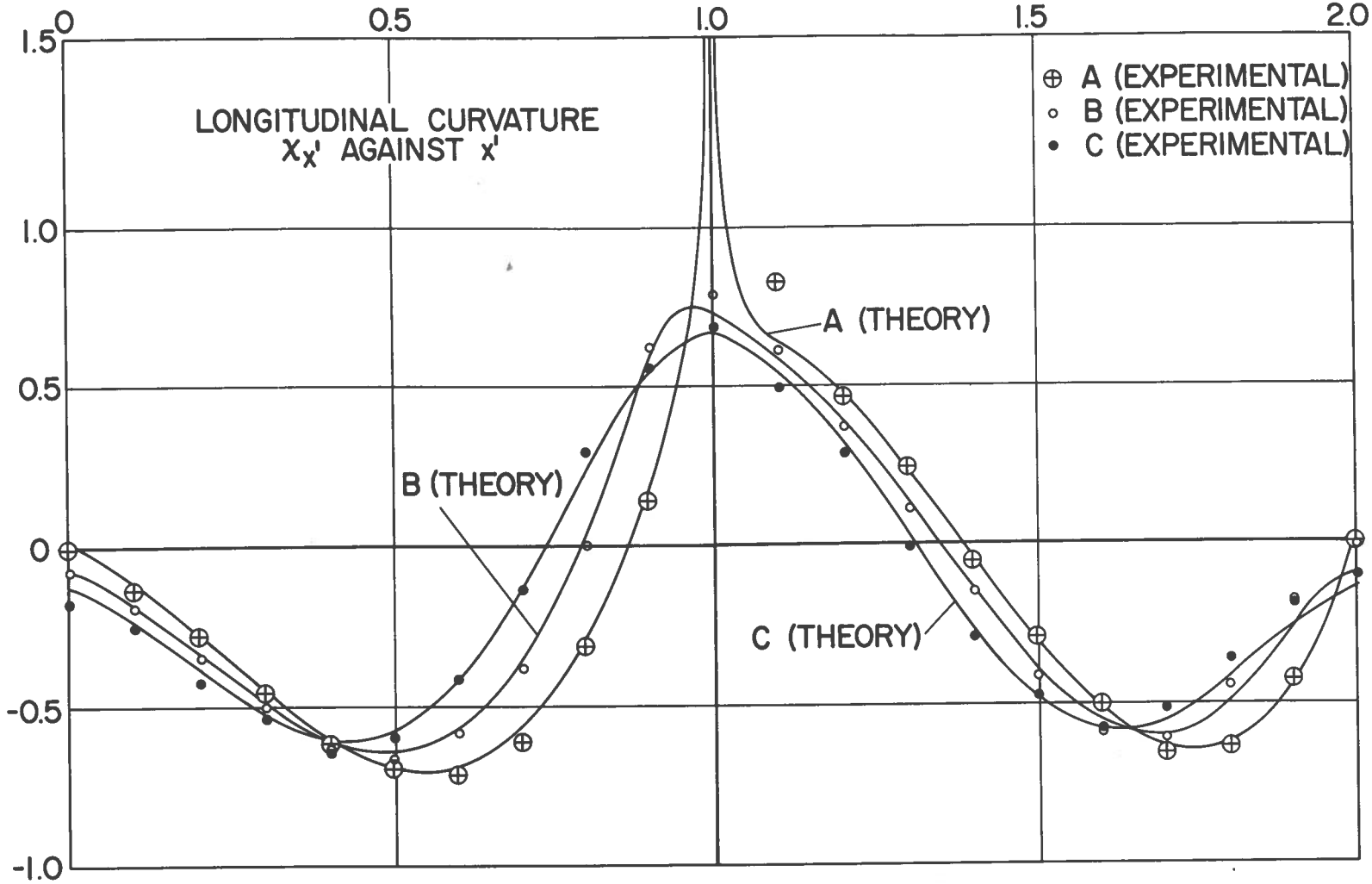

FIG. 5.24 COMPARISON OF ANALYTICAL AND EXPERIMENTAL RESULTS ALONG SECTIONS A, B, AND C
β = 45°, ASPECT RATIO = 0.5, LOAD CASE I

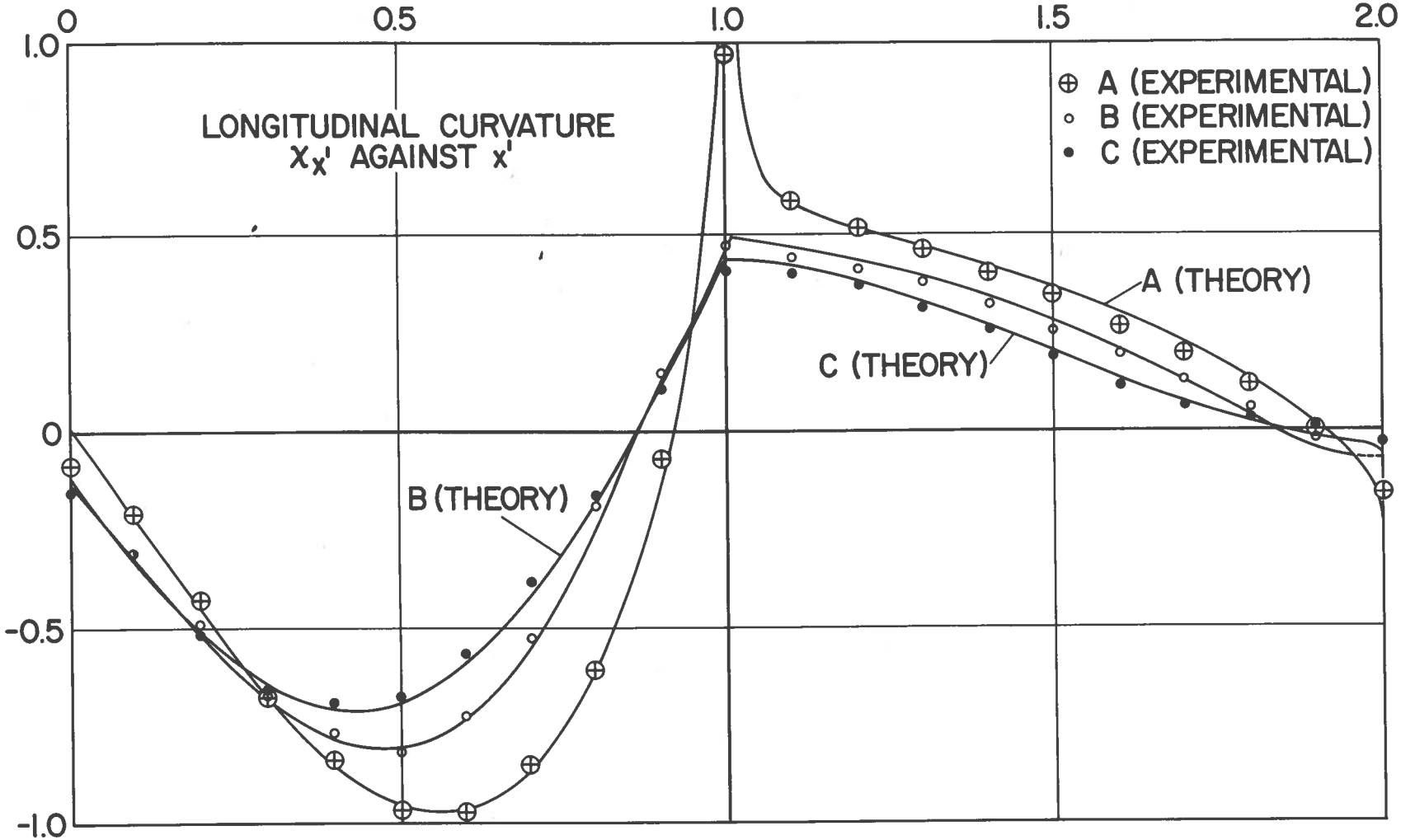

FIG. 5.25 COMPARISON OF ANALYTICAL AND EXPERIMENTAL RESULTS ALONG SECTIONS A, B, AND C
$\beta = 30°$, ASPECT RATIO = 1.0, LOAD CASE 2

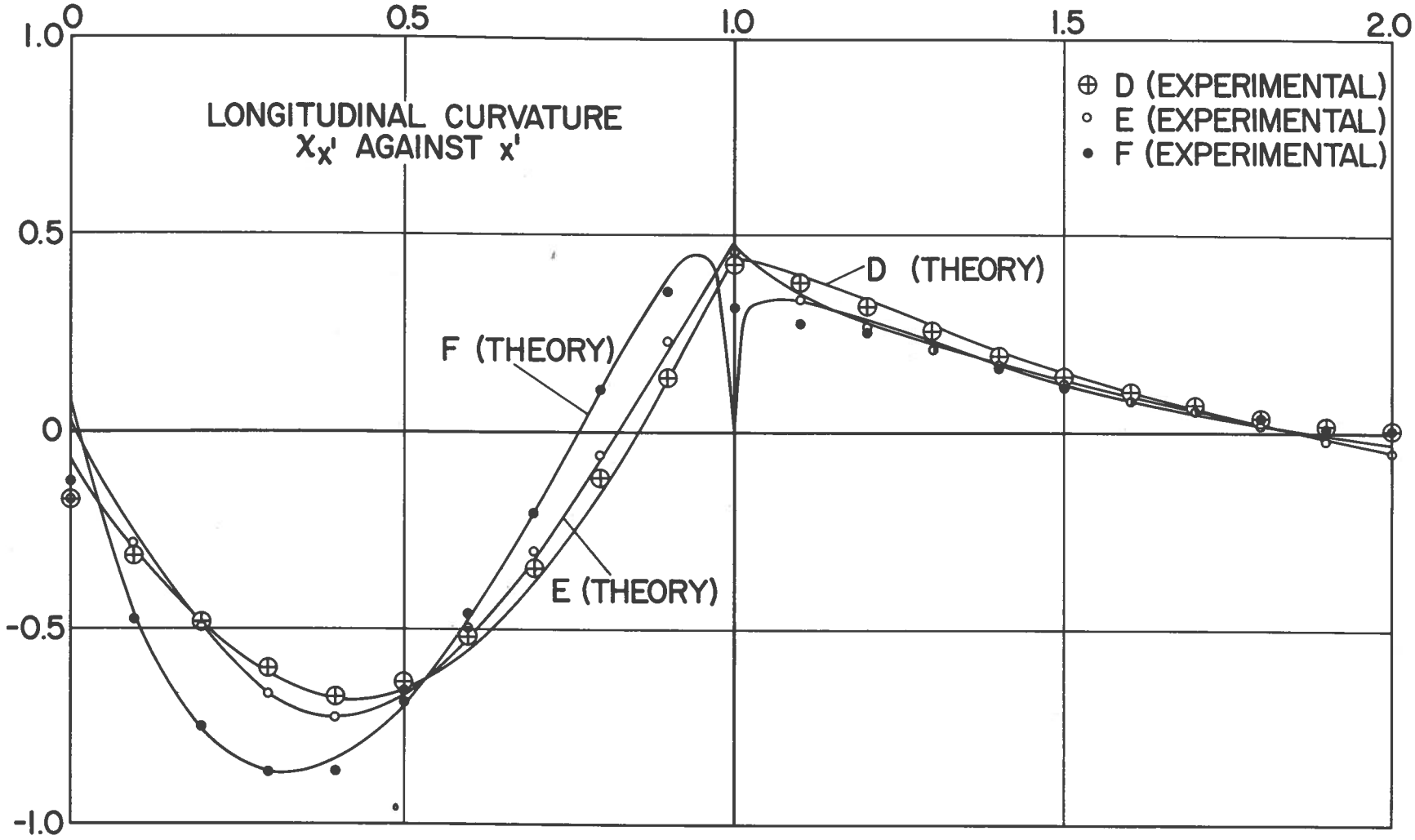

FIG. 5.26 COMPARISON OF ANALYTICAL AND EXPERIMENTAL RESULTS ALONG SECTIONS D, E, AND F
$\beta = 30°$, ASPECT RATIO = 1.0, LOAD CASE 2

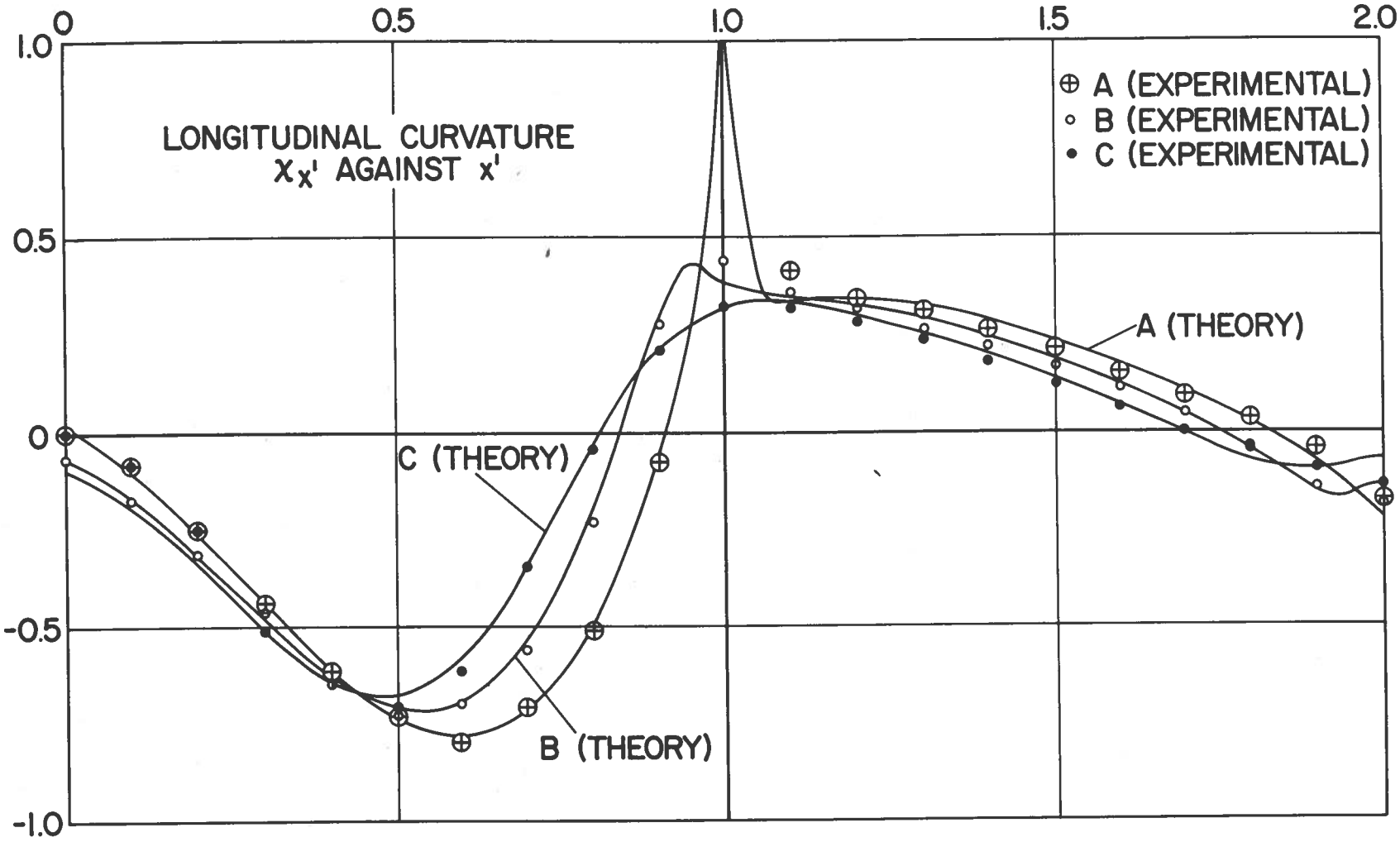

FIG. 5.27 COMPARISON OF ANALYTICAL AND EXPERIMENTAL RESULTS ALONG SECTIONS A, B, AND C
$\beta = 45°$, ASPECT RATIO = 0.5, LOAD CASE 2

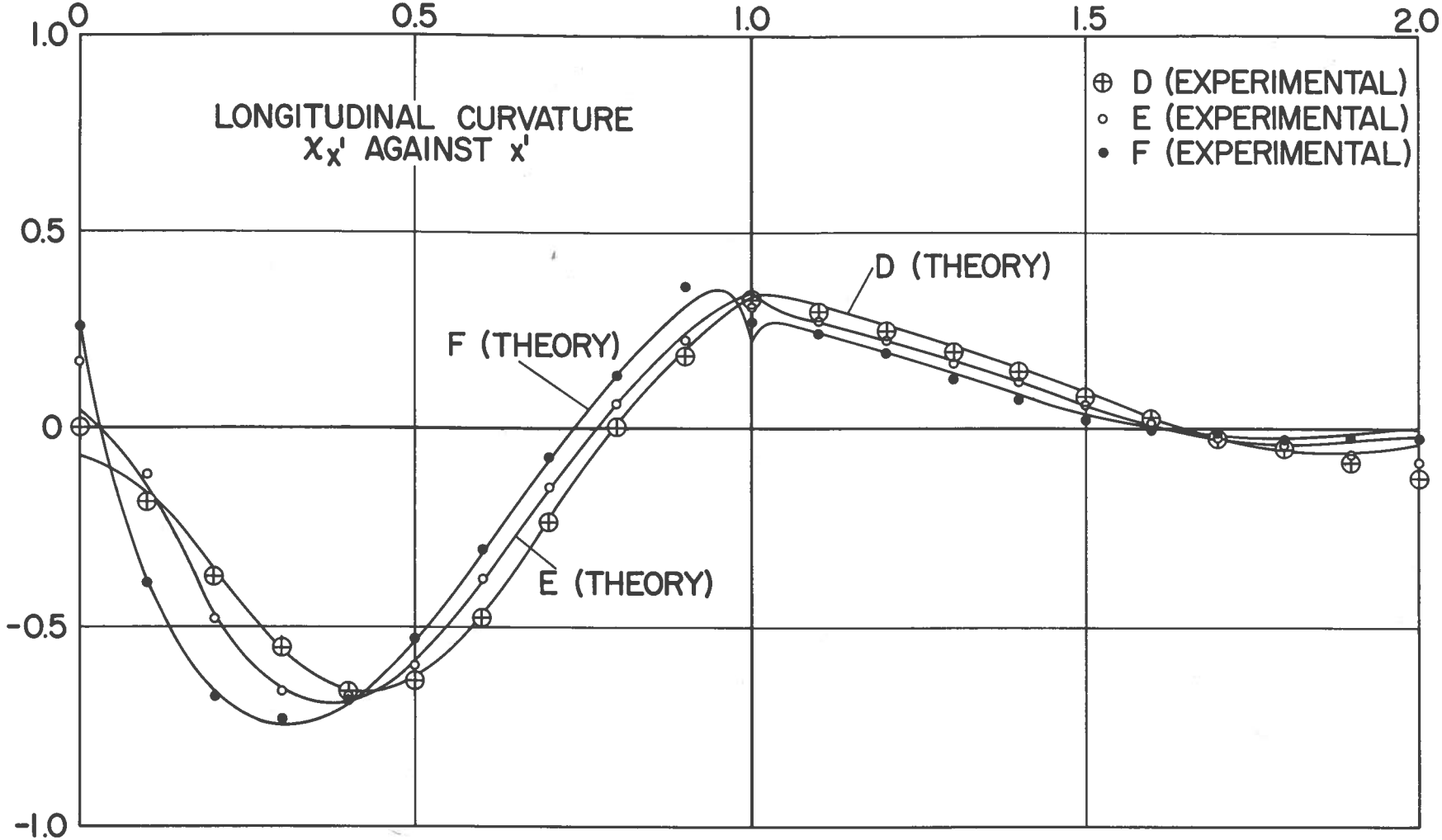

FIG. 5.28 COMPARISON OF ANALYTICAL AND EXPERIMENTAL RESULTS ALONG SECTIONS D, E, AND F
$\beta = 45°$, ASPECT RATIO = 0.5, LOAD CASE 2

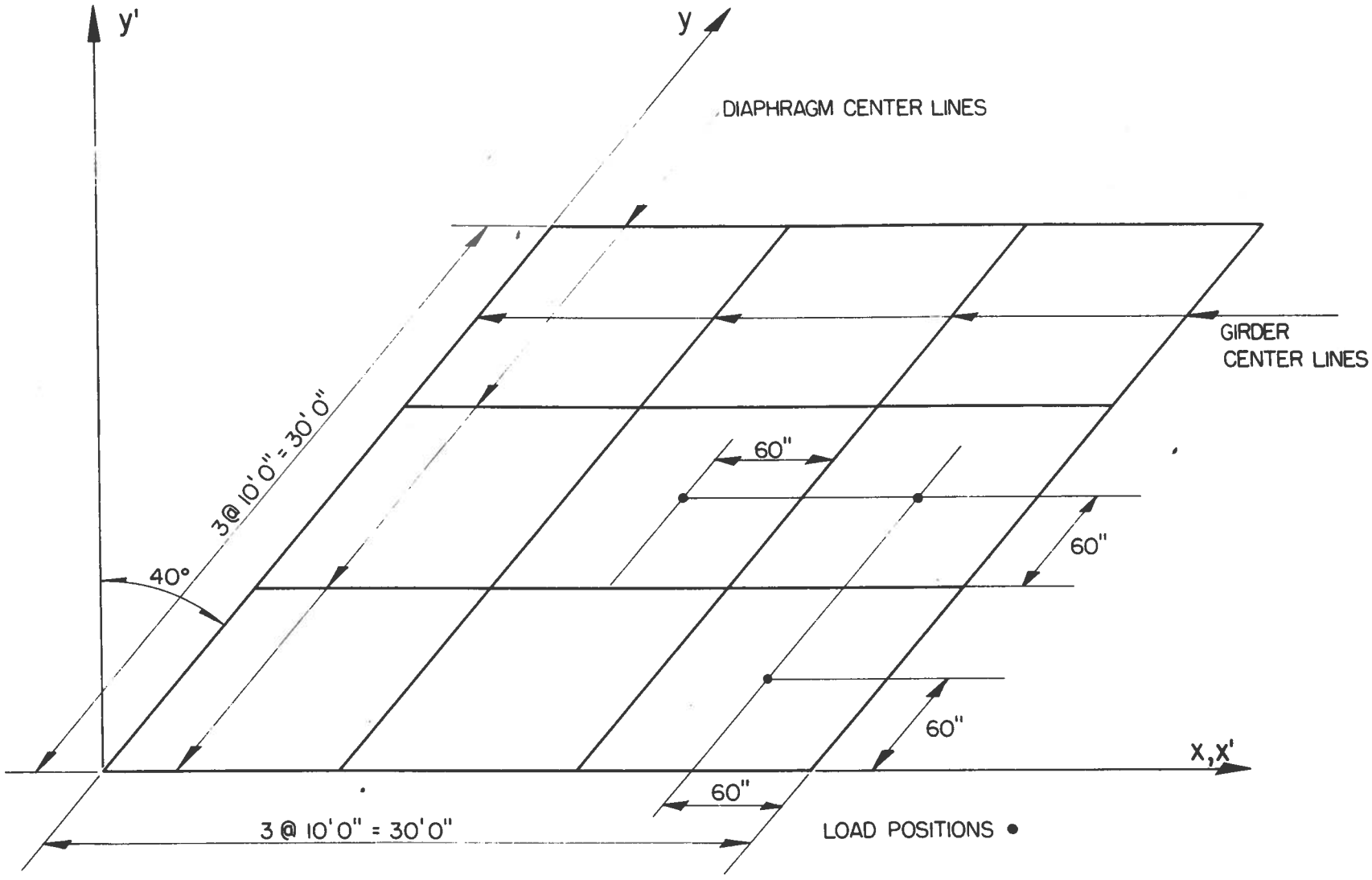

FIG. 6.1 PLAN VIEW OF DECK SLAB PANELS

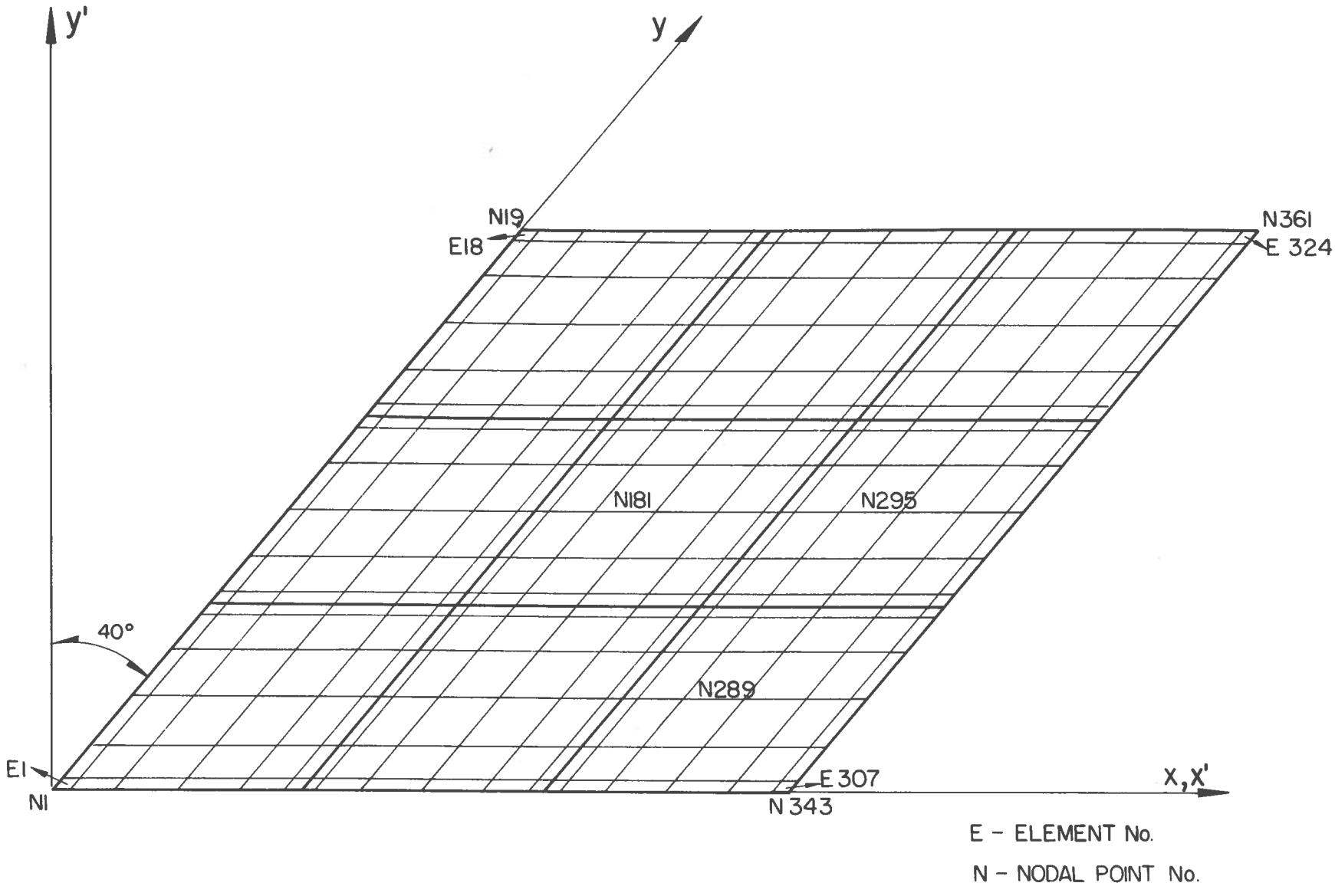

FIG. 6.2 FINITE ELEMENT MESH LAYOUT

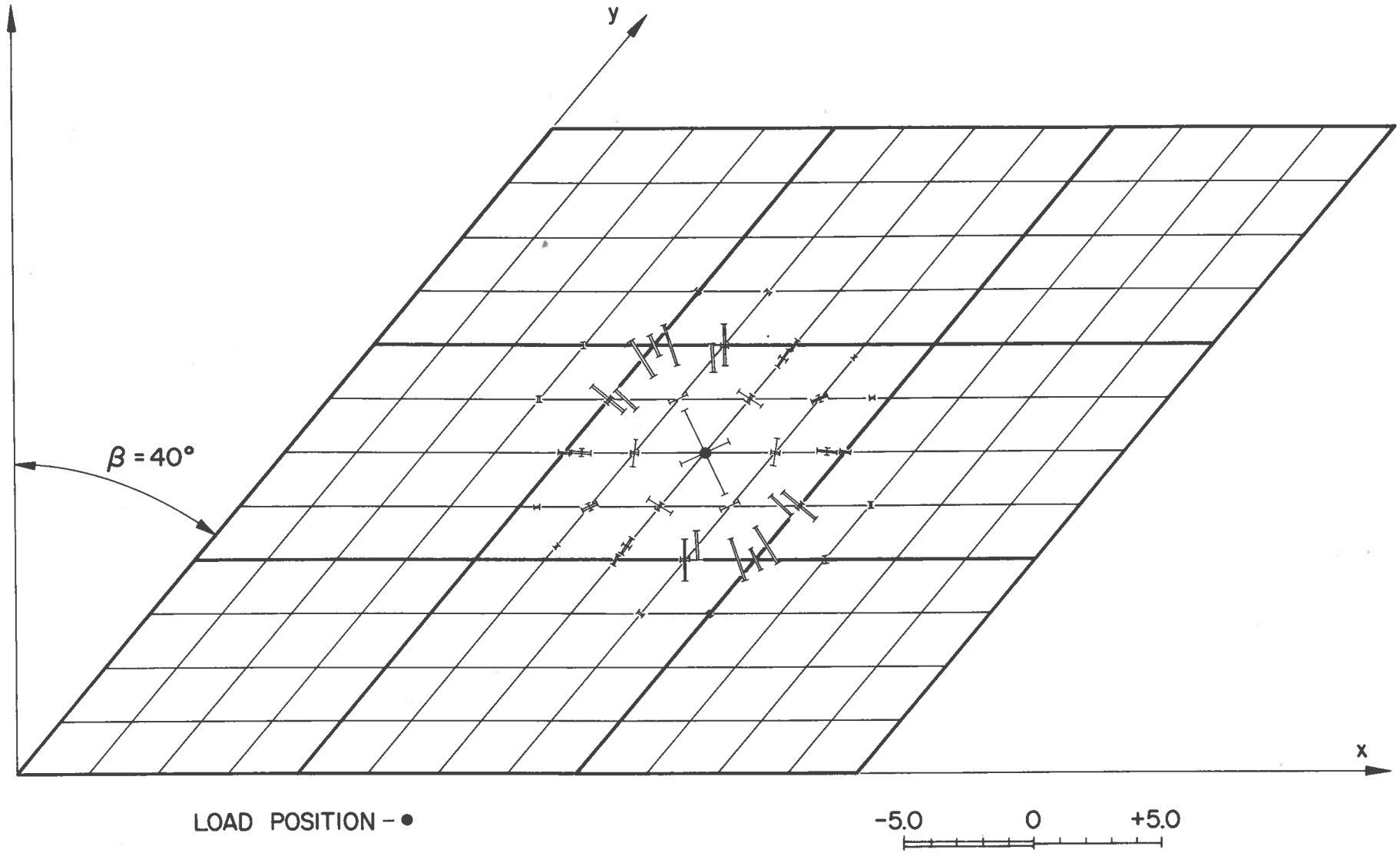

FIG. 6.3 PRINCIPAL MOMENTS IN SKEW DECK SLAB PANELS WITH DIAPHRAGM SUPPORTS

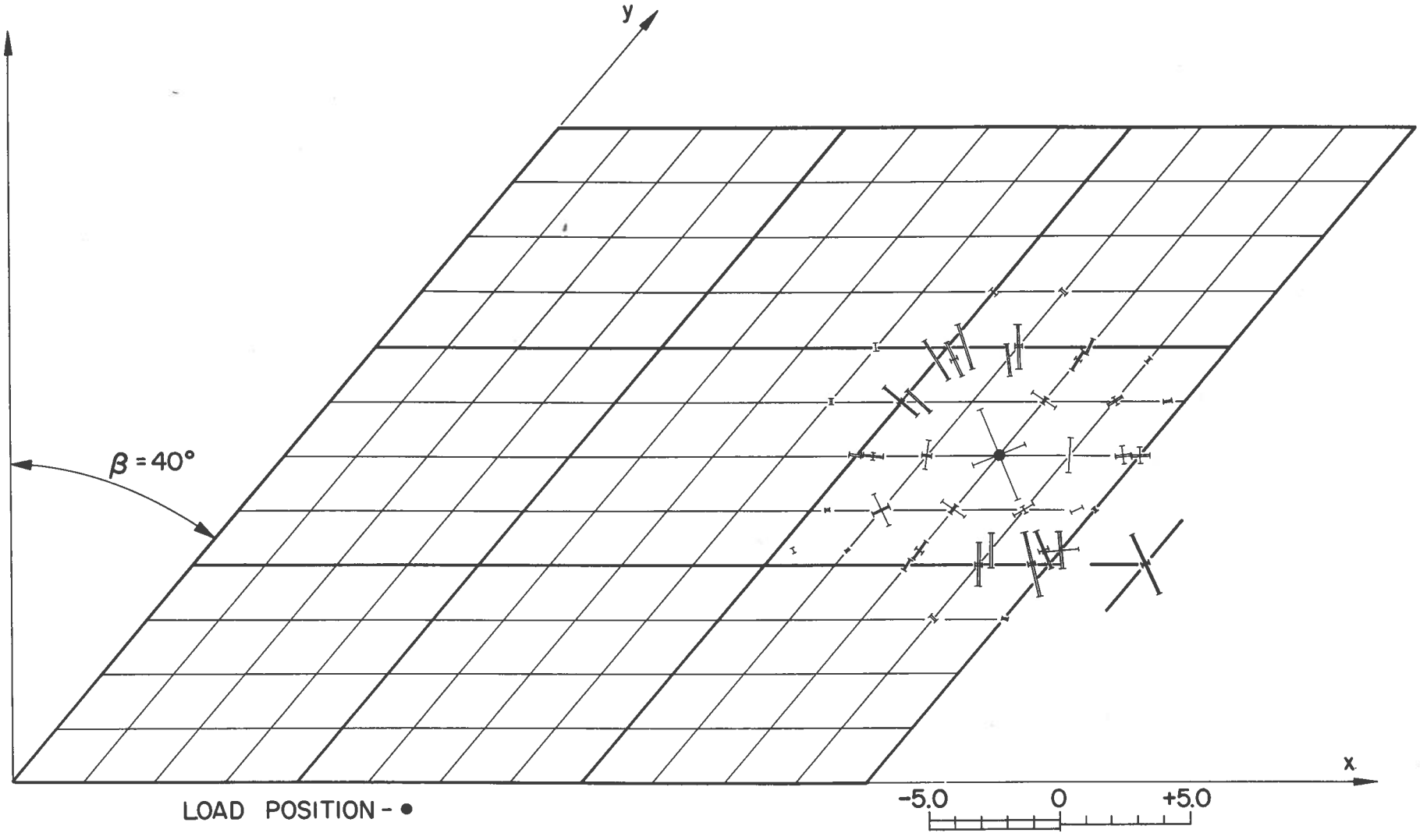

FIG. 6.4 PRINCIPAL MOMENTS IN SKEW DECK SLAB PANELS WITH DIAPHRAGM SUPPORTS

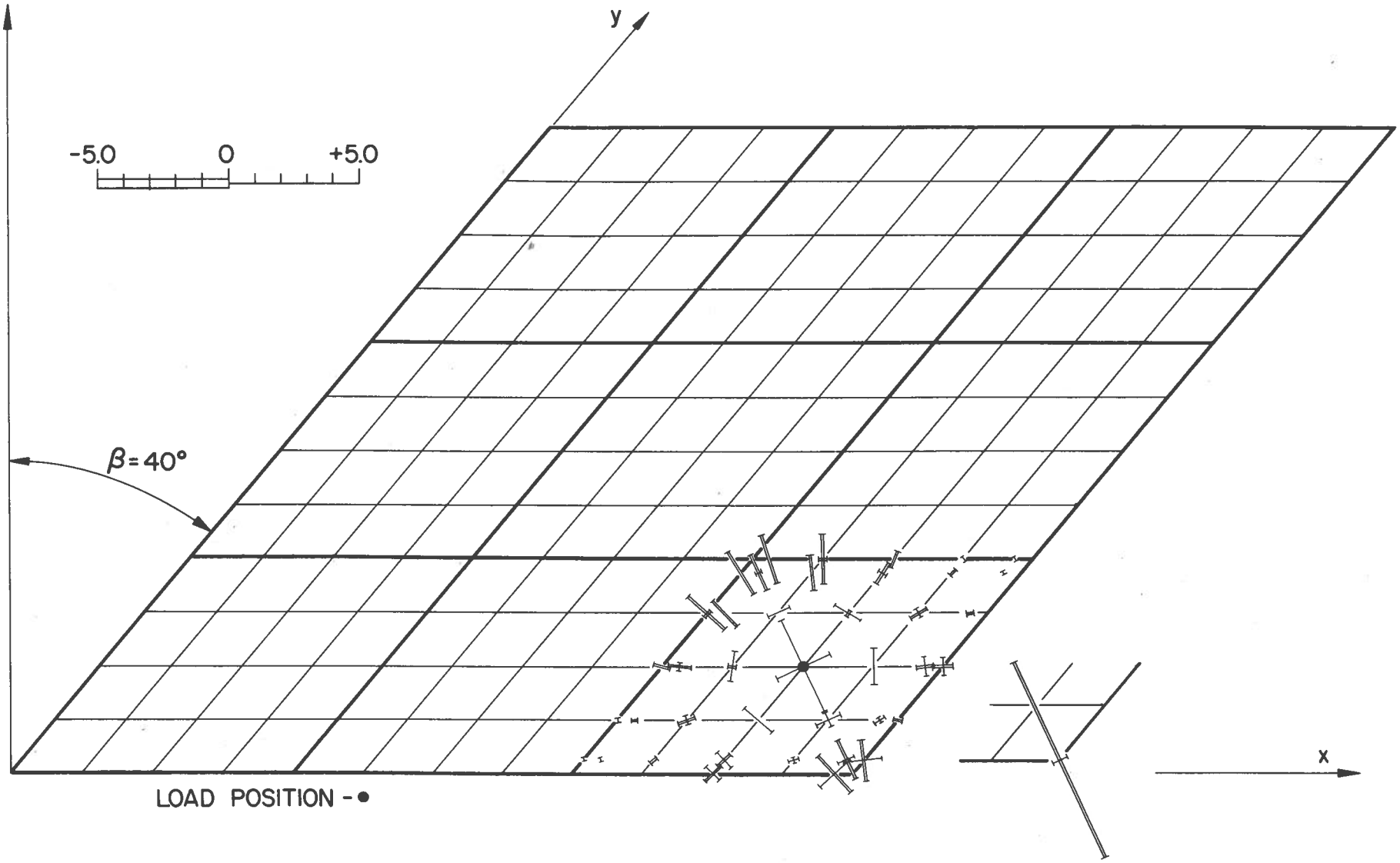

FIG. 6.5 PRINCIPAL MOMENTS IN SKEW DECK SLAB PANELS WITH DIAPHRAGM SUPPORTS

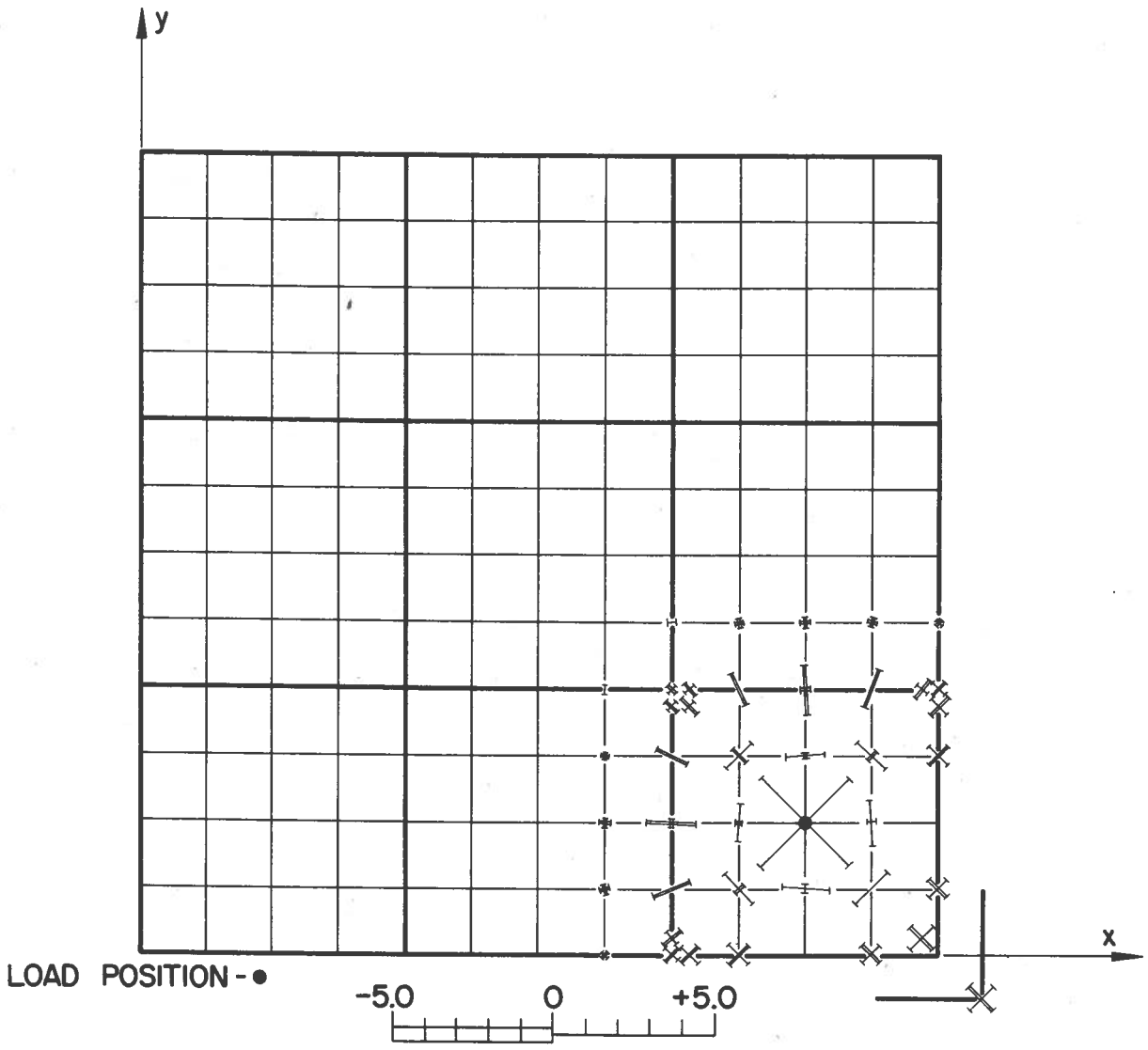

FIG. 6.6 PRINCIPAL MOMENTS IN RIGHT DECK SLAB PANELS WITH DIAPHRAGM SUPPORTS

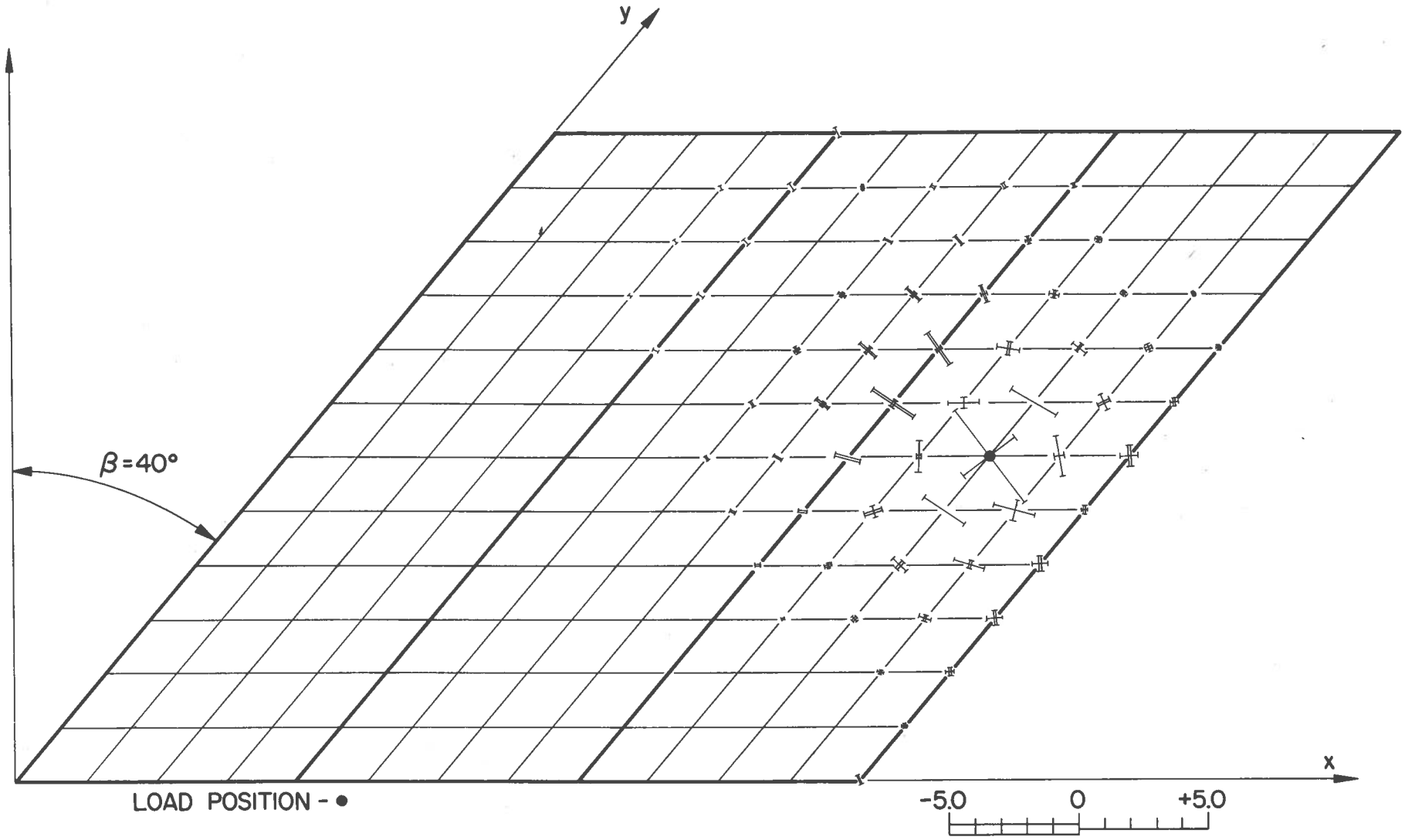

FIG. 6.7 PRINCIPAL MOMENTS IN SKEW DECK SLAB PANELS WITHOUT DIAPHRAGM SUPPORTS

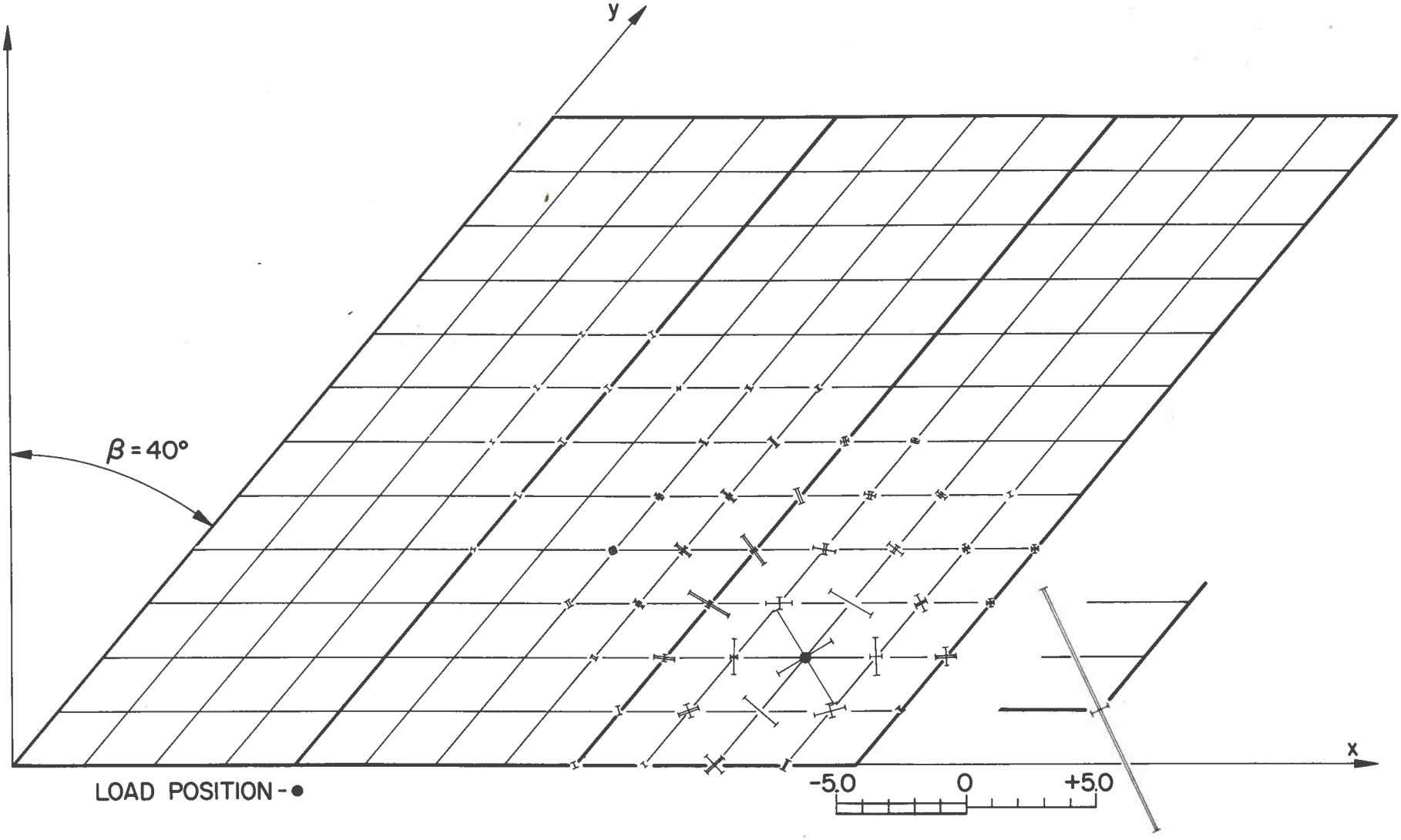

FIG. 6.8 PRINCIPAL MOMENTS IN SKEW DECK SLAB PANELS WITHOUT DIAPHRAGM SUPPORTS